

NUREG/CR-3690

SAND84-0402


R-4

Printed May 1984

# RELAP5 Assessment: Semiscale Natural Circulation Tests S-NC-3, S-NC-4, and S-NC-8

Chung-Nin Channy Wong, Lubomyra N. Kmetyk

Prepared by  
Sandia National Laboratories  
Albuquerque, New Mexico 87185 and Livermore, California 94550  
for the United States Department of Energy  
under Contract DE-AC04-76DP00789



8408310089 840731  
PDR NUREG  
CR-3690 R PDR

Prepared for  
**U. S. NUCLEAR REGULATORY COMMISSION**

**NOTICE**

This report was prepared as an account of work sponsored by an agency of the United States Government. Neither the United States Government nor any agency thereof, or any of their employees, makes any warranty, expressed or implied, or assumes any legal liability or responsibility for any third party's use, or the results of such use, of any information, apparatus product or process disclosed in this report, or represents that its use by such third party would not infringe privately owned rights.

Available from  
GPO Sales Program  
Division of Technical Information and Document Control  
U.S. Nuclear Regulatory Commission  
Washington, D.C. 20555  
and  
National Technical Information Service  
Springfield, Virginia 22161

NUREG/CR-3690  
SAND84-0402  
R-4

RELAP5 ASSESSMENT: SEMISCALE NATURAL CIRCULATION TESTS  
S-NC-3, S-NC-4, and S-NC-8

Chung-Nin Channy Wong

and

Lubomyra N. Kmetyk

Date Published: May 1984

Sandia National Laboratories  
Albuquerque, NM 87185  
Operated by  
Sandia Corporation  
U. S. Department of Energy

Prepared for  
Reactor Systems Research Branch  
Division of Accident Evaluation  
Office of Nuclear Regulatory Research  
U. S. Nuclear Regulatory Commission  
Washington, DC 20555  
Under Memorandum of Understanding DOE 40-550-75  
NRC FIN No. A-1205

## ABSTRACT

The RELAP5/MOD1 independent assessment project at Sandia National Laboratories (SNLA) is part of an overall effort funded by the NRC to determine the ability of various systems codes to predict the detailed thermal/hydraulic response of LWRs during accident and off-normal conditions. The RELAP5 code is being assessed at SNLA against test data from a number of integral and separate effects test facilities. As part of this assessment matrix, we have analyzed a number of natural circulation tests performed at the Semiscale facility. Our results for the single-loop and two-loop steady state basecase tests S-NC-2 and S-NC-7 have already been documented separately; this report gives the results of calculations for two single-loop degraded heat transfer tests, S-NC-3 and S-NC-4, and for the two-loop ultra-small break transient test S-NC-8.

For tests S-NC-3 and S-NC-4, our analyses show that RELAP5/MOD1 describes correctly the qualitative influence of steam generator secondary side heat transfer degradation on both two-phase and reflux natural circulation. The agreement between calculated and measured two-phase mass flow rates in test S-NC-3 is better with a primary mass inventory of 85% (where the peak two-phase mass flow rate is calculated to occur) instead of 92% (where the measured peak mass flow rate occurred in S-NC-2). Flow oscillations are calculated for both tests, and were seen during S-NC-3, but were not reported in the S-NC-4 experiment. Some of these predicted oscillations are real, but others are nonphysical and can be inhibited by reducing the time step being used (indicating problems in the time step control algorithm).

The results for test S-NC-8, an ultra-small (0.4%) cold leg break, also compare reasonably well with the outcome of that experiment. Mass flow rates calculated in the intact loop and in the downcomer match data, although there are some discrepancies in the broken loop mass flow rates. The calculated pressure response throughout the blowdown period is good. However, the mass flow rate at the break is underpredicted, resulting in discrepancies in the primary system mass inventory.

## TABLE OF CONTENTS

	<u>Page</u>
1.0 Introduction.....	1
2.0 Nodalizations.....	3
3.0 Single-Loop Degraded Heat Transfer Tests S-NC-3 and S-NC-4.....	15
3.1 Two-phase Natural Circulation Test S-NC-3.....	15
3.1.1 Description of Experiment.....	15
3.1.2 Calculated Results.....	16
3.2 Reflux Cooling Test S-NC-4.....	19
3.2.1 Description of Experiment.....	19
3.2.2 Calculated Results.....	20
3.3 Flow Oscillations.....	21
4.0 Two-Loop Ultra-Small Break Transient S-NC-8.....	47
4.1 Description of Experiment.....	47
4.2 Calculated Results.....	48
4.3 Comparison with S-NC-7 Results.....	52
5.0 Discussion and Conclusions.....	77
6.0 References.....	81
Appendix I Facility Description.....	83
Appendix II Input Listings.....	103
Appendix III Additional Updates Used for Cycle 18+.....	104

## LIST OF FIGURES

	<u>Page</u>
2.1	Isometric View of the Semiscale Mod-2A System..... 7
2.2	RELAP5 Nodalization for Tests S-NC-3 and S-NC-4..... 8
2.3	RELAP5 Nodalization for Test S-NC-8..... 9
2.4	Vessel Nodalization..... 10
2.5	Intact Loop Steam Generator Nodalization..... 11
2.6	Broken Loop Steam Generator Nodalization..... 12
2.7	Loss Coefficients Used in S-NC-3 and S-NC-4 Nodalizations..... 13
2.8	Loss Coefficients Used in S-NC-8 Nodalization..... 14
3.1	Relationship between the Secondary Liquid Level and the Heat Transfer Area in the Steam Generator..... 25
3.1.1	Measured and Calculated Mass Flow Rates for Test S-NC-2 (60 kW Power Case)..... 26
3.1.2	Measured and Calculated Mass Flow Rates for Test S-NC-3..... 27
3.1.3	Measured and Calculated Primary System Pressures for Test S-NC-3..... 28
3.1.4	Measured and Calculated Hot Leg Temperatures for Test S-NC-3..... 29
3.1.5	Measured and Calculated Cold Leg Temperatures for Test S-NC-3..... 30
3.1.6	Measured and Calculated Mass Flow Rates for Test S-NC-3 (Including Results of Calculations with Reduced Primary Inventories)..... 31
3.1.7	Measured and Calculated Primary System Pressures for Test S-NC-3 (Including Results of Calculations with Reduced Primary Inventories)..... 32
3.1.8	Measured and Calculated Hot Leg Temperatures for Test S-NC-3 (Including Results of Calculations with Reduced Primary Inventories)..... 33

3.1.9	Measured and Calculated Cold Leg Temperatures for Test S-NC-3 (Including Results of Calculations with Reduced Primary Inventories).....	34
3.2.1	Measured and Calculated Reflux Mass Flow Rates for Test S-NC-4 (60 kW Power Case).....	35
3.2.2	Measured and Calculated Carryover Mass Flow Rates for Test S-NC-4 (60 kW Power Case).....	36
3.2.3	Measured and Calculated Primary System Pressures for Test S-NC-4 (60 kW Power Case).....	37
3.2.4	Measured and Calculated Core Outlet Temperatures for Test S-NC-4 (60 kW Power Case).....	38
3.2.5	Measured and Calculated Core Inlet Temperatures for Test S-NC-4 (60 kW Power Case).....	39
3.2.6	Measured and Calculated Reflux Mass Flow Rates for Test S-NC-4 (30 kW Power Case).....	40
3.2.7	Measured and Calculated Carryover Mass Flow Rates for Test S-NC-4 (30 kW Power Case).....	41
3.2.8	Measured and Calculated Primary System Pressures for Test S-NC-4 (30 kW Power Case).....	42
3.2.9	Measured and Calculated Core Outlet Temperatures for Test S-NC-4 (30 kW Power Case).....	43
3.2.10	Measured and Calculated Core Inlet Temperatures for Test S-NC-4 (30 kW Power Case).....	44
3.3.1	Calculated Steady State Flow Oscillations in Test S-NC-4 (60 kW Power Case).....	45
3.3.2	Measured (Top) and Calculated (Bottom) Steady State Flow Oscillations in Test S-NC-3 (Both Primary Inventories Equal to 92%).....	46
4.2.1	Measured and Calculated Primary System Pressures vs Time for Test S-NC-8.....	56
4.2.2	Measured and Calculated Intact Loop Secondary Pressures vs Time for Test S-NC-8.....	57
4.2.3	Measured and Calculated Broken Loop Secondary Pressures vs Time for Test S-NC-8.....	58

	<u>Page</u>
4.2.4 Measured and Calculated Break Mass Flow Rates vs Time for Test S-NC-8.....	59
4.2.5 Measured and Calculated Fluid Densities Upstream from the Break vs Time for Test S-NC-8.....	60
4.2.6 Measured and Calculated Broken Loop Cold Leg Mass Flow Rates vs Time for Test S-NC-8.....	61
4.2.7 Measured and Calculated Intact Loop Cold Leg Mass Flow Rates vs Time for Test S-NC-8.....	62
4.2.8 Measured and Calculated Downcomer Mass Flow Rates vs Time for Test S-NC-8.....	63
4.2.9 Calculated Collapsed Liquid Level in the Reactor Core vs Time for Test S-NC-8.....	64
4.2.10 Measured and Calculated Clad Temperatures at 291 cm above the Bottom of Heated Length vs Time for Test S-NC-8.....	65
4.2.11 Measured and Calculated Clad Temperatures at 322 cm above the Bottom of Heated Length vs Time for Test S-NC-8.....	66
4.2.12 Measured and Calculated Intact Loop Cold Leg Fluid Temperatures vs Time for Test S-NC-8.....	67
4.2.13 Measured and Calculated Broken Loop Cold Leg Fluid Temperatures vs Time for Test S-NC-8.....	68
4.2.14 Measured and Calculated Intact Loop Hot Leg Fluid Temperatures vs Time for Test S-NC-8.....	69
4.2.15 Measured and Calculated Broken Loop Hot Leg Fluid Temperatures vs Time for Test S-NC-8.....	70
4.3.1 Measured and Calculated Primary System Mass Inventories vs Time for Test S-NC-8.....	71
4.3.2 Measured and Calculated Cold Leg Mass Flow Rates vs Primary Mass Inventory for Test S-NC-8.....	72
4.3.3 Measured and Calculated Hot Leg Mass Flow Rates vs Primary Mass Inventory for Test S-NC-8.....	73
4.3.4 Measured and Calculated Cold Leg Mass Flow Rates vs Primary Mass Inventory for Tests S-NC-7 and S-NC-8.....	74



	<u>Page</u>
4.3.5 Measured and Calculated Downcomer Mass Flow Rates vs Primary Mass Inventory for Tests S-NC-7 and S-NC-8.....	75
AI.1 Isometric View of the Semiscale Mod-2A System.....	92
AI.2 Intact Loop Spool Pieces.....	93
AI.3 Broken Loop Spool Pieces.....	94
AI.4 Break Orifice for S-NC-8.....	95
AI.5 Steam Generator Assembly.....	96
AI.6 Pressurizer Vessel.....	97
AI.7 Semiscale Mod-2A Vessel Assembly.....	98
AI.8 Semiscale Mod-2A Vessel Downcomer Inlet and Upper Plenum Region.....	99
AI.9 Semiscale Mod-2A Vessel Core Region.....	100
AI.10 Core Axial Power Profile.....	101
AI.11 Semiscale Mod-2A Vessel Lower Plenum and Lower Downcomer Region.....	102

LIST OF TABLES

	<u>Page</u>
2.1 Test Matrix for the NC Test Series.....	6
3.1 Experimental System Parameters for Test S-NC-3.....	23
3.2 Experimental System Parameters for Test S-NC-4.....	24
4.1 Measured and Calculated Initial Conditions for Test S-NC-8.....	54
4.2 Test S-NC-8 Core Power.....	54
4.3 Sequences of Observed and Predicted Events for Test S-NC-8.....	55
AI.1 Semiscale Primary Coolant System Elevations.....	88
AI.2 Intact Loop Spool Pieces.....	89
AI.3 Broken Loop Spool Pieces.....	90
AI.4 Type II Steam Generator Data.....	91

#### ACKNOWLEDGEMENTS

We would like to express our appreciation for the effort of other Sandia staff involved in the RELAP5 assessment project: Mike McGlaun for the S-NC-2 analyses referenced, John Orman for modifying and maintaining RELAP5 on the Sandia computer system, Katherine McFadden for graphics support, and Jan Frey for construction of the reports.

## 1.0 INTRODUCTION

The RELAP5 independent assessment project at Sandia National Laboratories in Albuquerque (SNLA) is part of an overall effort funded by the U. S. Nuclear Regulatory Commission (NRC) to determine the ability of various systems codes to predict the detailed thermal/hydraulic response of LWRs during accident and off-normal conditions. The RELAP5 code [1] is based on a non-homogeneous and nonequilibrium one-dimensional model for two-phase systems, and has been under development at the Idaho National Engineering Laboratory (INEL) for an extended period, with the first version released in May 1979. The version first used for this assessment project was RELAP5/MOD1/CYCLE14, the latest publicly released version available at the time the project started. In June 1982, we received the formally-released updates creating cycle 18 together with some unreleased, but recommended, updates then being used at INEL. [2] These changes have been used to create and run a MOD1 version at Sandia we call cycle 18+, which was used on the Cray-1S computer as the assessment code for these analyses.

The RELAP5 code is being assessed at SNLA against test data from various integral and separate effects test facilities. The assessment test matrix includes a number of natural circulation tests for various power levels and primary side inventories [3] which were performed at the Semiscale test facility [4,5,6] at INEL. These tests investigate the different decay heat removal mechanisms which can occur in a small-break scenario if the pumps are tripped off, by studying mass and energy transport phenomena in the primary and secondary systems when the primary inventory is less than 100%. (Small breaks are characterized by a slow voiding of the primary system. A substantial inventory may therefore be maintained over a long period of time, and during this time period the energy may be removed from the primary system by loss of primary fluid, environmental heat losses and heat transfer to the steam generators.)

Our assessment analysis results [7] for the single-loop and two-loop Semiscale basecase steady state natural circulation tests (S-NC-2 and S-NC-7, respectively) have previously been documented. This report summarizes our analyses of three other Semiscale natural circulation tests. The RELAP5 models used for these analyses are described in Section 2, and the calculational results for tests S-NC-3 and S-NC-4, and test S-NC-8, are presented in Sections 3 and 4, respectively. The overall conclusions and their possible relevance to future RELAP5 code application and development are discussed in Section 5. The appendices provide a brief description of the test facility, input listings, and a list of the additional INEL updates used to create cycle 18+ from cycle 18, for reference.

## 2.0 NODALIZATIONS

The Semiscale Mod-2A test facility [4,5,6] is located at the Idaho National Engineering Laboratory and supported by the NRC. This scaled integral test facility, shown in Figure 2.1, is used to investigate the thermal and hydraulic phenomena accompanying various hypothesized loss-of coolant accidents and operational transients in a PWR system. It is an approximately 2:3411 scale model of a four-loop PWR, and consists of two primary coolant loops connected to an electrically-heated reactor pressure vessel model which has an external downcomer. While both experimental loops are active loops containing a circulation pump and a steam generator, one (the intact loop) has three times the water volume and mass flow of the other (the single or broken loop).

The main objective of the Semiscale NC test series (summarized in Table 2.1) was to provide thermal/hydraulic data for use in assessing and developing computer codes used to evaluate PWR safety, since natural circulation may be an important core heat removal mechanism during certain kinds of accidents or transients in a PWR, such as small break LOCAs or loss of forced pump circulation.[3] Two basic types of experiments were performed: steady state separate effects tests and transient integral tests.

Several of the separate effects tests used only a subsystem of the Mod-2A facility so that important system parameters during natural circulation could be better examined. This partial system consisted of the intact loop and vessel/downcomer. The intact loop pump was replaced by a pump replacement spool piece to eliminate leakage from the pump, and the upper head was removed from the vessel and capped off to minimize heatup difficulty and thus prevent distortions introduced from the presence of cold structures. The entire Mod-2A system (exclusive of the intact loop pump) was used for the final separate effects test and for the integral tests, with the upper head reinstalled for some of the integral tests. (A brief description of the Semiscale Mod-2A facility is given in Appendix I.)

The RELAP5 nodalization we developed to analyze the single-loop natural circulation tests is shown in Figure 2.2; this model was used for our S-NC-2 [7], S-NC-3 and S-NC-4 analyses. This nodalization consists of 127 volumes, 126 junctions and 175 heat slabs. Of this total, 33 are used in the intact loop piping and 13 in the pressurizer and surge line. The steam generator primary (6 U-tubes lumped together) is modelled with 20 cells, and the secondary side consists of 29 cells. The vessel/downcomer is represented by a total of 32 volumes, with 4 cells in the lower plenum, 8 in the core, 5 in the upper plenum and 1 cell each for the simulated guide tube and support columns; the downcomer nodalization uses 2 cells for the inlet distribution annulus, 10 for the downcomer pipe and 1 for the downcomer distribution annulus.

The RELAP5 nodalization we developed to analyze the two-loop transient natural circulation test S-NC-8 is shown in Figure 2.3; this model is similar to that used for our S-NC-7 analyses [7], with the addition of the cold leg break and the cold leg accumulators. This nodalization contains 203 volumes, 204 junctions and 265 heat slabs. The intact loop model shown on the left and the vessel model in the center are identical to the single loop nodalization, except that the intact loop pump suction bend is now modelled with two 45° cells rather than one horizontal cell, and four cells have been added to the vessel to model the bypass line and shortened upper head cap. The added broken loop is shown on the right. The broken loop steam generator primary (2 U-tubes lumped together) is modelled with 18 cells and its secondary side consists of 25 cells. The broken loop piping is represented by 24 cells, including one for the inactive broken loop pump and a time-dependent volume providing the break boundary condition. Two accumulators and their associated surge line volumes have been connected to the intact and broken loop cold legs.

The details of the vessel and external downcomer nodalization are shown in Figure 2.4. The relative elevations of the cell boundaries are given (for comparison with facility values given in Appendix I), as are either flow areas for open pipes or cell volumes for more complex regions. The choice of the core axial levels was based on the axial power profile given in Figure AI.10, to avoid interpolation problems, rather than on the location of the grid spacers in the core. Besides the core rod heat slabs, additional heat slabs have been included for most of the major vessel structure -- the pressure vessel itself, the downcomer annulus and piping walls, and the simulated guide tube, support column and bypass line piping. A time-dependent junction and time-dependent volume (not shown in Figures 2.2 and 2.4) were connected to the lower plenum of the vessel. The primary fluid was drained out of the system through this junction, with controllers allowing outflow until the desired primary side mass inventory was achieved and then stopping further flow.

The intact and broken loop steam generator nodalizations are shown in more detail in Figures 2.5 and 2.6. As for the vessel nodalization in Figure 2.4, the relative elevations of the cell boundaries are given, together with either flow area or cell volume data. The elevations have been chosen to correspond to the location of baffle plates in the boiler sections, allowing these to be modelled explicitly. As already mentioned, all the U-tubes in either steam generator are lumped into a single flow path. Besides the U-tubes themselves, heat slabs representing the external walls, the shroud, and the filler pieces are included in the model.

Before performing the S-NC-8 calculation, we received corrected information from INEL for the secondary side fluid volumes. Comparison of this new data with our input decks for tests S-NC-2, S-NC-3, S-NC-4 and S-NC-7 revealed small differences in flow areas and volumes in the intact loop steam generator riser region; no changes were seen in the broken loop steam generator model. We made the appropriate corrections in our S-NC-8 input deck, but did not go back and rerun any of the previously completed analyses. The corrections should have no effect on our results for S-NC-2 and S-NC-7, since the steam generator tubes remain covered throughout; the changes were judged small enough to have no significant impact on the secondary side U-tube heat transfer area fraction in tests S-NC-3 and S-NC-4.

All area changes and elbows in the piping are accounted for in the model. Figures 2.7 and 2.8 show the loss coefficients used in the calculations. These loss coefficients can be either user-input, as for elbow losses, or code-calculated using abrupt area change models. The user-input numbers are given first; two values are given, for the forward and reverse loss coefficients respectively, if they are different. The code-calculated numbers are shown in parentheses, and are single-phase values in the direction of normal flow which may change in two-phase flow. (If two numbers are given in parentheses, they correspond to different values used for liquid and vapor loss coefficients for two-phase flow.)

The broken loop pump homologous curves used were those handed out at the LOFT/Semiscale modelling workshop [5]. All the loop piping walls are represented as heat slabs, but environmental heat loss, pipe insulation, tape and band heaters, etc. are ignored -- the exterior piping heat slabs are assumed to be adiabatic on their outer surfaces in the calculations, since the tape and band heaters on the piping walls were designed to achieve such a condition.

Table 2.1

## Test Matrix for the NC Test Series

Test Number	Type of Test	System Configuration	Principal Test Parameters	Test Objectives
S-NC-1	Steady-state separate effect	Partial system <sup>a</sup>	Core power, primary system pressure	Single-phase NC tests. Evaluate: effects of power, predictive methods and instrument capability. Provide data for comparison to other facilities to examine scaling.
S-NC-2	Steady-state separate effect	Partial system <sup>a</sup>	Core power, system mass inventory	Baseline, single-phase, two-phase, and reflux NC test. Establish thermal hydraulic response during the three modes of NC. Evaluate predictive methods.
S-NC-3	Steady-state separate effect	Partial system <sup>a</sup>	Core power, system mass inventory SG secondary conditions	Two-phase NC test. Examine the effect of different SG secondary condition on 2 $\phi$ natural circulation. Evaluate predictive methods and instrument capability.
S-NC-4	Steady-state separate effect	Partial system <sup>a</sup>	Core power, system mass inventory SG secondary conditions	Reflux NC test. Examine the effect of different SG secondary conditions that might occur during a transient on reflux natural circulation. Evaluate predictive methods and instrument capability.
S-NC-5	Steady-state separate effect	Partial system <sup>a</sup>	Core power, system mass inventory Amount of noncondensibles	Two-phase NC test with noncondensibles. Evaluate predictive methods. Evaluate effects of noncondensibles on steam generator heat transfer.
S-NC-6	Steady-state separate effect	Partial system <sup>a</sup>	Core power, system mass inventory. Amount of noncondensibles.	Reflux NC test with noncondensibles. Examine the effect of noncondensibles on the reflux mode of natural circulation. Evaluate predictive methods.
S-NC-7	Steady-state separate effect	Whole system <sup>b</sup>	System mass inventory, SG secondary conditions	Two-phase NC test. Examine imbalances between intact loop and broken loop steam generator during 2 $\phi$ natural circulation. Evaluate predictive methods and instrument capability.
S-NC-8	Transient Integral	Whole system <sup>c</sup>	0.4% cold leg break, No ECCS	Small break test without ECCS. Examine the various modes of natural circulation and transitions during a small break without ECC injection. Evaluate predictive methods and instrument capability.
S-NC-9	Transient Integral	Whole system <sup>c</sup>	0.4% cold leg break ECCS	Small break test with ECCS. Examine the various modes of natural circulation and transitions during a small break with ECC injection. Examine the effect of ECC on natural circulation. Evaluate predictive methods and instrument capability.

a. The partial system includes the intact loop with a pump replacement spool, and vessel/downcomer without the upper head.

b. The whole system includes the entire Mod-2A system except the intact loop pump which will be replaced by a pump replacement spool and the upper head will be removed.

c. The whole system includes the entire Mod-2A system except the intact loop pump which will be replaced by a pump replacement spool.



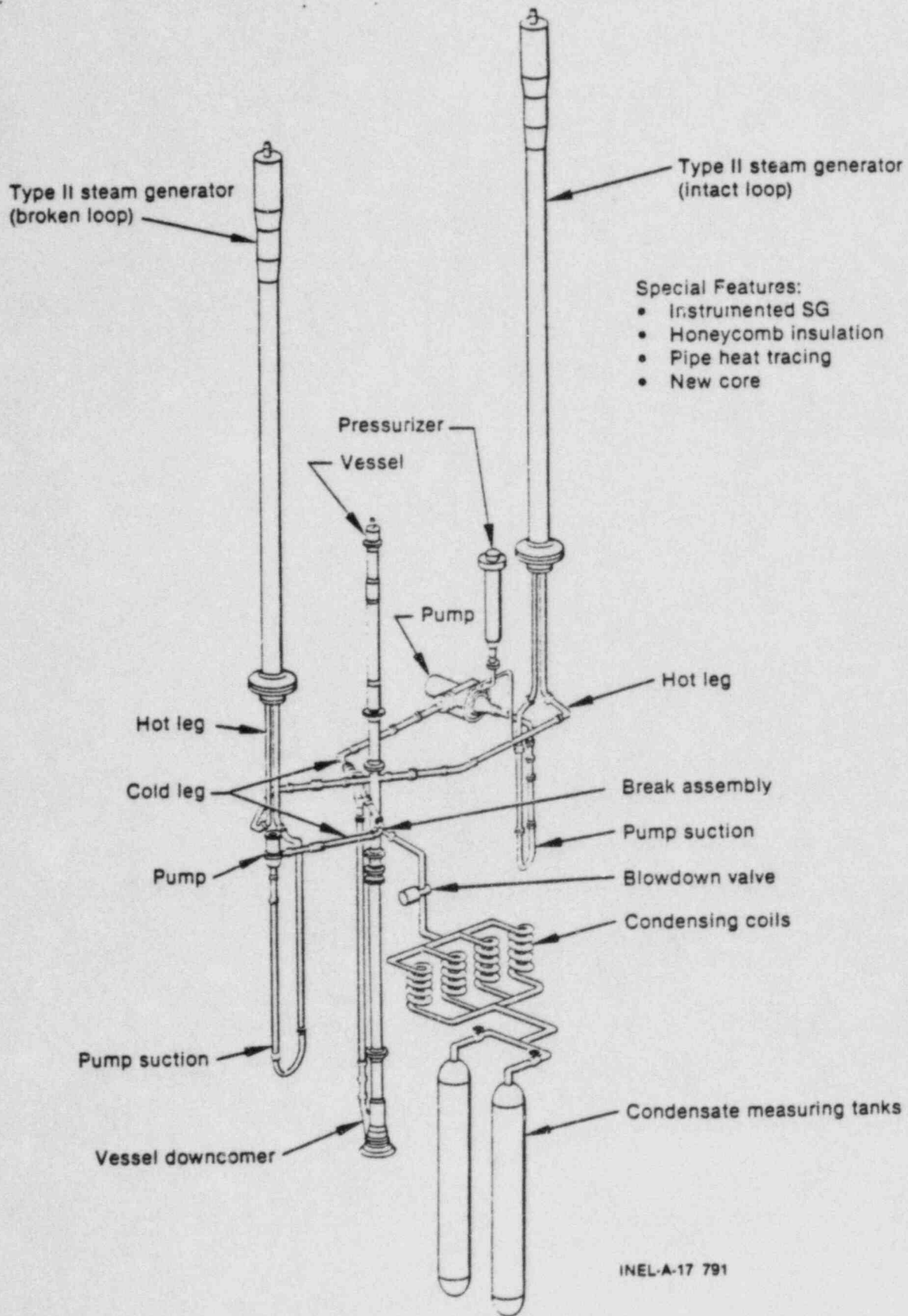


Figure 2.1 Isometric View of the Semiscale Mod-2A System

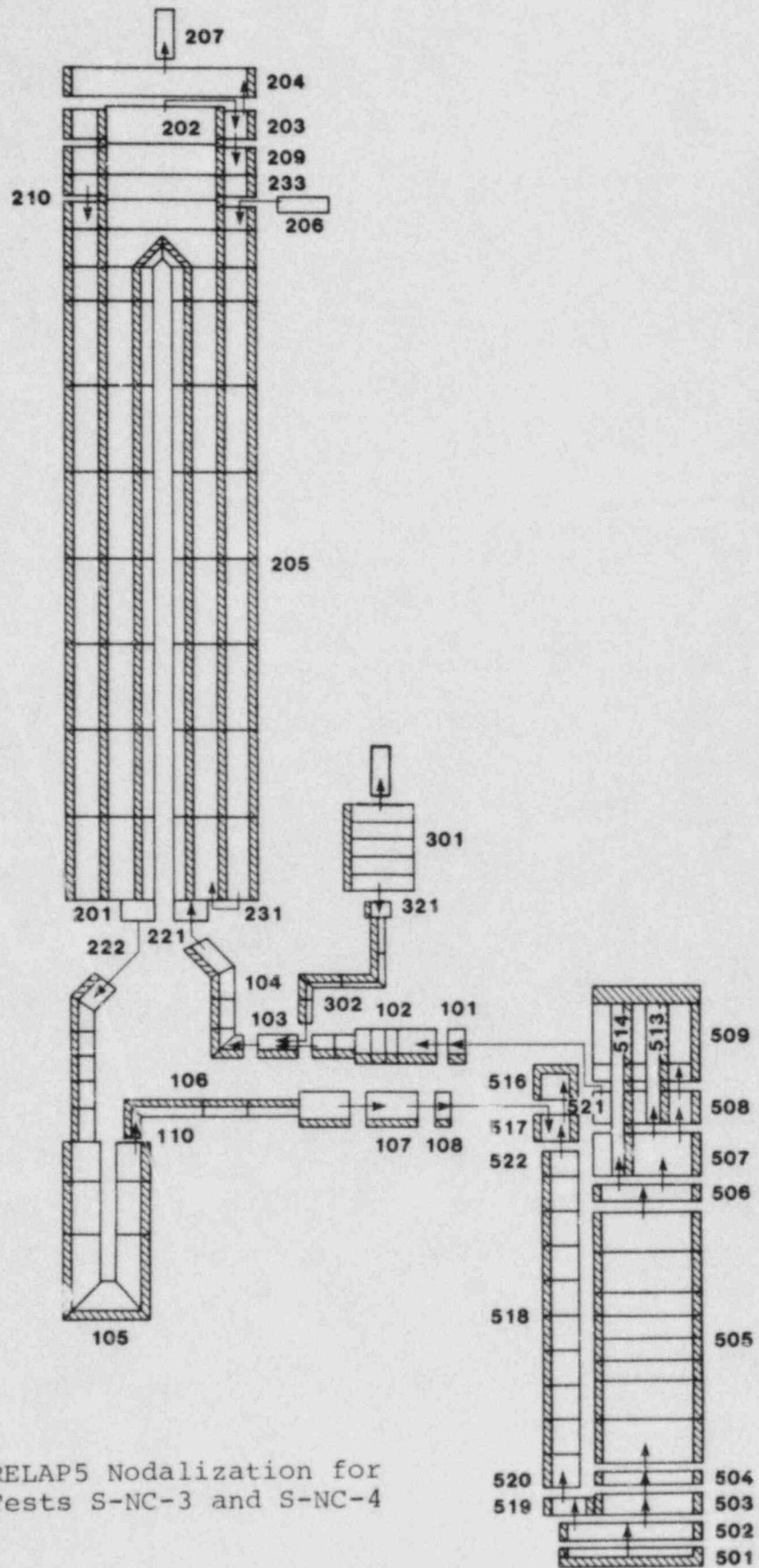


Figure 2.2 RELAP5 Nodalization for Tests S-NC-3 and S-NC-4

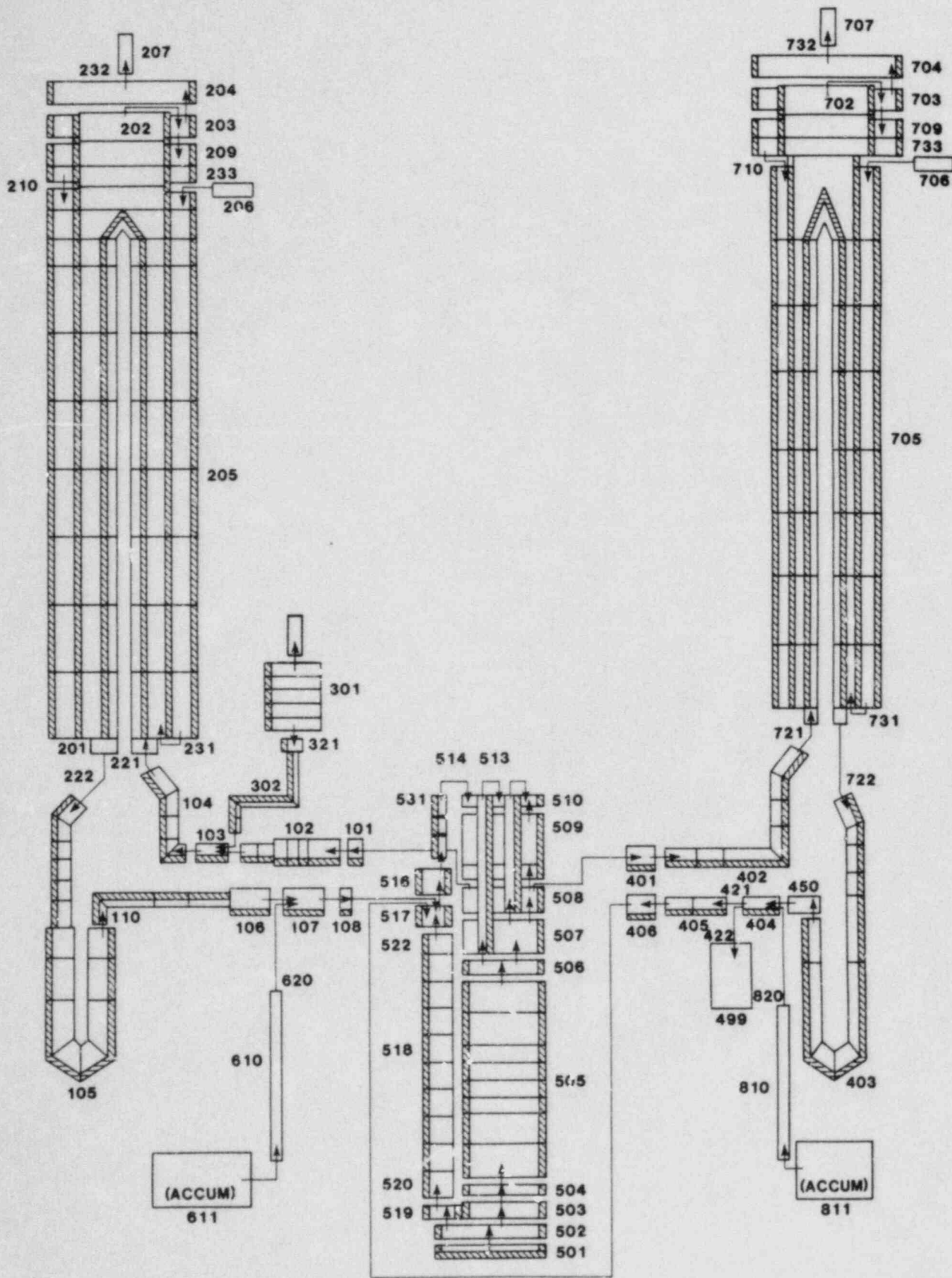


Figure 2.3 RELAP5 Nodalization for Test S-NC-8

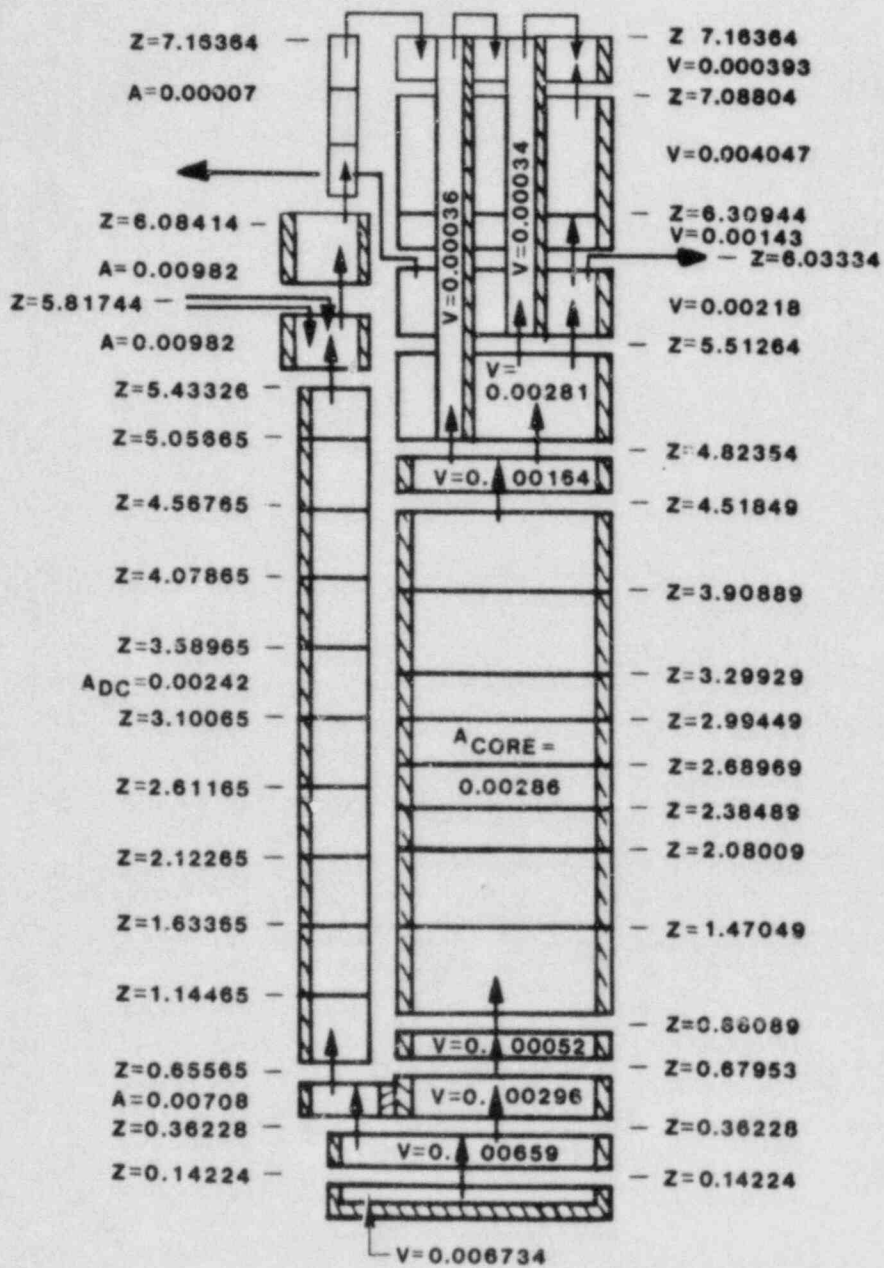


Figure 2.4 Vessel Nodalization

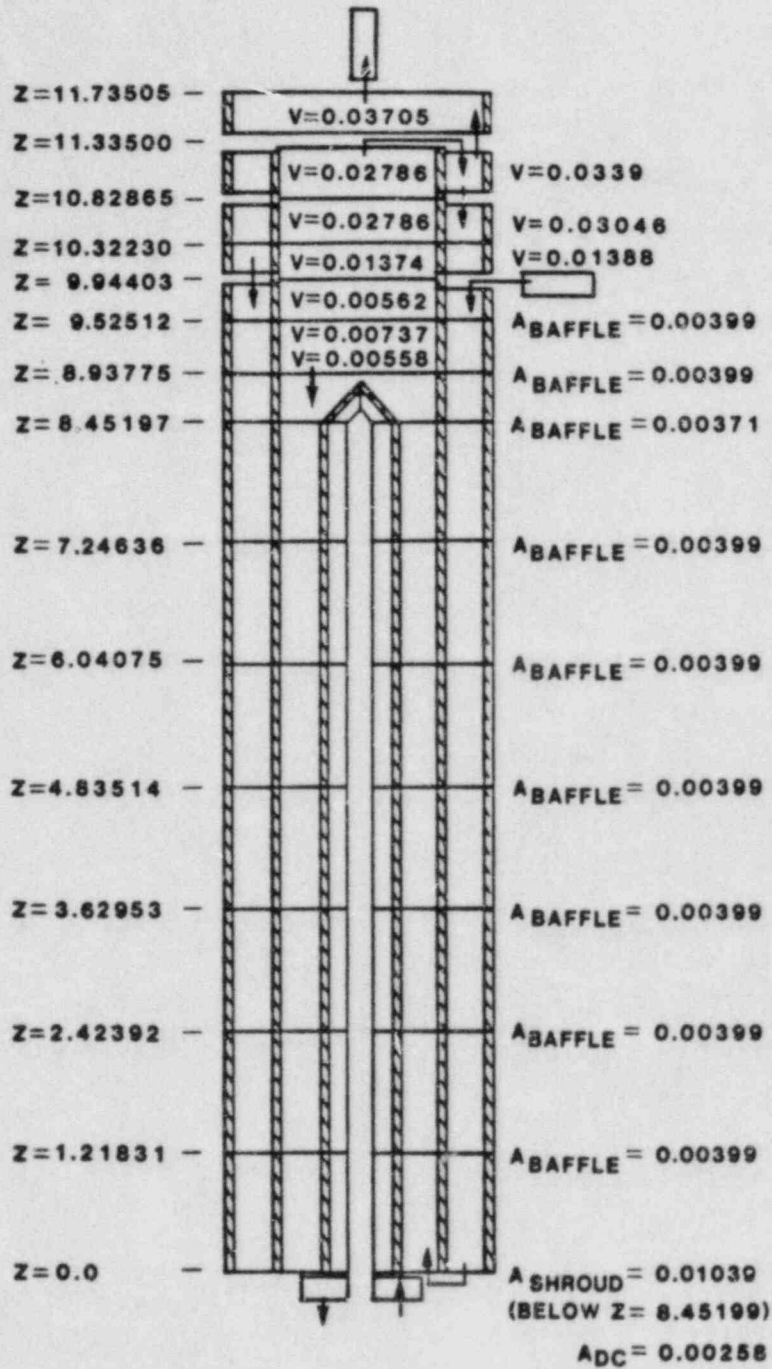


Figure 2.5 Intact Loop Steam Generator Nodalization

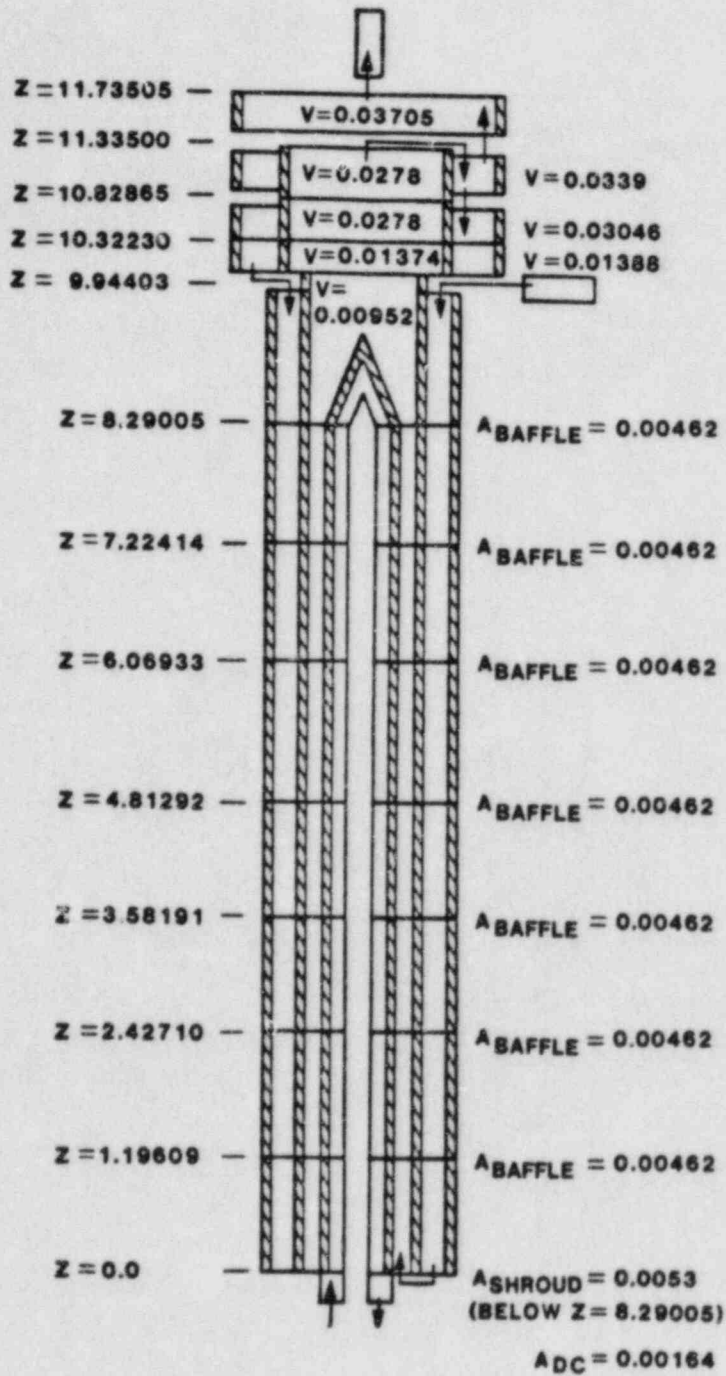


Figure 2.6 Broken Loop Steam Generator Nodalization

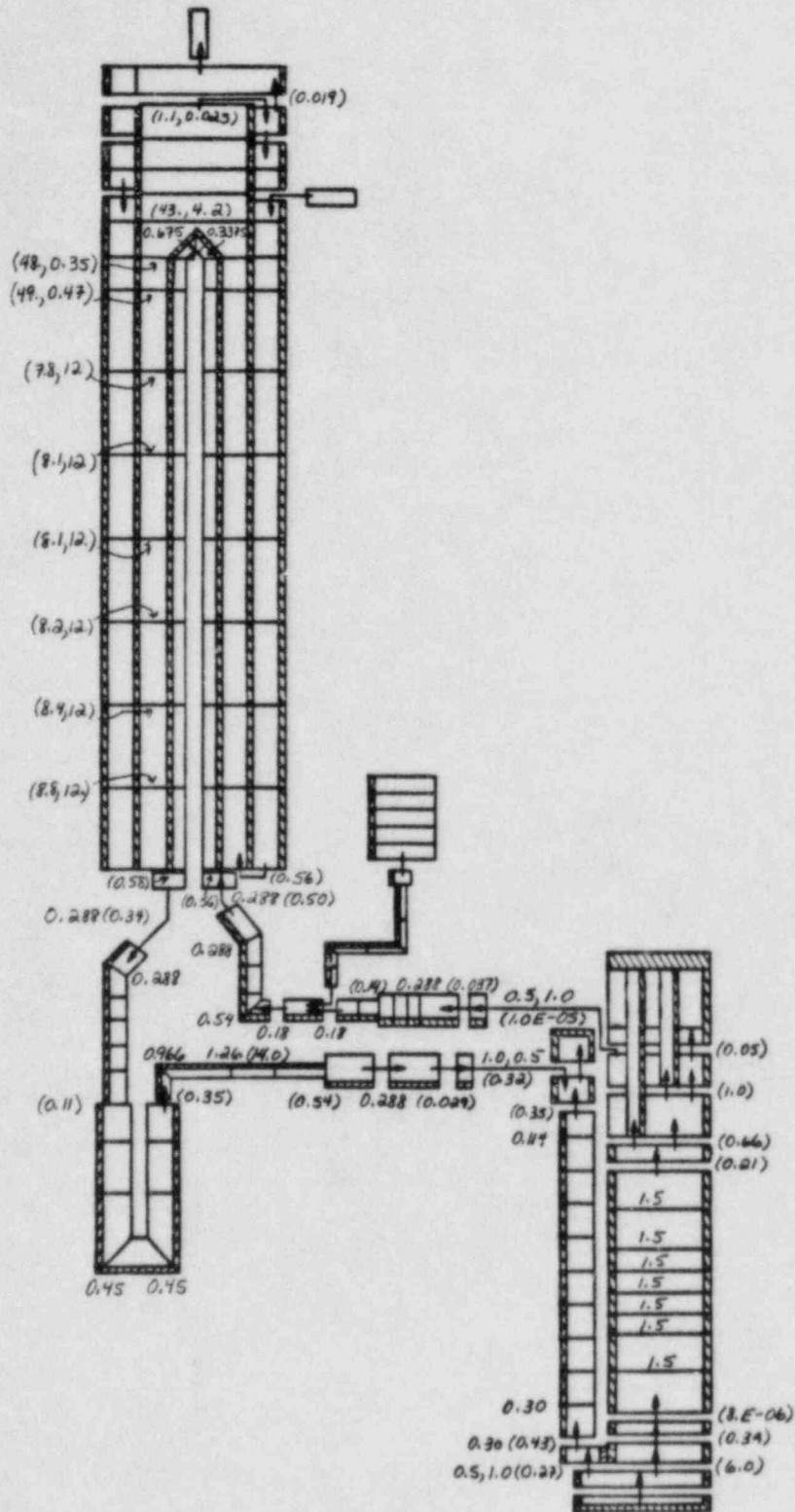


Figure 2.7 Loss Coefficients Used in S-NC-3 and S-NC-4 Nodalizations

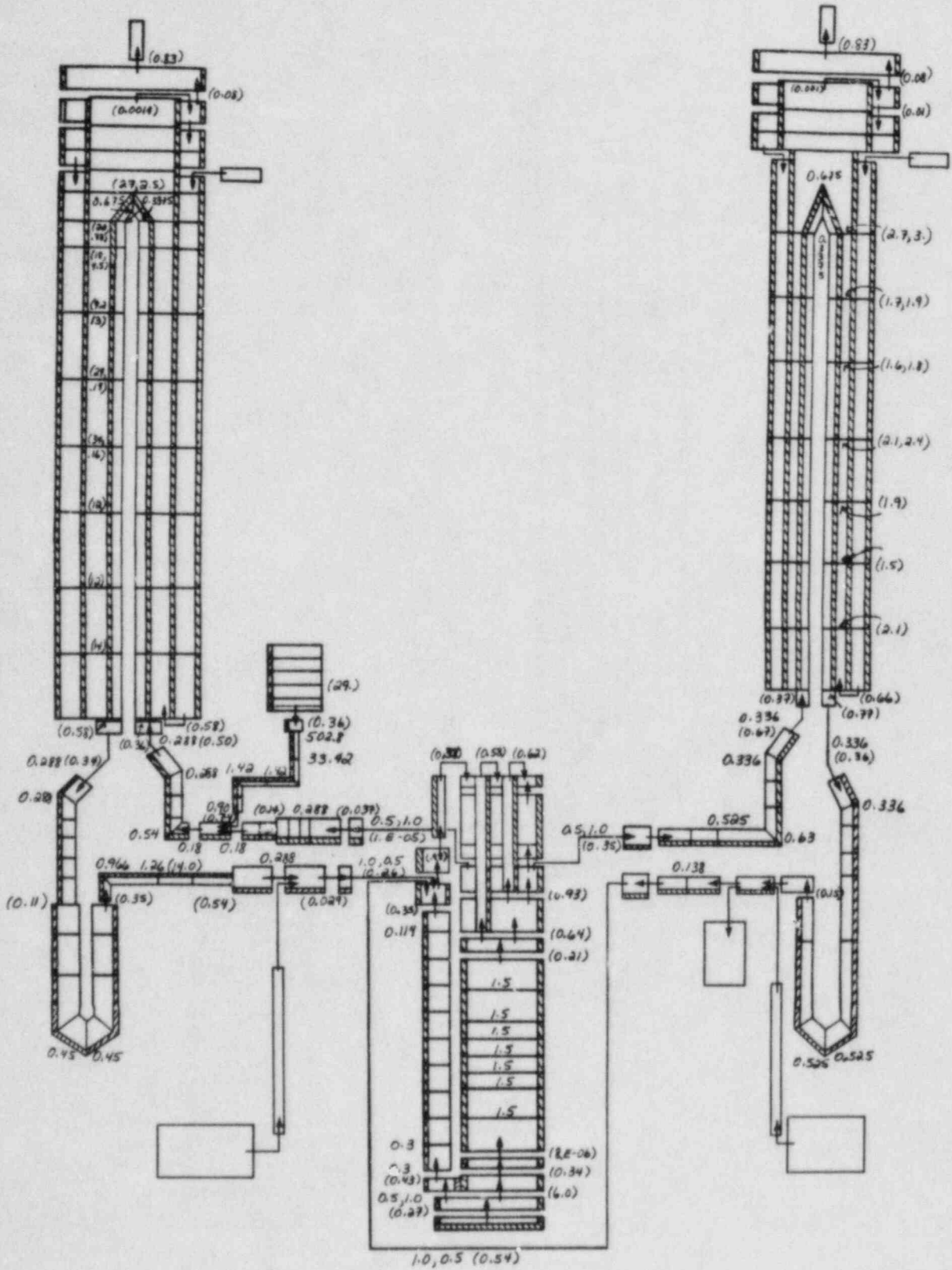


Figure 2.8 Loss Coefficients Used in S-NC-8 Nodalization



### 3.0 SINGLE LOOP DEGRADED HEAT TRANSFER TESTS S-NC-3 AND S-NC-4

We have previously performed and documented [7] RELAP5 assessment analyses for the single-loop basecase natural circulation test S-NC-2, a test which provided data on the occurrence of and transition between the single-phase, two-phase and reflux natural circulation modes with normal steam generator cooling available. The S-NC test series also included two derivative single-loop tests which studied the effects of varying secondary side conditions on particular data points identified during S-NC-2. Thus, test S-NC-3 studied the effect of degraded secondary side heat transfer on peak two-phase flow in the primary system, measured to occur at 92% primary inventory in test S-NC-2. Similarly, test S-NC-4 investigated any effects on reflux cooling at low primary inventories (50-70%) of decreasing secondary side liquid inventory.

Figure 3.1 shows the relationship between the collapsed liquid level and the effective heat transfer area in the Semiscale intact loop steam generator secondary side. As the inverted U-tubes slowly uncover on the secondary side, the effective heat transfer area decreases and the steam generator begins losing its heat sink capability. This reduces the density difference between the upside and the downside of the U-tubes, which in turn decreases the natural circulation flow in the loop. Eventually, natural circulation ceases and the primary system loses a valuable heat removal mechanism.

#### 3.1 Two-phase Natural Circulation Test S-NC-3

Test S-NC-3, a single-loop test, studied the effect of various steam generator secondary side thermal/hydraulic conditions, such as pressure and collapsed liquid level, on two-phase natural circulation in the primary system. [3,8,9] Two-phase natural circulation was established by starting with a liquid-full primary system in single-phase natural circulation, and slowly draining the primary side inventory to 92%. This specific value was chosen because it corresponded to the inventory where the primary loop mass flow rate was at its peak in the basecase Semiscale natural circulation test S-NC-2. After the system had reached equilibrium, the steam generator secondary fluid was drained in discrete steps. Between each step, some length of time was allowed for the primary system natural circulation to stabilize. The major parameters examined were natural circulation flow rates and system temperature distribution.

##### 3.1.1 Description of Experiment

Some modifications of the basic Mod-2A facility were made for these single-loop natural circulation experiments: the vessel upper head was removed, an isolation valve was installed in the

pressurizer surge line, the intact loop pump was replaced with an instrumented spool piece with the expected locked-rotor hydraulic resistance, and the broken loop was isolated from the system. External surfaces were covered with insulation and heaters to approximate adiabatic boundary conditions. S-NC-3 was conducted at a constant power level of 60 kW.

System parameters for 19 steady state natural circulation data points were measured in three sets, and are summarized in Table 3.1. In the first set, the liquid in the primary system was slowly drained from the bottom of the vessel lower plenum, and two-phase natural circulation flow rates were measured at various primary mass inventories. This procedure was then repeated with an increased pressure in the secondary system, showing that changing the secondary side pressure from 5 to 6 MPa did not have any significant effect on single-phase natural circulation flow rates.

However, changing the secondary side collapsed liquid level in the third set of experiments, by draining the liquid in the secondary side from the bottom of the steam generator downcomer, did have a significant effect upon the system, because it resulted in a reduction of tube heat transfer surface area and steam generator heat sink capability. As observed in the experiment, when the liquid level decreased as low as 55% of the total tube heat transfer area, the primary side natural circulation mass flow rate did not change much at all; however, reducing the heat transfer area below 55% caused a corresponding reduction in loop mass flow. Also, large oscillations in the primary loop flow occurred for tube effective heat transfer areas below 43.6% of the total area.

The effect of degrading steam generator heat transfer rate on the fluid temperature distribution was quite similar to that on the mass flow rate. Temperature measurements indicated that the fluid temperature distribution in the steam generator tubes was fairly uniform (indicating a fairly uniform tube-to-tube flow distribution) when more than 55% of the tube secondary side heat transfer area was covered. However, with further draining of the secondary liquid, a non-uniform temperature distribution was observed, indicating a possibly non-uniform flow distribution.

### 3.1.2 Calculated Results

As mentioned in the introduction, we used RELAP5/MOD1/CYCLE18+ to simulate these natural circulation experiments. However, before beginning calculations for test S-NC-3, we repeated one S-NC-2 calculation (the 60 kW case); our previous analyses for S-NC-2 and S-NC-7 [7] had been run with cycle 14 and we wanted to check if cycle 18+ produced results similar to those of cycle 14. Figure 3.1.1 compares the results of both cycles 14 and 18+ with experimental data for the 60 kW S-NC-2 case. The two calculations give

very similar results, with both code versions predicting a higher peak mass flow rate, but at a lower primary mass inventory, than the data.

In each of our initial S-NC-3 calculations, the core power was held at 62 kW and the primary mass inventory at 92% full (corresponding to the inventory of measured peak mass flow rate in test S-NC-2); we also reduced the steam generator feedwater mass flow rate and let the secondary liquid boil off slowly until the collapsed liquid level in the steam generator downcomer dropped to the specified value. We stopped each calculation when the system reached a steady state equilibrium condition. The results of these first S-NC-3 calculations are presented in Figures 3.1.2 through 3.1.5.

Of the 19 experiments in test S-NC-3, only 9 data points (the third set of tests) relate to the effect of secondary inventory on two-phase natural circulation flow rate in the primary system, and are thus used in our comparisons with experimental data. We suspect that data point 11 in Table 3.1, indicating 0.69 kg/s at 99.1% secondary side heat transfer area, and the apparent rise in primary flow with decreased secondary side effective area, is in error. Data point 10, of 0.75 kg/s at 100% secondary heat transfer area at the same primary conditions, implies a more believable plateau occurring at the higher secondary inventories, as do the corresponding points in S-NC-2 [7,10], of 0.77 kg/s and 0.74 kg/s at 93.1% and 90.9% primary inventories, respectively (with the S-NC-2 points for 60 kW core power and 100% secondary side heat transfer area).

Figure 3.1.2 compares the calculated and measured mass flow rates in the primary system for different effective steam generator heat transfer areas. Qualitatively, RELAP5 does reasonably well predicting the two-phase natural circulation flow rate and the flow oscillations which occurred in the experiment. Both the calculated and the experimental results show that, for effective heat transfer areas in the steam generator above 50%, changes in secondary inventory do not affect the steady two-phase natural circulation flow rate (if the 99.1% data point is assumed to be in error); when the heat transfer area falls below 50%, the natural circulation flow rate decreases with decreasing secondary inventory, and flow oscillations appear. Quantitatively, RELAP5 does not predict as sharp a decrease in flow rate at low secondary inventories as seen in the experiment, and the amplitude of the flow oscillations calculated at low secondary inventories (shown by the "uncertainty bars") is smaller than that measured.

In Figure 3.1.3, calculated primary system pressures are plotted against experimental data. When the effective heat transfer area in the steam generator is above 50%, the calculated

pressures are higher than those measured, probably related to the lower mass flow rates being predicted for these conditions. Similarly, the overprediction of the natural circulation flow rate when the heat transfer area falls below 50% is likely the reason that the calculated pressure is then lower than the measured value. Since the fluid in the hot leg is generally saturated and two-phase, the calculated hot leg temperature is also high at high secondary inventories and low at low secondary inventories relative to data (as shown in Figure 3.1.4). The comparison of calculated and measured cold leg temperatures is reasonably good, except at lower secondary inventories (Figure 3.1.5).

In our S-NC-2 results [7], RELAP5 gave a higher peak natural circulation flow rate at a lower primary inventory than the experiment for 60 kW core power, as shown in Figure 3.1.1. For the S-NC-3 calculations above, the primary inventory was always set at 92% full, the cited experimental value, which corresponds to the inventory where the peak two-phase natural circulation flow was measured in S-NC-2. The occurrence of this peak two-phase flow implies that bubbles are just reaching the top of the U-tubes and being pulled over into the downside. At the same inventory, our S-NC-2 calculation shows all the bubbles condensing out lower in the upside of the U-tubes; the primary inventory must be dropped to 85% before the predicted primary inventory distribution has bubbles at the U-tube bend and the calculated two-phase natural circulation flow peaks. Matching the height and distribution of the two-phase mixture within the U-tubes relative to the height and distribution of secondary side liquid should be very important in correctly calculating the degraded heat transfer behavior seen in S-NC-3.

An additional set of calculations were then performed. As shown in Figure 3.1.6, draining the primary inventory to 85%, where the peak mass flow rate is calculated to occur and the primary mass inventory distribution should be more like the experimental data, produces better qualitative and quantitative agreement with measured results. The mass flow remains nearly constant while the steam generator effective heat transfer area is above 55%, with the calculated peak two-phase natural circulation flow rate being somewhat (~10-15%) higher than that measured, and further reduction of the effective heat transfer area results in a sharp drop in mass flow and in progressively larger flow oscillations.

Figures 3.1.7 and 3.1.8, respectively, compare predicted primary system pressures and hot leg temperatures with experimental results, for both the original and additional calculations. When the primary mass inventory is 85%, the calculated primary pressures and hot leg temperatures decrease and compare better with experimental data for effective heat transfer areas above 50%.

However, for the lower effective heat transfer areas, reducing the primary mass inventory does not change either primary pressure or hot leg temperature very much, although both variables do increase more in the 85% primary inventory calculations as the secondary heat transfer area drops from 40% to 20%, in better qualitative agreement with the data. In Figure 3.1.9, calculated and measured cold leg temperatures are compared. Agreement is excellent for both primary inventories as long as the effective heat transfer area is above 50%. When the heat transfer area drops below 50%, unlike the experimental data, both sets of calculated results show that changing the heat transfer area does not affect the cold leg temperature much. However, the 85% inventory calculations are in slightly better quantitative agreement with the cold leg temperature data.

### 3.2 Reflux Cooling Test S-NC-4

Test S-NC-4 was the reflux cooling counterpart to the two-phase flow test S-NC-3, further examining the influence of steam generator secondary side liquid inventory on natural circulation flow rate and other primary system conditions. [3,9,11] The reflux mode of natural circulation consists of countercurrent two-phase flow with a continuous vapor field developed at the center and a liquid film deposited on the wall. This flow pattern occurs at the steam generator (primary) inlet and is characterized by countercurrent liquid flow returning to the vessel. In this test, reflux natural circulation was studied with primary system fluid inventory varied between 48% and 70% and secondary side collapsed liquid level varied from 100% to 25%. The major parameters studied included reflux vs carryover flow split, and system fluid and temperature distribution.

Test S-NC-4 is not a very good experiment for quantitative code assessment; the instrumentation seriously perturbs the system by draining relatively large amounts of liquid inventory from the hot leg/steam generator inlet plenum area and injecting makeup liquid at different conditions into the cold leg/vessel downcomer area. The reflux and carryover mass flow rates being measured are very small compared to the possible measurement uncertainties, and the measurements really provide only an average value. However, combined with the preceding S-NC-2 and S-NC-3 experiments, it does offer some valuable qualitative data on natural circulation flow phenomena.

#### 3.2.1 Description of Experiment

The same modified Mod-2A facility was used for S-NC-4 as for S-NC-2 and S-NC-3; i.e., the vessel upper head was removed, an isolation valve was installed in the pressurizer surge line, the intact loop pump was replaced with an instrumented spool piece

with the proper locked-rotor hydraulic resistance, and the broken loop was isolated from the system. External surfaces were covered with insulation and heaters to approximate adiabatic boundary conditions.

In addition, for this test, a specially-designed flowmeter was used to measure the reflux mass flow rate; a spool piece was installed at the inlet to the steam generator which would divert the refluxing liquid film into a standpipe, where the liquid was collected and measured. After each measurement, liquid was injected into the primary system from a heated tank to re-establish the primary system mass inventory, because enough liquid had been drained into the reflux meter to significantly decrease the primary inventory (by ~10%). Lenses and video equipment in the steam generator inlet plenum, and inlet and outlet piping, were also used to verify the occurrence of reflux conditions. The carryover liquid was measured differently; a valve in the intact loop pump replacement spool was closed, causing liquid to accumulate in the vertical piping between the steam generator outlet and the pump suction. The collected liquid was then measured using differential pressure cells and finally the mass flow rate was inferred from these results. Each test point measured either reflux or carryover mass flow rate, but not both simultaneously, to avoid compounding system perturbations.

A total of 12 measurements of reflux mass flow or carryover mass flow were obtained (summarized in Table 3.2), for various combinations of thermal/hydraulic conditions in the primary and secondary systems. The collapsed liquid level in the secondary was changed in discrete increments from 100% (tubes fully covered) to 24%. Two core power levels (31.4 and 60.9 kW) were used. The pressurizer was valved out of the system after initial conditions were established, and the primary pressure system pressure was allowed to vary; however, the steam generator secondary side pressure was maintained constant at ~5.7-5.8 MPa.

The experiment showed that the reflux-to-carryover flow split was approximately 1:1 for both the 30 kW and 60 kW core power cases; a small decrease in this ratio occurred at secondary side inventories below 50% for the 30 kW core power case. Reducing the secondary side inventory had little impact on primary pressure for secondary inventories above 50%, but at a secondary inventory of 24% the primary pressure rose from 6.2 MPa to 6.9 MPa. For a core power of 30 kW, conditions in the primary provided adequate core cooling for all data points, but core dryout was seen for secondary inventories below 50% at the higher core power of 60 kW.

### 3.2.2 Calculated Results

The results of our calculations for the 60 kW power case of test S-NC-4 are shown in Figures 3.2.1 through 3.2.5. The comparisons between calculated and measured reflux and carryover flow

rates are shown in Figures 3.2.1 and 3.2.2, respectively. The "uncertainty bars" in the graphs represent the amplitude of calculated flow oscillations, which should be distinguished from high frequency numerical oscillations. From our past experience [7,12], numerical oscillations usually disappeared if the time step was reduced sufficiently. In our S-NC-4 calculations, the time step had to be reduced to ~0.005 s before such numerical oscillations were damped out. However, for low secondary side inventories (collapsed liquid levels below 89%), substantial flow oscillations still persisted in the calculations, unaffected by changes in time step (as in S-NC-3).

In general, the agreement between calculated and measured primary pressures, and core inlet and outlet temperatures, for the 60 kW core power case is reasonably satisfactory. Figures 3.2.3 through 3.2.5 show these comparisons as a function of steam generator effective heat transfer area. There is good agreement between the calculated and measured primary pressures (Figure 3.2.3), and therefore good agreement in the saturation temperatures. The "uncertainty bars" on the core outlet temperatures in Figure 3.2.4 correspond to predicted temperature fluctuations caused by superheated steam being generated in the core, not seen in the experiment until the secondary side effective heat transfer area had dropped below ~50%. The differences between calculated and measured results for the core inlet temperatures (Figure 3.2.5) are due to subcooled liquid being injected into the cold leg in the test to make up for fluid lost to the reflux flowmeter.

Figures 3.2.6 through 3.2.10 show the results of the RELAP5 analyses for 30 kW core power. The overall thermal/hydraulic behavior of the system is quite similar to that seen for 60 kW core power. All the important parameters such as primary pressure, cold leg temperature, hot leg temperature, reflux mass flow rate and carryover mass flow rate are not affected much by the changes in steam generator effective heat transfer area. The calculated carryover flow oscillations, if compared to the 60 kW case, are relatively small, while the reflux flow oscillations are of similar magnitude. No temperature fluctuations are observed in the core outlet temperature in either the calculations or the data. The measured increase in primary pressure (Figure 3.2.8) and associated saturation temperature (Figure 3.2.9) at low secondary inventories is not calculated; this is similar to the results for S-NC-3, where the primary pressure increased less and at lower inventories than shown in the data.

### 3.3 Flow Oscillations

In both tests S-NC-3 and S-NC-4, nonphysical flow oscillations were calculated in the primary system when the time step was too large; these were high frequency numerical oscillations, which could be inhibited by reducing the time step sufficiently. Figure

3.3.1 shows these nonphysical oscillations damping out as the time step was incrementally reduced for one of our S-NC-4 analyses. For different time steps, the code gave somewhat different results for the reflux mass flow rate (with all other parameters held constant). The smaller the time step, the better the answer, but also the longer the CPU time required to run any given length of calculation.

In the two-phase natural circulation test S-NC-3, flow oscillations were both measured and calculated for low secondary side inventories, as shown in Figure 3.3.2; the calculated flow oscillations were unaffected by changes in the time step and thus are likely to be real and physical. When the U-tubes were mostly covered on the secondary side, the oscillations were negligibly small. Under these conditions, there was sufficient liquid in the secondary side to condense the steam bubbles in the upside of the U-tubes. Hence, the density gradient between the upside and downside of the tubes remained steady, as did the buoyancy-driven mass flow rate. As the U-tubes became uncovered on the secondary side, there was not enough heat sink capability to collapse the bubbles before they reached the top of the tubes; they started to accumulate in the U-tube bends and, from time to time, a big steam bubble was driven over to the downside of the U-tubes. When this bubble was then collapsed in the downside of the tubes, adjacent liquid quickly filled up the space and caused a drastic change in the density gradient between the upside and downside of the tubes. Flow oscillations followed. This process accelerated as more and more bubbles were carried over the top of the tubes and collapsed on the downside of the tubes. Hence, these flow oscillations grew bigger as more and more heat transfer area in the U-tubes was uncovered.

In test S-NC-4, flow oscillations were calculated by RELAP5 (as shown in Figures 3.2.1, 3.2.2, 3.2.6 and 3.2.7) but were not reported in the experiment. This could be explained by the difficulty of obtaining precise measurements using the existing reflux flowmeter. The technique to measure reflux flow rate involved draining and measuring the total amount of the countercurrent liquid film which fell back into the hot leg from the inlet region of steam generator. When these measurements were made, the period between each data acquisition was large, and it would be hard to observe flow oscillations occurring since the measurements effectively time-averaged the data.



Table 3.1 Experimental System Parameters for Test S-NC-3

Case	Number	Mass Inventory (% of Total)	Primary Pressure (MPa)	Fluid Temperature		Core $\Delta T$ (K)	SG $\Delta T$ (K)	Steam Generator Condition			Core Power (kW)	Mass Flow Rate (kg/s)
				Cold Leg (K)	Hot Leg (K)			Heat Transfer		Liquid Level <sup>a</sup> (cm)		
								Pressure (MPa)	Area (%)			
1	1	100	11.2	540	560	20	23	5.0	100	1080	32.8	0.33
	2	100	12.5	539	569	30	32	5.0	100	1073	62.6	0.39
	3	94.1	8.2	540	569	29	32	5.0	100	1039	62.6	0.40
	4	93.1	8.3	540	569	29	32	5.0	100	1011	62.6	0.40
2	5	100	10.1	549	577	28	30	5.9	100	1067	62.6	0.40
	6	98.0	9.2	550	577	28	30	5.9	100	1067	62.6	0.40
	7	95.7	8.0	550	572 <sup>b</sup>	23	24	5.9	100	1039	62.6	0.50
	8	93.6	7.2	550	563 <sup>b</sup>	14	15	5.9	100	1053	62.6	0.63
	9	92.6	6.9	550	560 <sup>b</sup>	10	12	5.9	100	1067	62.6	0.70
	10	91.8	6.9	550	557	7	9	5.9	100	1067	62.6	0.75
3	11	91.8	7.0	550	558	8	10	5.9	99.1	970	62.0	0.69
	12	91.8	6.9	550	557	7	8	5.9	86.9	804	62.0	0.76
	13	91.8	6.8	551	556	6	8	5.9	75.5	694	62.0	0.75
	14	91.8	6.8	551	556	5	7	6.0	67.4	624	62.0	0.77
	15	91.8	6.9	553	557	5	7	6.0	55.5	514	62.0	0.68
	16	91.8	7.4	556	561	6	8+1	6.0	43.6	404	62.0	0.59 + 0.06 <sup>c</sup>
	17	91.8	7.8	559	566	8	9+1	6.0	33.2	307	62.0	0.45 + 0.11 <sup>c</sup>
	18	91.8	8.7	564	572	13	11+2	6.0	22.7	210	62.0	0.30 + 0.17 <sup>c</sup>
	19	91.8	9.6	566	580	17	13+7	6.0	15.2	141	62.0	0.20 + 0.13

a. Collapsed liquid level as measured from the top of the tube sheet.

b. Rapidly decreasing trend.

c. Large oscillation was observed.

d. External heaters were used for making up heat loss hot leg (4.8 kW), the cold leg (2.7 kW), and the pump suction (8.5 kW) and the vessel (20.0 kW), throughout the test.

Table 3.2 Experimental System Parameters for Test S-NC-4

Number	Primary System Mass Inventory <sup>a</sup>		Effective Steaming Rate (kg/s)	Refluxing Rate			
	Start of Measurement (%)	End of Measurement (%)		Carry-Over		Reflux	
	(%)	(%)		(kg/s)	(%) <sup>b</sup>	(kg/s)	(%) <sup>b</sup>
1	58.5	48.1	0.035	--	--	0.0162	46
2	61.1	52.3	0.035	--	--	0.0154	44
3	60.7	53.8	0.017	--	--	0.0092	54
4	62.4	62.4	0.017	0.0101	59	--	--
5	62.4	62.4	0.035 <sup>b</sup>	0.0116	33	--	--
6	64.4	51.9	0.035	--	--	0.0154	44
7	65.9	58.6	0.035	--	--	0.0158	45
8	71.7	71.7	0.035	0.0175	50	--	--
9	71.7	71.7	0.017	0.0127	75	--	--
10	71.7	71.7	0.017	0.0229	134	--	--
11	70.1	65.8	0.017	--	--	0.0092	54
12	69.9	63.2	0.017	--	--	0.0070	41

a. The system mass was 113 kg when full.

b. Percent of the effective steaming rate.

c. Steaming rate plus superheating rate.

Number	Primary Pressure (MPa)	Core Inlet Temperature (K)	Core Outlet Temperature (K)	Core Power (kW)	Steam Generator Conditions		
					Pressure (MPa)	Liquid Level (m)	Heat Transfer Area (K)
1	6.2	540	550	60.9	5.72	10.67	100
2	6.2	539	550	60.9	5.74	8.18	89
3	6.1	530	549	31.4	5.74	8.18	89
4	6.1	545	549	31.4	5.74	0.59	93
5	6.2	540	567-596 <sup>a</sup>	60.9	5.74	8.59	93
6	6.2	535	550	60.9	5.74	7.49	81
7	6.2	535	551	60.9	5.75	6.52	71
8	6.4	550	552	60.9	5.75	6.52	71
9	6.2	548	551	31.4	5.75	6.52	71
10	6.2	548	550	31.4	5.76	4.52	49
11	6.2	538	550	31.4	5.76	4.52	49
12	6.9	535	558	31.4	5.79	2.24	24

a. The core was partially uncovered.

b. The external heaters were operated to compensate for system heat loss as shown below:

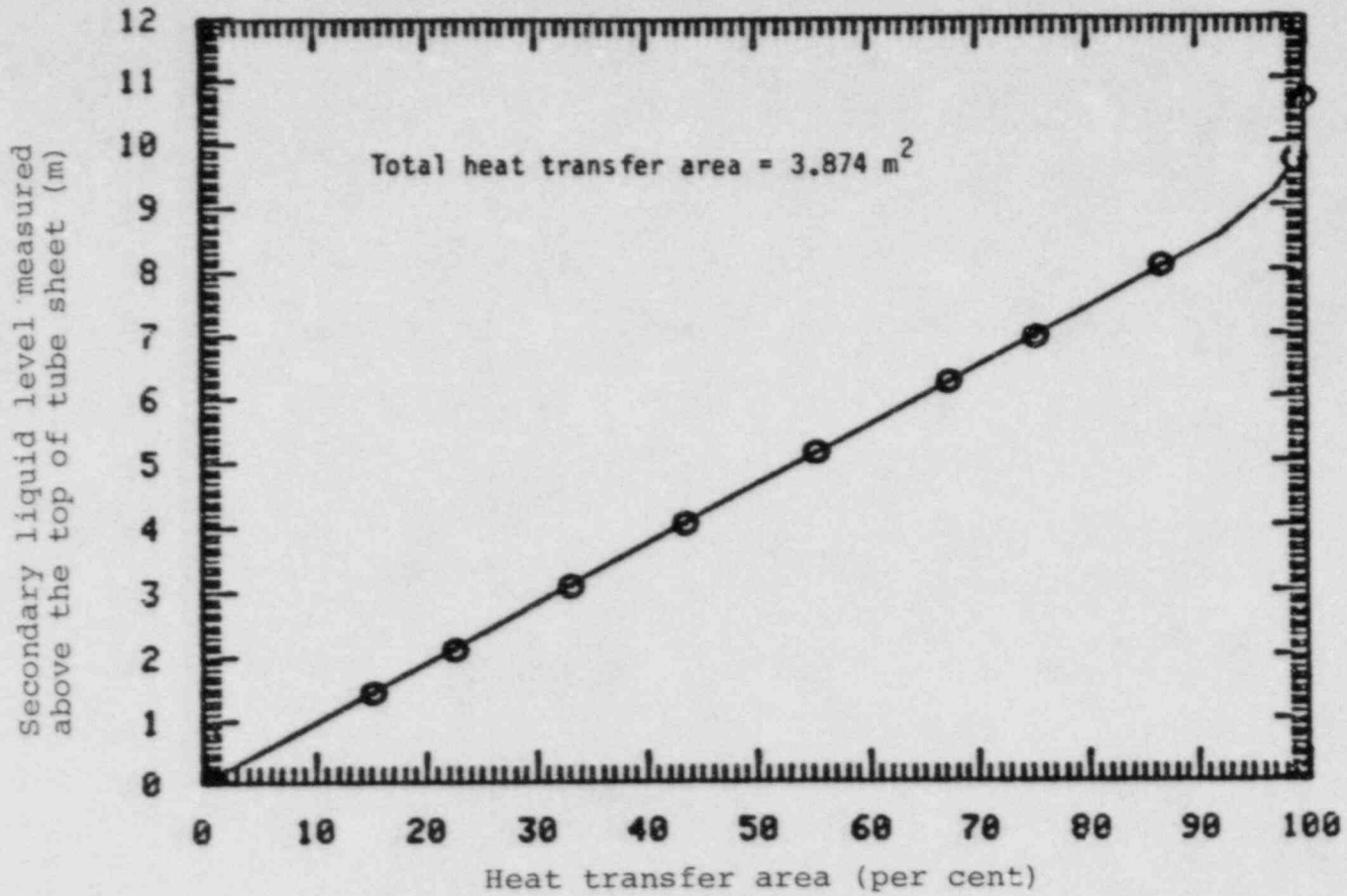


Figure 3.1 Relationship between the Secondary Liquid Level and the Heat Transfer Area in the Steam Generator

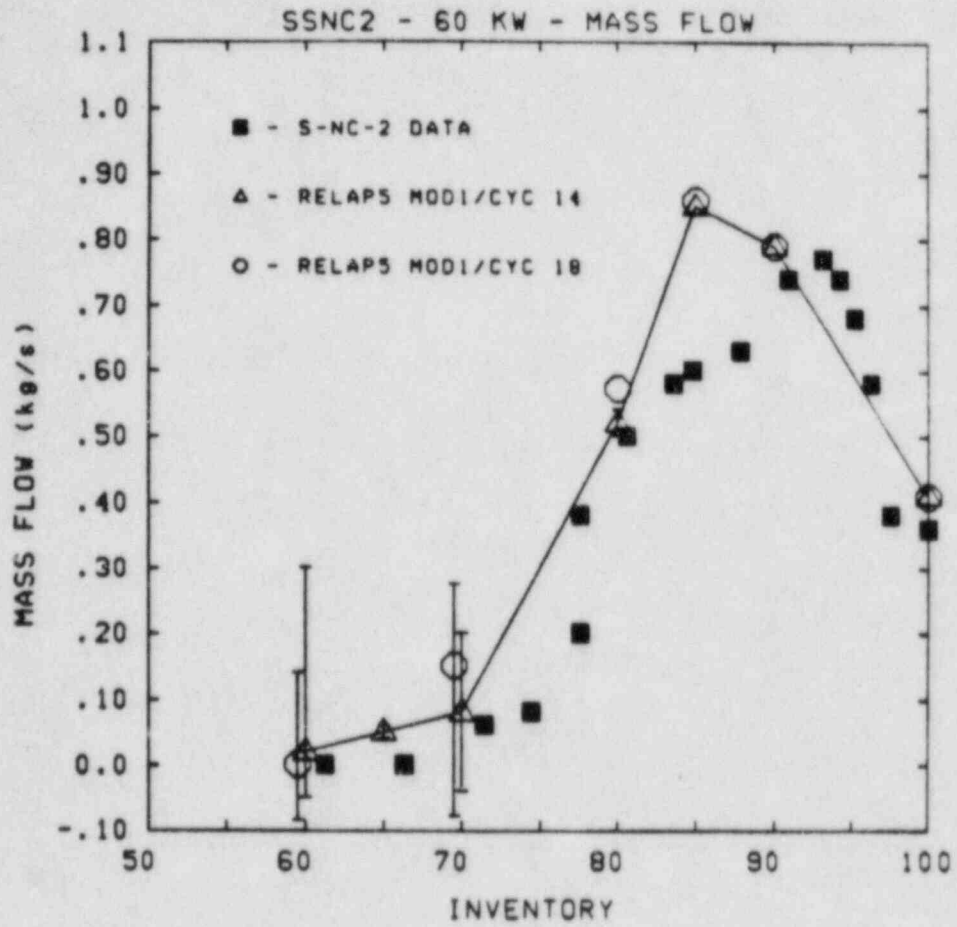


Figure 3.1.1 Measured and Calculated Mass Flow Rates for Test S-NC-2 (60 kW Power Case)

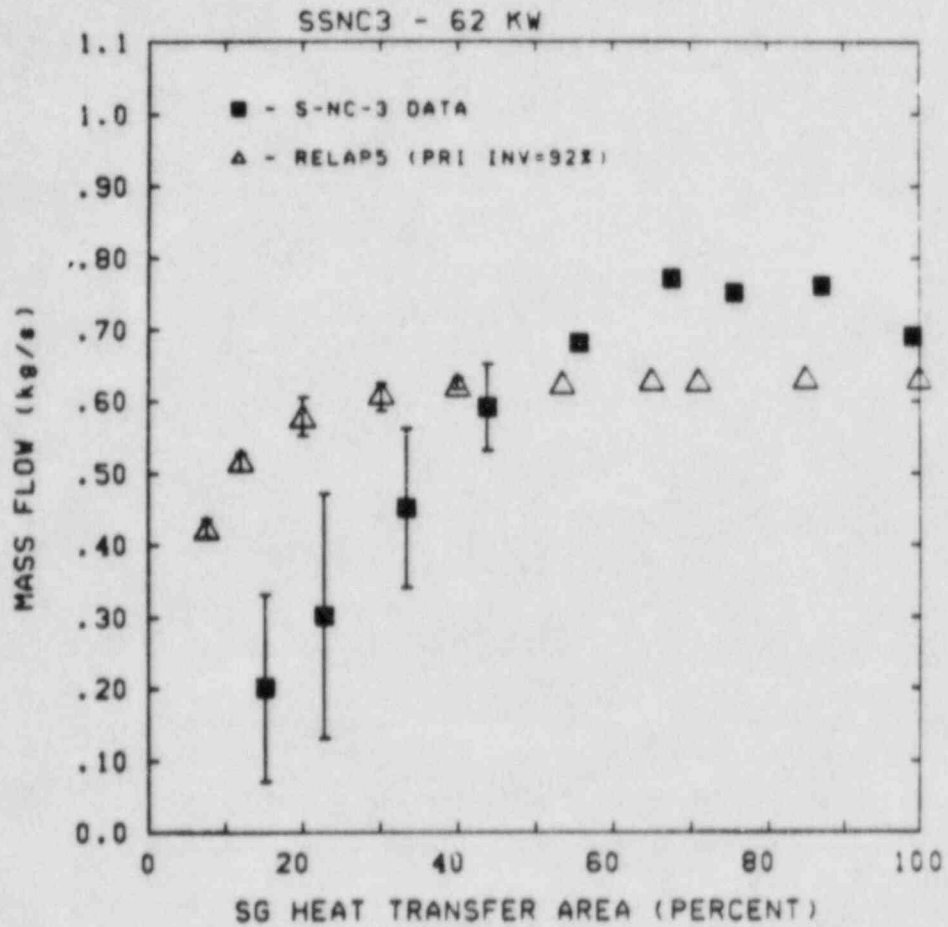


Figure 3.1.2 Measured and Calculated Mass Flow Rates for Test S-NC-3

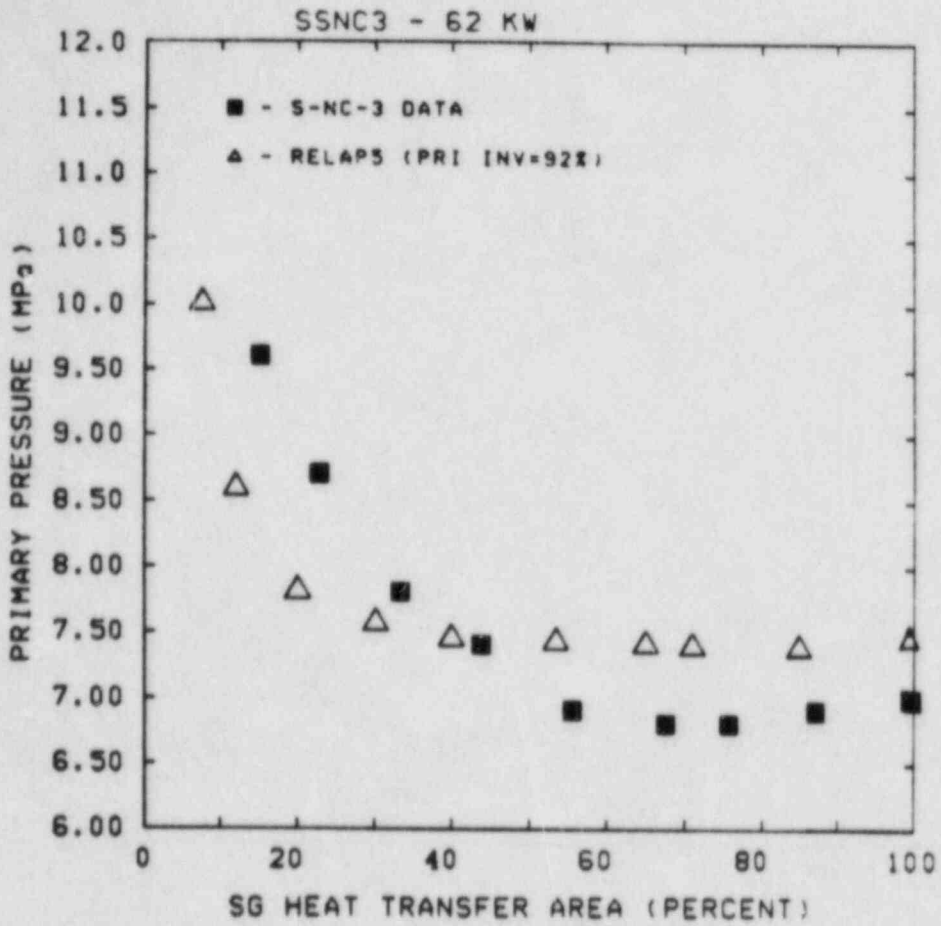


Figure 3.1.3 Measured and Calculated Primary System Pressures for Test S-NC-3

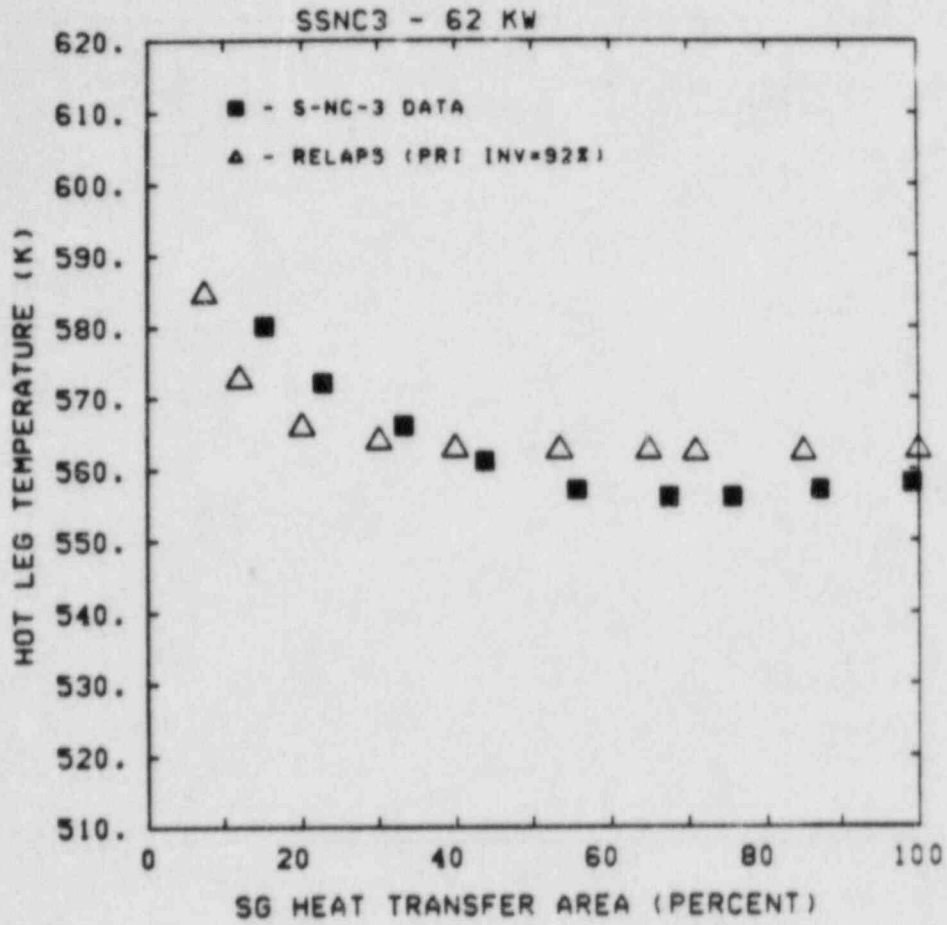


Figure 3.1.4 Measured and Calculated Hot Leg Temperatures for Test S-NC-3

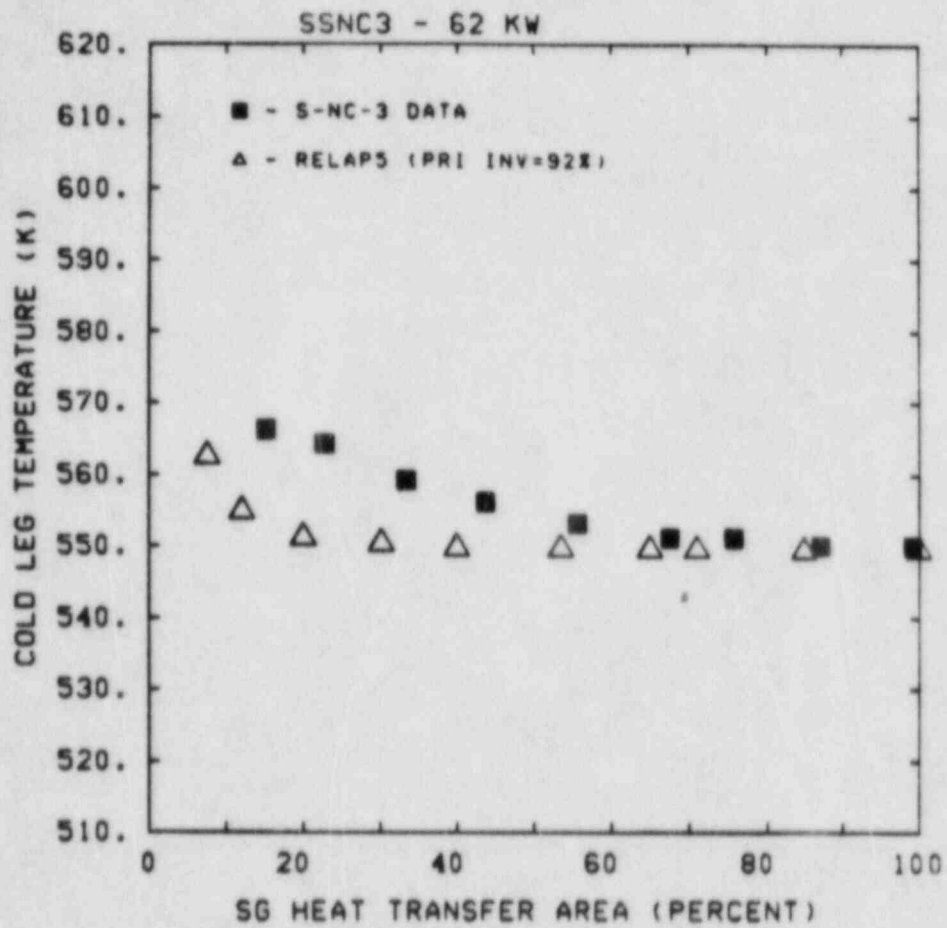


Figure 3.1.5 Measured and Calculated Cold Leg Temperatures for Test S-NC-3



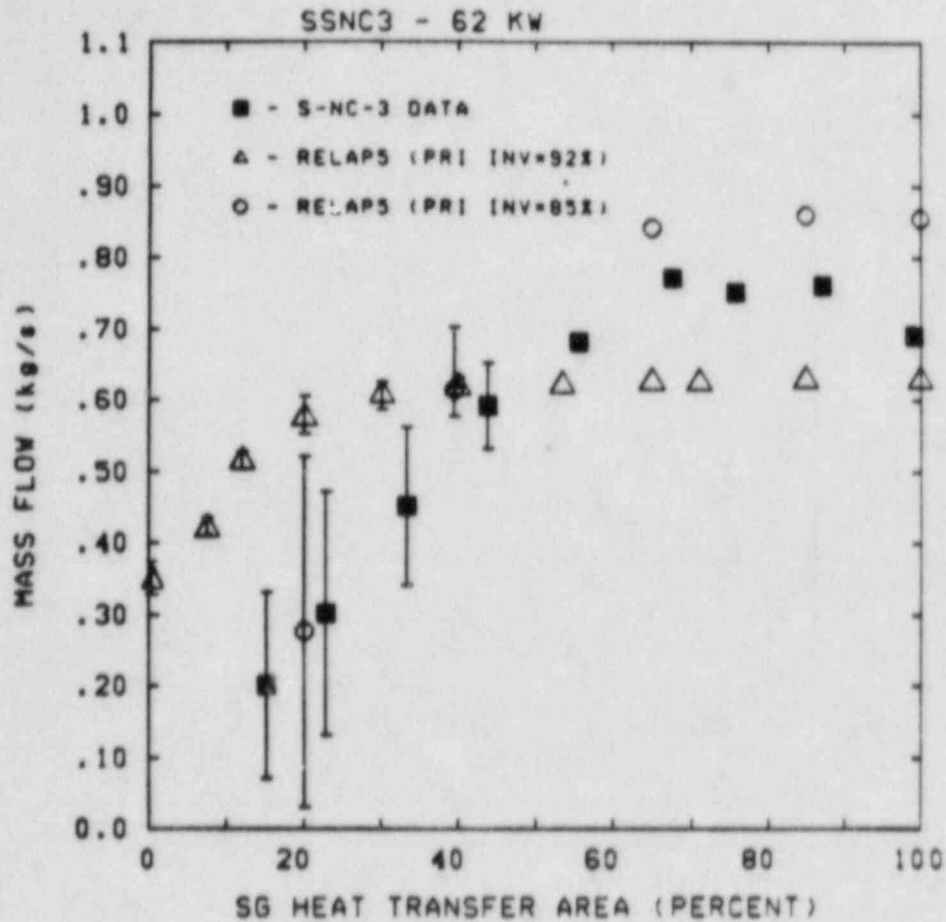


Figure 3.1.6 Measured and Calculated Mass Flow Rates for Test S-NC-3 (Including Results of Calculations with Reduced Primary Inventory)

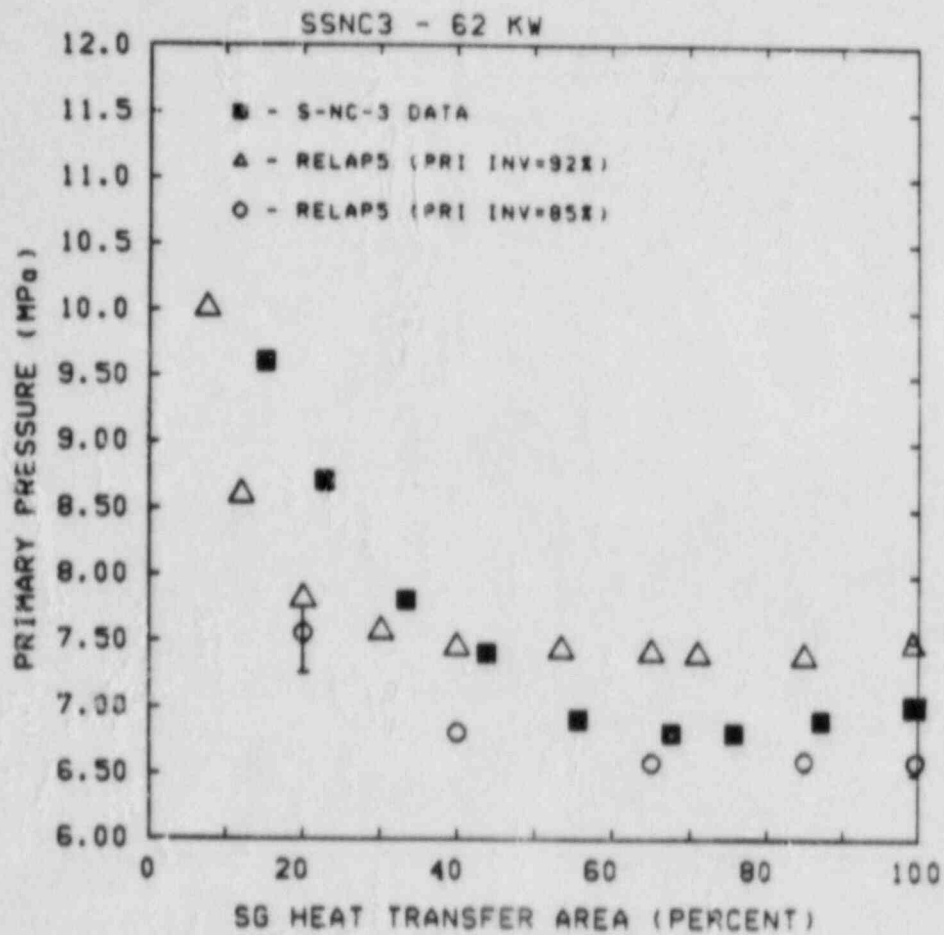


Figure 3.1.7 Measured and Calculated Primary System Pressures for Test S-NC-3 (Including Results of Calculations with Reduced Primary Inventory)

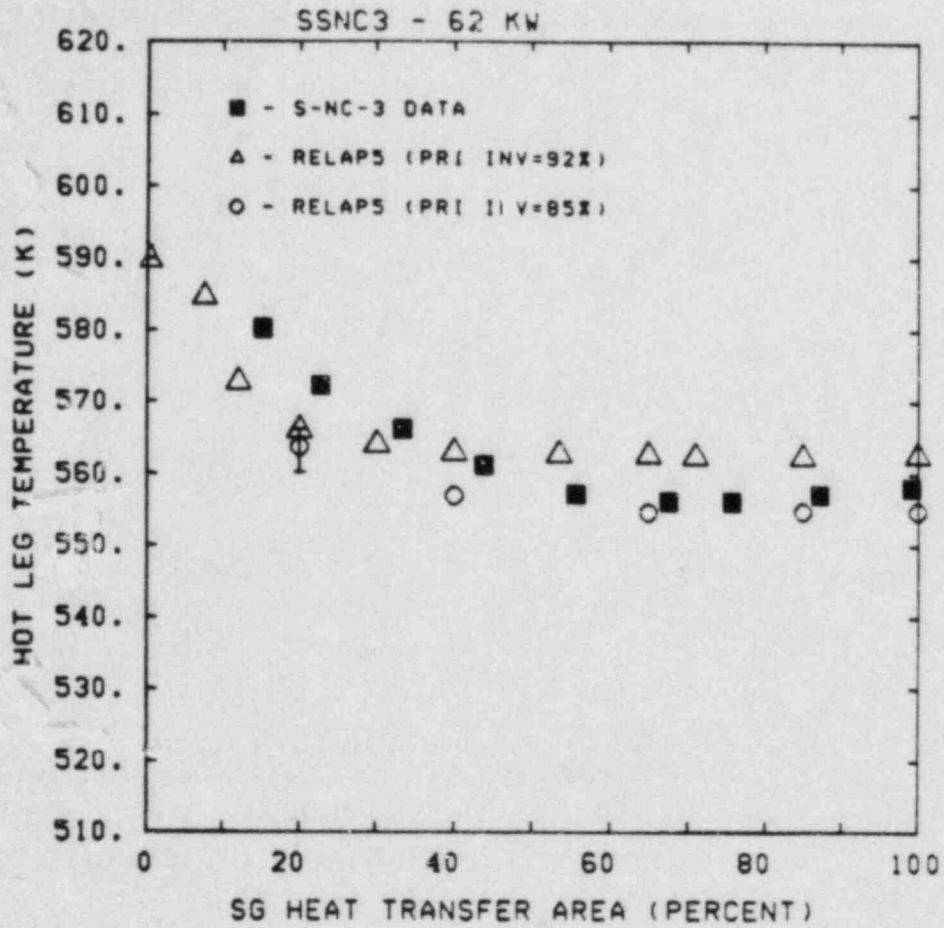


Figure 3.1.8 Measured and Calculated Hot Leg Temperatures for Test S-NC-3 (Including Results of Calculations with Reduced Primary Inventory)

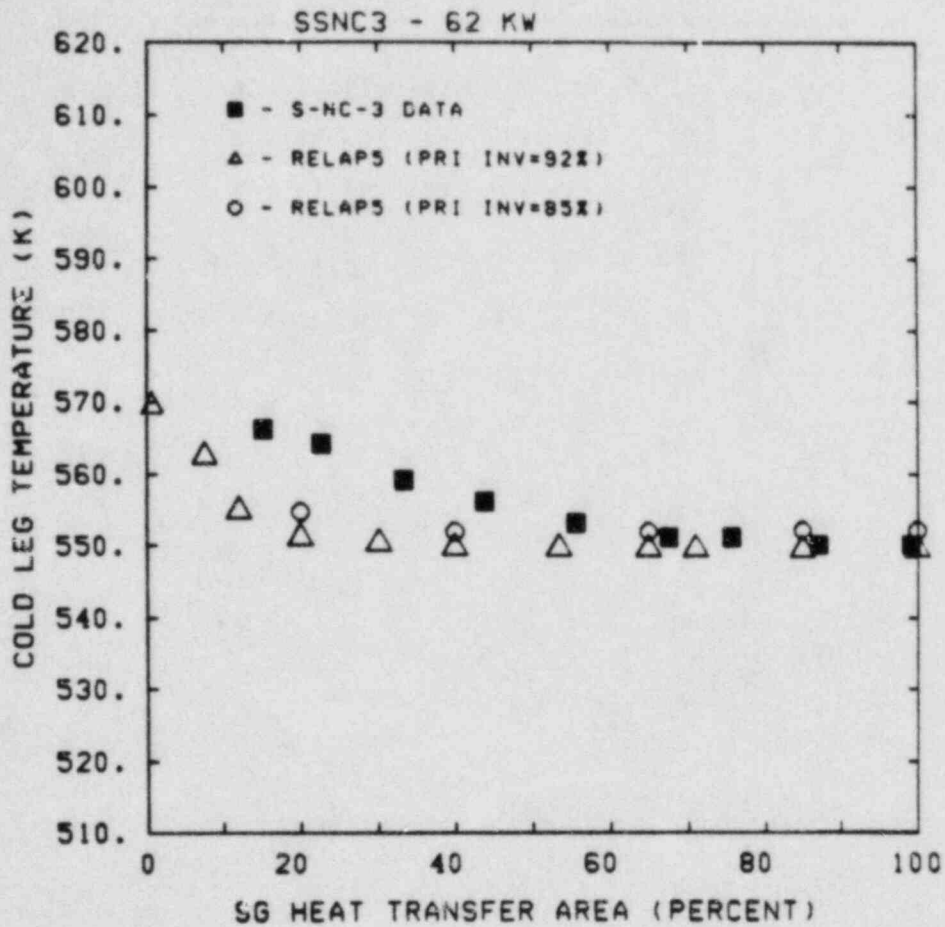


Figure 3.1.9 Measured and Calculated Cold Leg Temperatures for Test S-NC-3 (Including Results of Calculations with Reduced Primary Inventory)

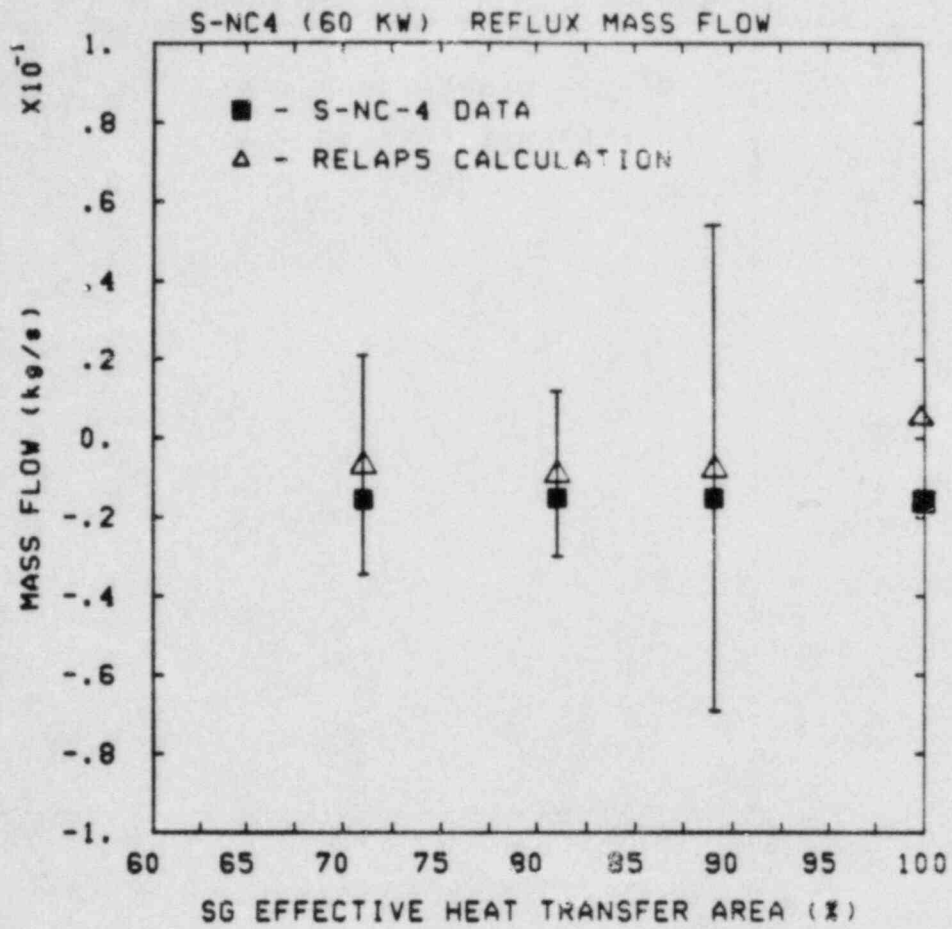


Figure 3.2.1 Measured and Calculated Reflux Mass Flow Rates for Test S-NC-4 (60 kW Power Case)

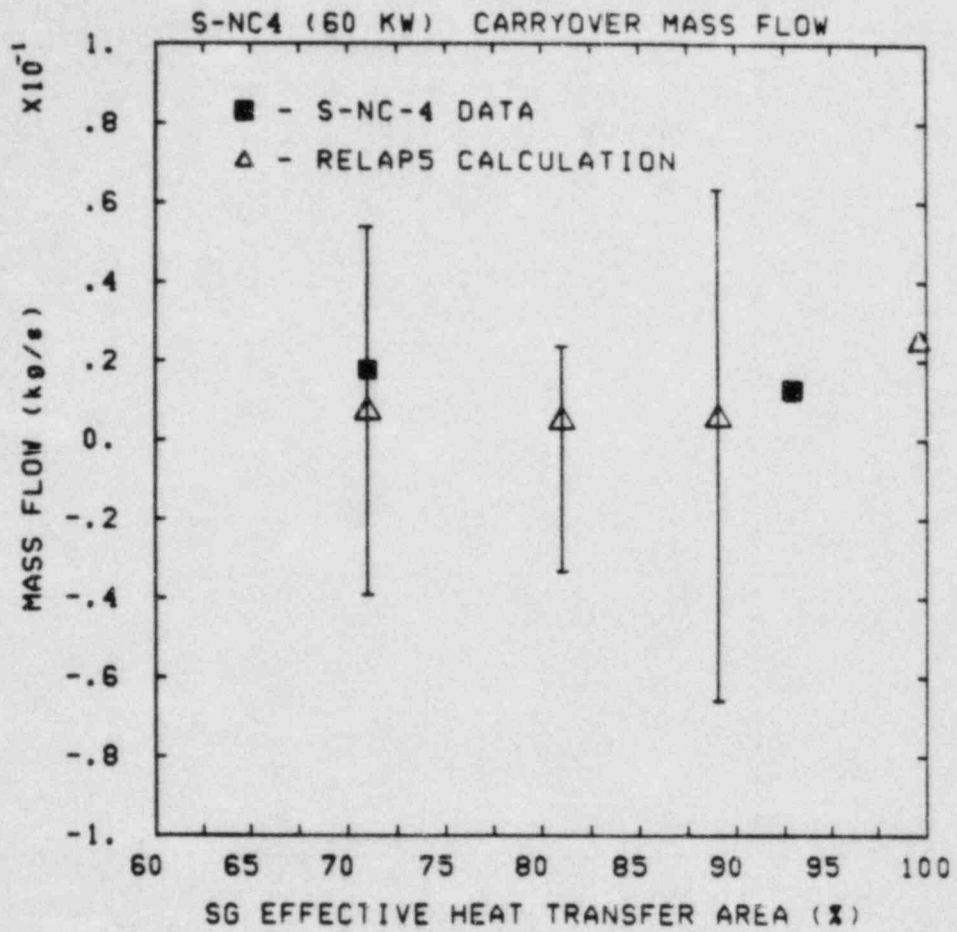


Figure 3.2.2 Measured and Calculated Carryover Mass Flow Rates for Test S-NC-4 (60 kW Power Case)

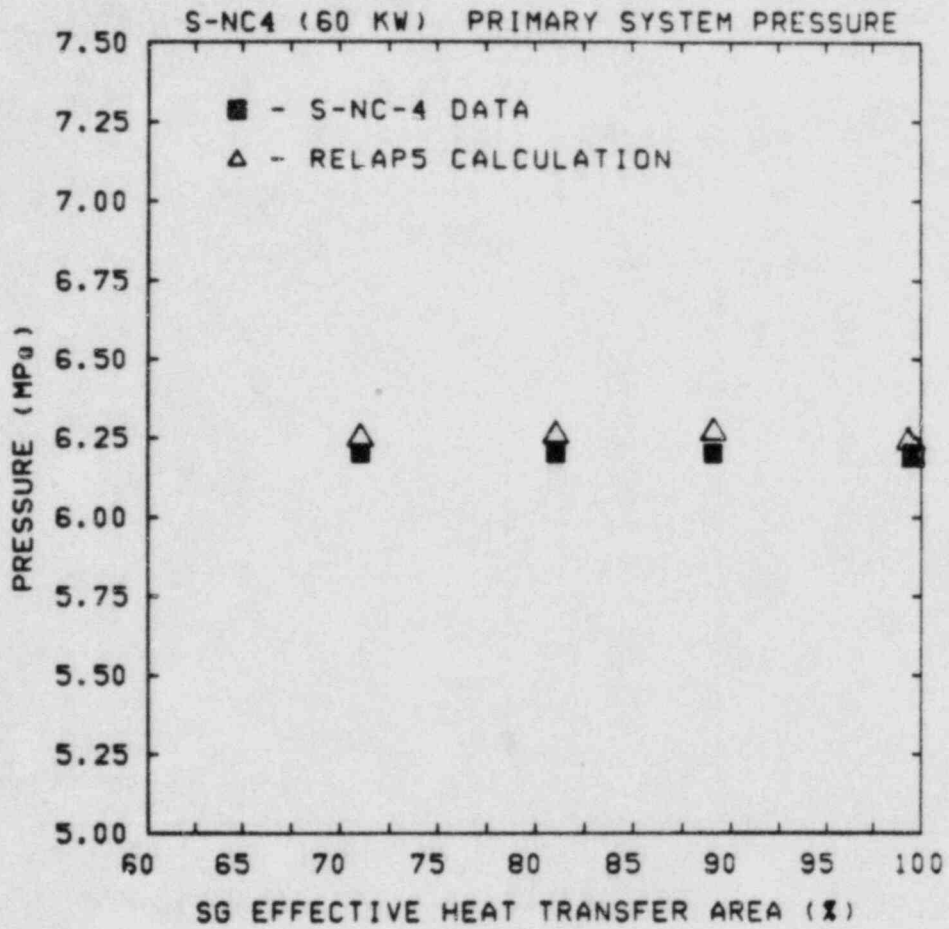


Figure 3.2.3 Measured and Calculated Primary System Pressures for Test S-NC-4 (60 kW Power Case)

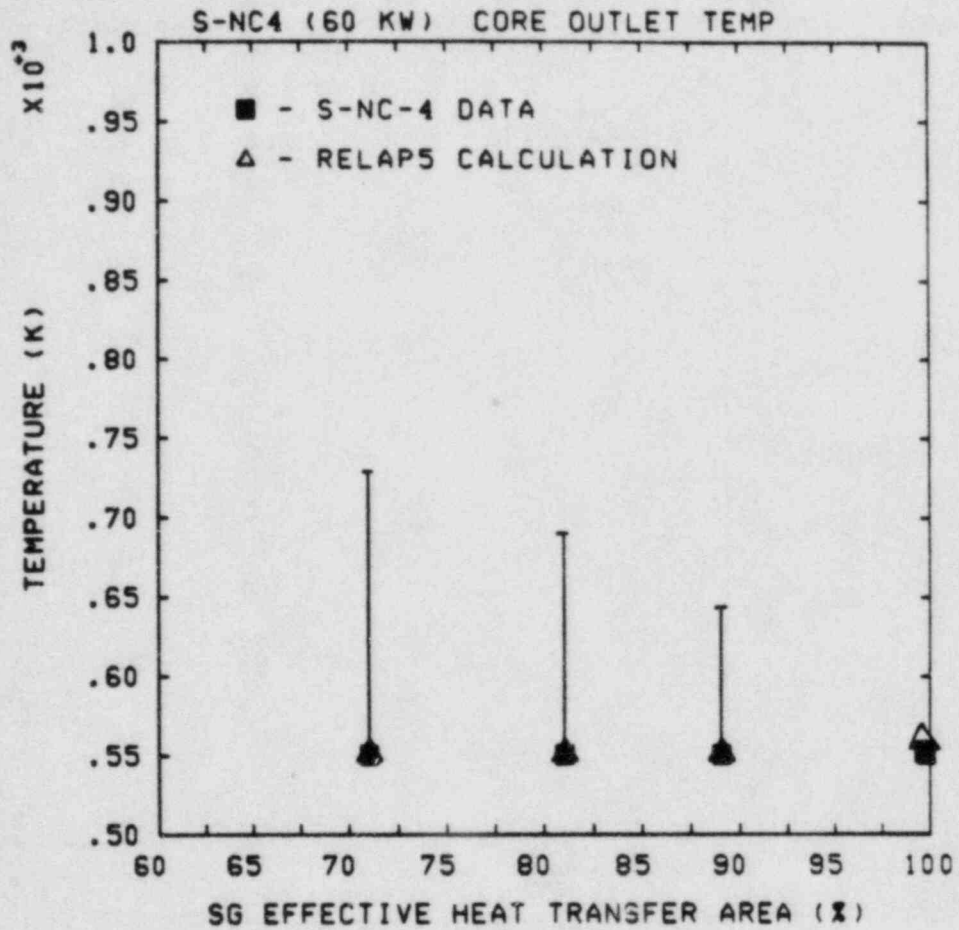


Figure 3.2.4 Measured and Calculated Core Outlet Temperatures for Test S-NC-4 (60 kW Power Case)



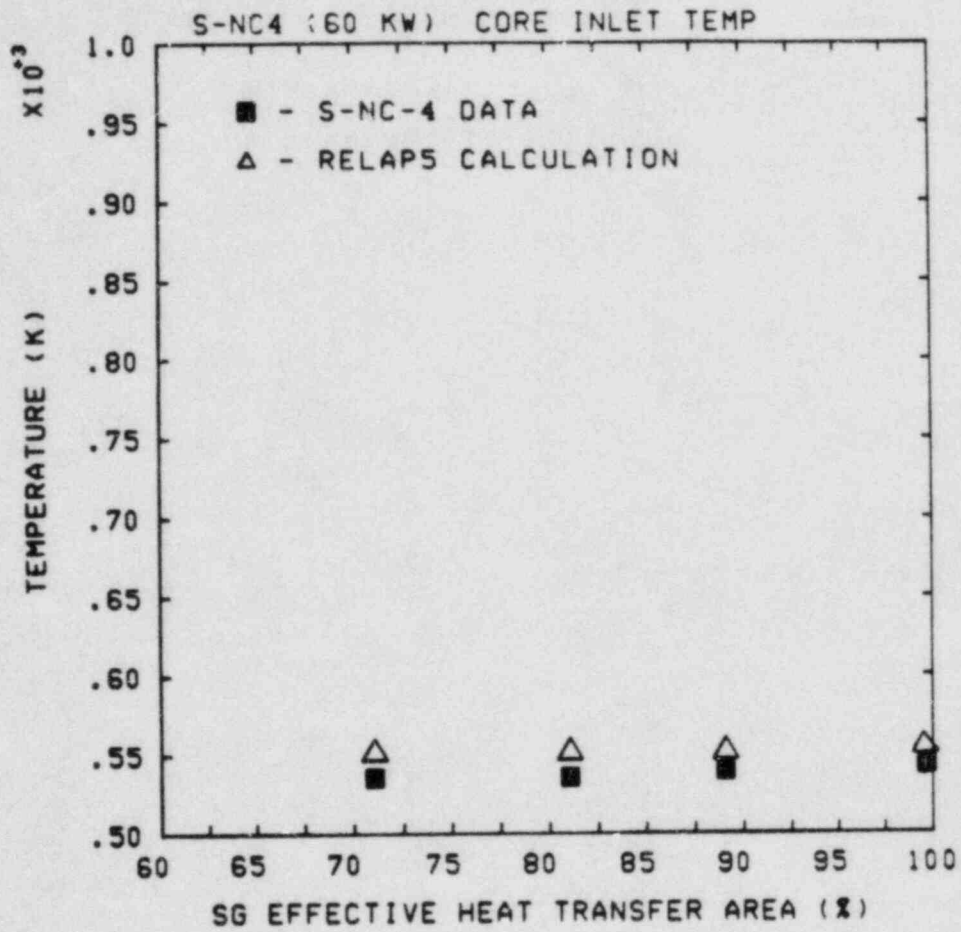


Figure 3.2.5 Measured and Calculated Core Inlet Temperatures for Test S-NC-4 (60 kW Power Case)

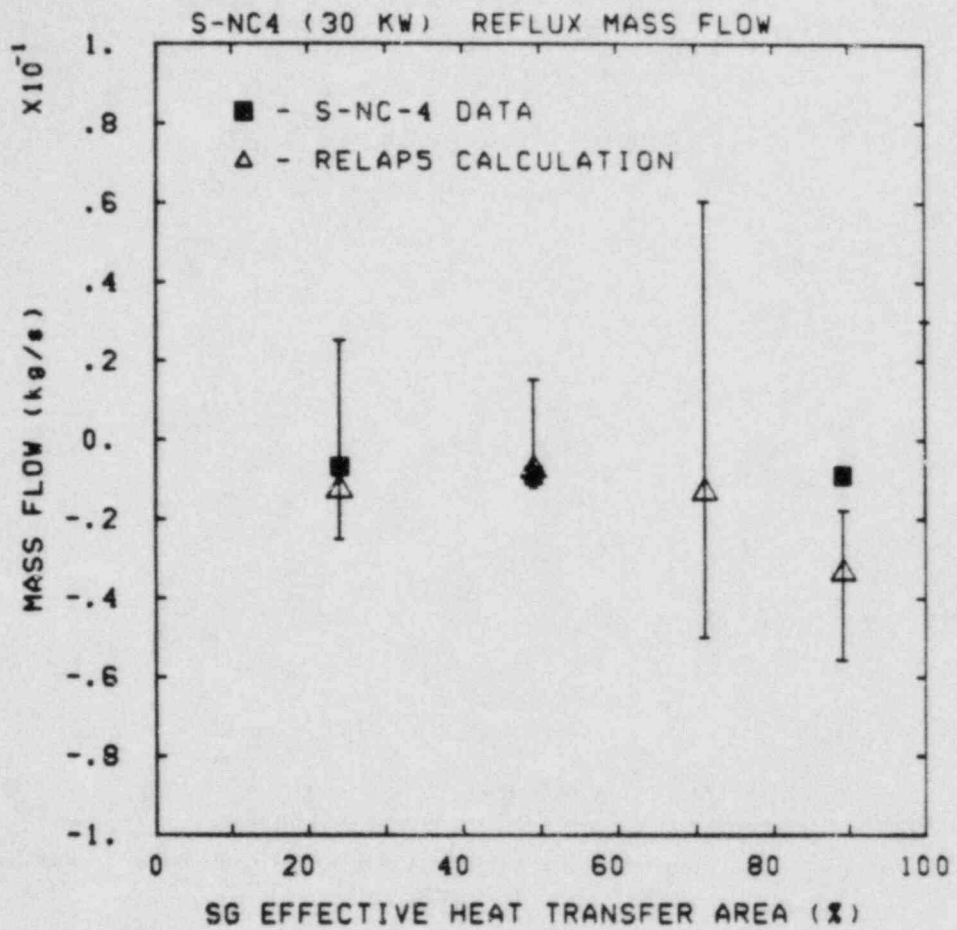


Figure 3.2.6 Measured and Calculated Reflux Mass Flow Rates for Test S-NC-4 (30 kW Power Case)

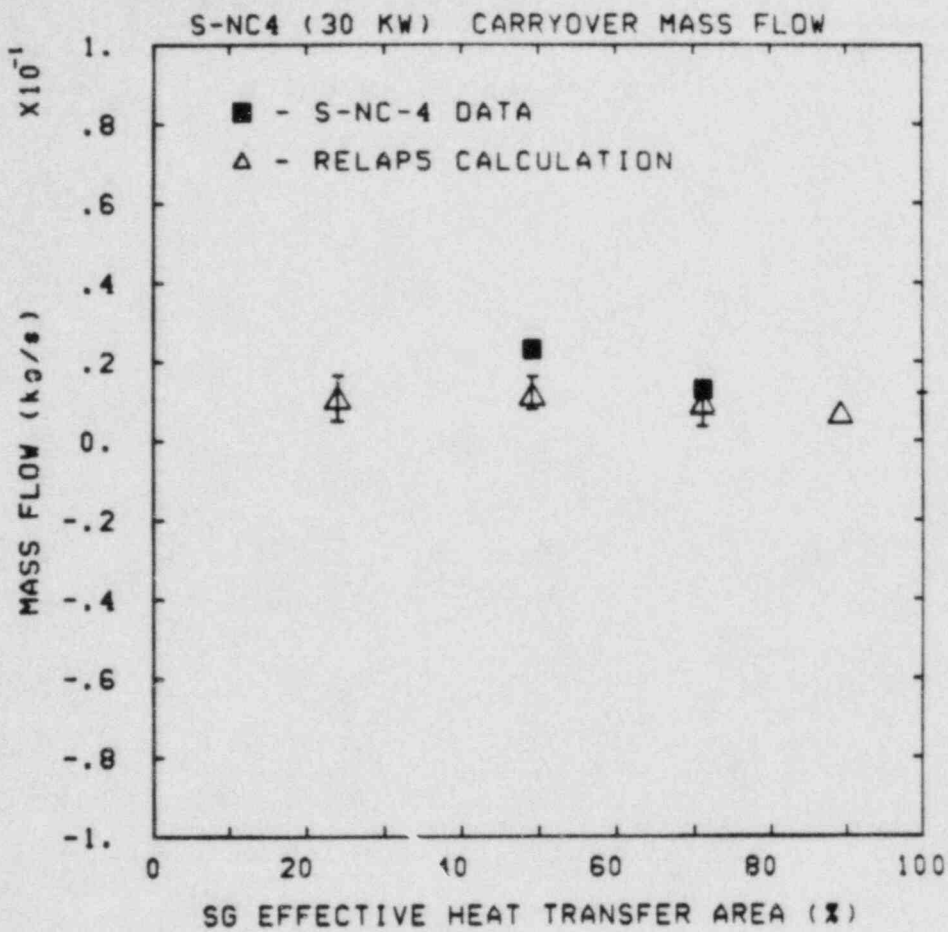


Figure 3.2.7 Measured and Calculated Carryover Mass Flow Rates for Test S-NC-4 (30 kW Power Case)

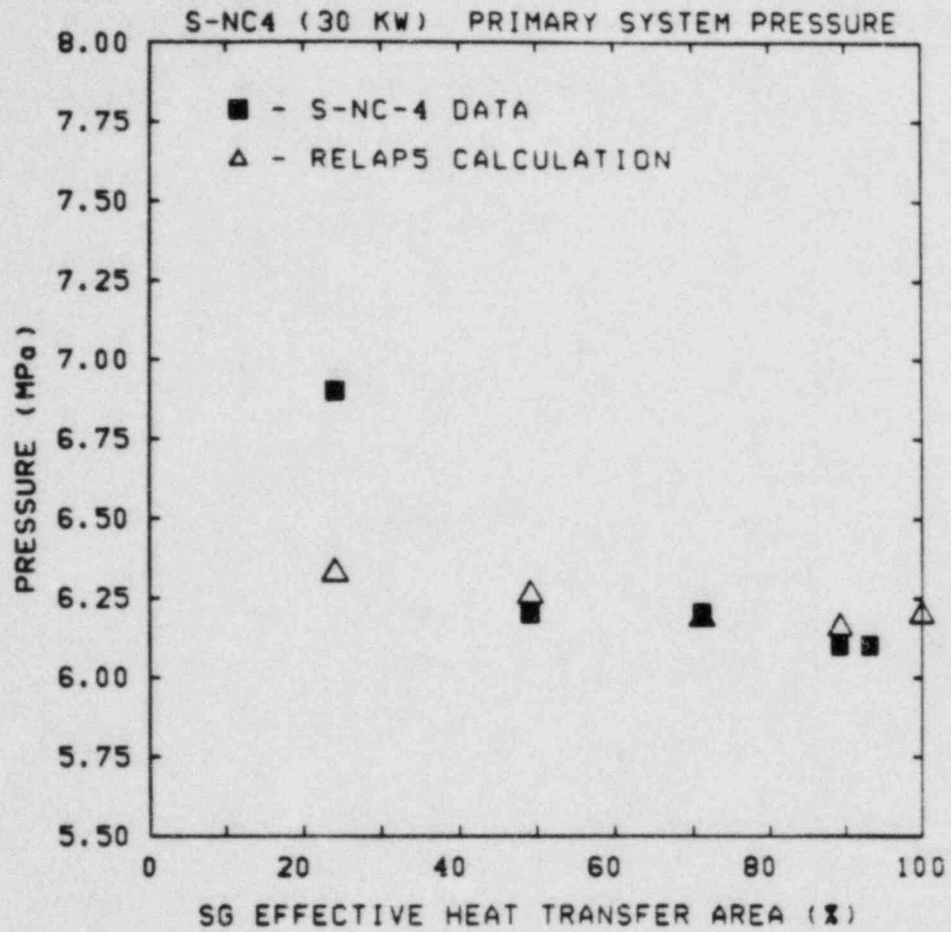


Figure 3.2.8 Measured and Calculated Primary System Pressures for Test S-NC-4 (30 kW Power Case)

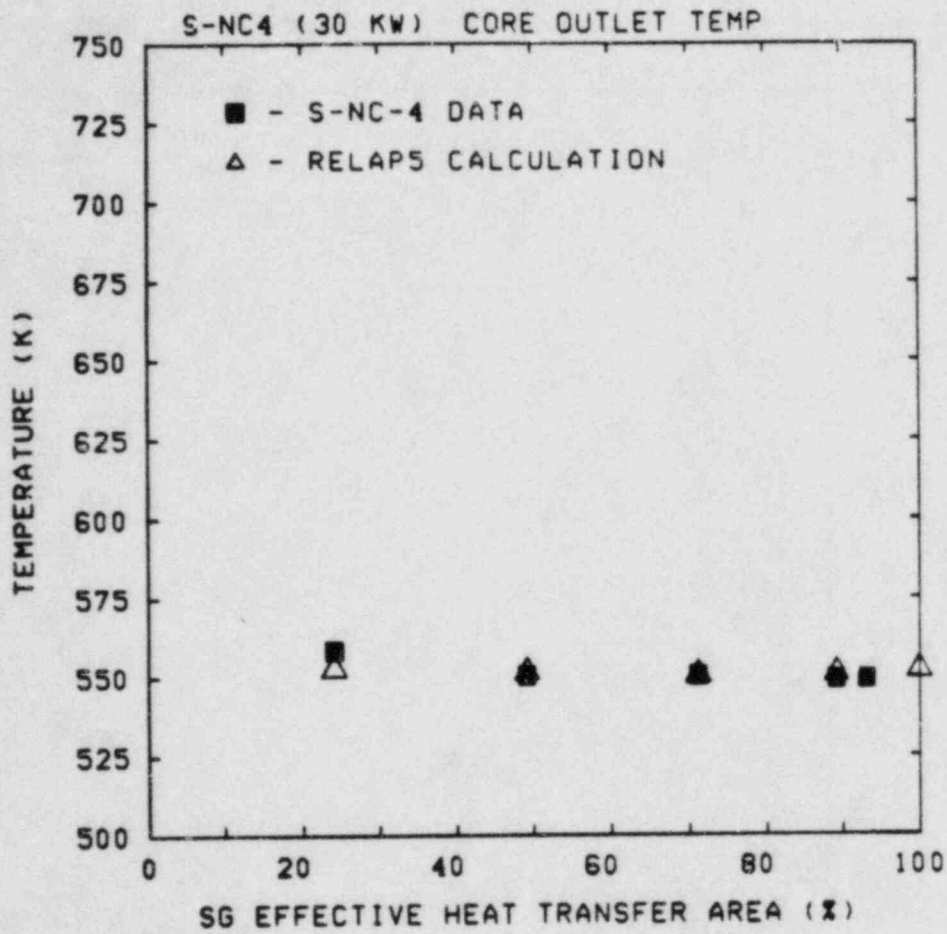


Figure 3.2.9 Measured and Calculated Core Outlet Temperatures for Test S-NC-4 (30 kW Power Case)

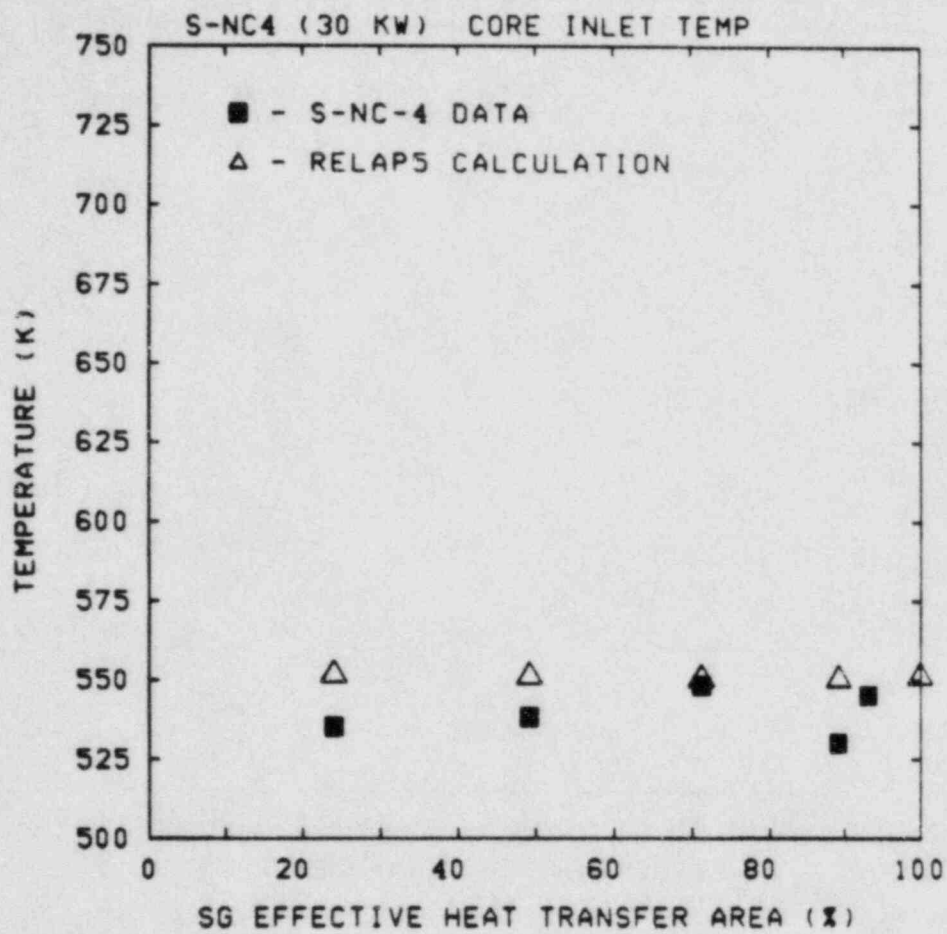


Figure 3.2.10 Measured and Calculated Core Inlet Temperatures for Test S-NC-4 (30 kW Power Case)

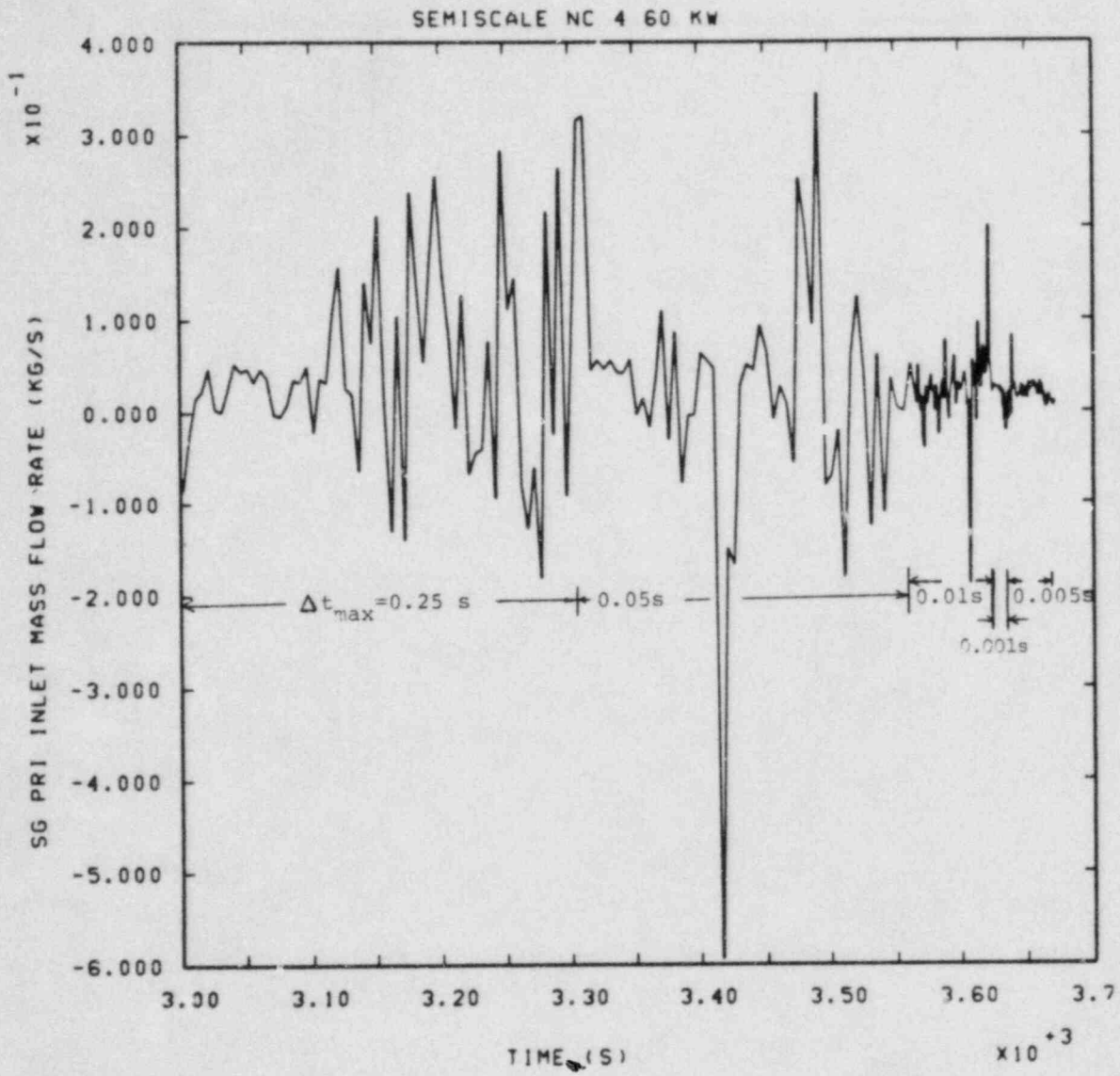


Figure 3.3.1 Calculated Steady State Flow Oscillations in Test S-NC-4 (60 kW Power Case)

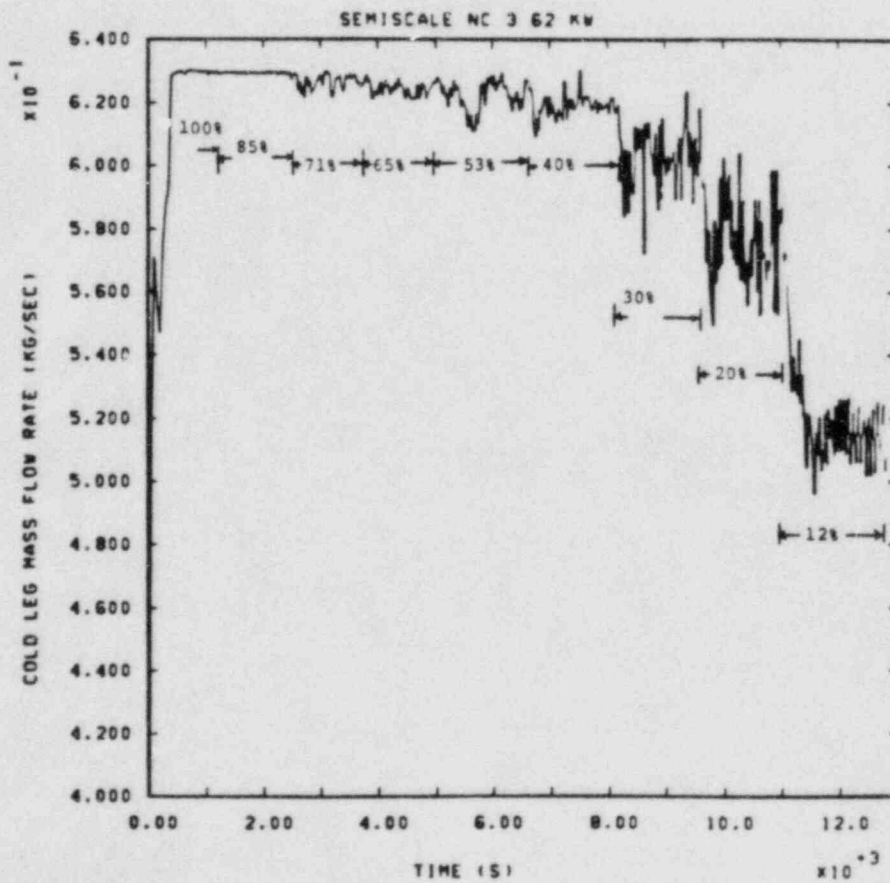
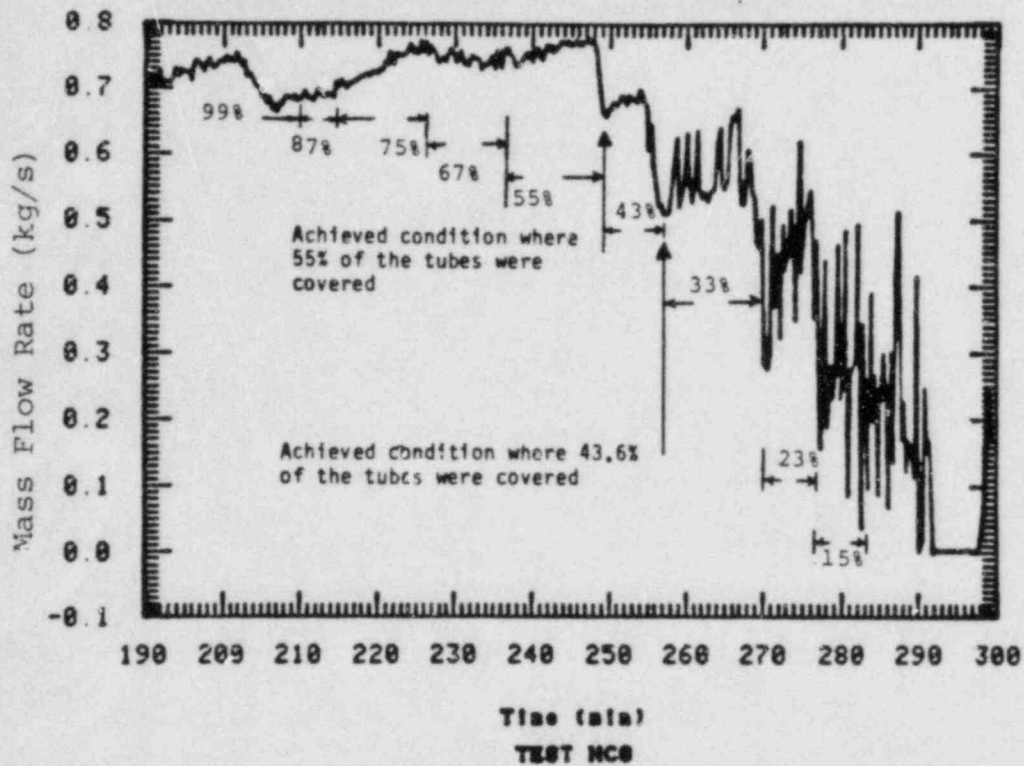


Figure 3.3.2 Measured (Top) and Calculated (Bottom) Steady State Flow Oscillations in Test S-NC-3 (Both Primary Inventories Equal to 91.8%)



#### 4.0 TWO-LOOP ULTRA-SMALL BREAK TRANSIENT S-NC-8

Test S-NC-8, a two-loop natural circulation experiment, simulated a loss-of-coolant accident resulting from a 0.4% cold leg break. [3,13,14] Its objective was to investigate the occurrence and transition between single-phase, two-phase and reflux natural circulation and core recovery procedures during an ultra-small break transient without pumped emergency core cooling flow. Recovery procedures attempted include steam generator auxiliary feed and bleed, accumulator injection, and primary system venting through a pressure-operated relief valve. The thermal/hydraulic response of the reactor system and the effectiveness of safety components and operator actions during this simulated abnormal event were the main concern in this experiment. Transient data obtained from this experiment also complements steady state separate effects data previously obtained during the natural circulation test series, primarily in the two-loop steady state basecase test S-NC-7.

#### 4.1 Description of Experiment

A modified two-loop Mod-2A system was used for this experiment, similar to the two-loop configuration used in test S-NC-7, except that the pressurizer remained active during S-NC-8. The vessel upper head was removed, the intact loop pump was replaced with an instrumented spool piece with the properly-scaled locked-rotor hydraulic resistance, a bypass line between the upper plenum and downcomer was installed to ensure uniform heating in the entire system, and a break flow condensing and measuring system was added to allow more accurate break flow measurements. External surfaces were covered with insulation and heaters to approximate adiabatic boundary conditions.

In the test, steady conditions were first established in the system during single-phase natural circulation, for 95 kW core power. (Since no primary system pumped flow was used, this initial core power was considerably lower than the nominal 2 MW, and is characteristic of ~5% decay heat levels.) Next, blowdown was initiated by opening a valve downstream of the break nozzle. A rapid subcooled depressurization occurred for about 200 s, followed by a much slower saturated depressurization. The core power was held at 95 kW until it intersected the nominal 2 MW decay curve, after which the core power was ramped down accordingly.

When the cold leg break began to expel a two-phase mixture, the system slowly established saturated conditions with two-phase natural circulation in the loops. After the vessel collapsed liquid level dropped to the hot leg elevation, the two-phase natural circulation flow rate rapidly peaked as the result of an

increase in the overall system density gradient. Eventually, as enough mass was expelled from the system, first the intact loop and then the broken loop went into the reflux mode. This reflux natural circulation was an important heat removal mechanism, preventing any heatup in the core until 2000 s. At 2000 s, the upper portions of the core rods were totally uncovered and began to heat up substantially. This required rapid operator intervention to recover the core and prevent any more heatup.

Since no HPI was allowed, the attempted recovery procedures involved various methods of reducing primary system pressure to the low pressure injection system (LPIS) setpoint. After core uncover and heatup began, steam generator auxiliary feed and bleed was first used to depressurize the primary system to the accumulator setpoint. The accumulators were then effective in maintaining sufficient liquid in the core to keep the heater rods cool. Following depletion of the accumulator tanks, steam generator feed and bleed was capable of maintaining reflux cooling. However, in an effort to increase the rate of depressurization further in order to reach the LPIS setpoint sooner, the PORV was then opened; this precipitated a core uncover and rod temperature excursion. The PORV was then closed, and steam generator "fill and dump" begun, which led to further core uncover and rod heatup. The rod temperatures turned over (but did not quench) at about 750 K, coincident with the time the LPIS setpoint was finally reached.

#### 4.2 Calculated Results

Initial conditions for the S-NC-8 transient calculation were obtained from steady state results with constant boundary conditions. In the steady state analysis, the reactor core power was kept constant at 95 kW, and the broken loop pump was locked and kept at zero velocity, producing single-phase natural circulation in the primary system. A time-dependent volume with saturated steam at a constant pressure of 15.4 MPa was connected to the top of the pressurizer; pressure in the steam generator secondaries was maintained at 5.85 MPa by other time-dependent volumes connected to the secondary side steam outlets.

Unlike the primary and secondary pressures, matching the collapsed liquid levels in various components during the steady state was not easy. We neglected slight differences between calculated and measured collapsed liquid levels in the steam generator secondary sides, because we did not consider it very important to obtain the correct liquid level as long as the U-tubes were fully covered. However, we could not neglect similar differences between calculated and measured pressurizer water levels because any water in the pressurizer is included in the primary mass inventory, and the exact amount of inventory determines the subsequent natural circulation mode. We artificially added extra liquid until the water level in the pressurizer and the total primary mass inventory was consistent with data.

We ran this steady state calculation for 200 s of problem time to establish both hydraulic and thermal equilibrium conditions. Table 4.1 compares the calculated and experimental initial conditions for test S-NC-8. Our results were generally within the uncertainty of the measured initial conditions. However, the higher calculated mass flow resulted in a core  $\Delta T$  ~10% lower than measured, even though the individual hot and cold leg temperatures were within their individual uncertainties.

Boundary conditions for the S-NC-8 transient analysis were core power, environmental heat loss, feedwater and steam outlet flow rates in the steam generators, and pump speed. The core power was maintained at 95 kW until 131 s (28 s after the pressure power trip was reached), after which the power followed the standard 2 MW decay power curve, as shown in Table 4.2. No environmental heat loss from the primary system was accounted for during the calculation; we assumed that the primary system was adiabatic. However, in the steam generator secondaries, heat loss from the downcomer was modelled, with a heat transfer coefficient of  $6.8 \text{ W/m}^2\text{-K}$  and an ambient temperature of 300 K. Throughout the transient, the speed of the locked-rotor broken loop pump was set to zero, as in the test.

The feedwater and outlet steam conditions in the steam generators were modelled in detail. As in the experiment, steam valves were closed at 117 s. We also kept the U-tubes covered with water until the operators turned on the feedwater and opened the steam outlet valves at 2100 s. When the feedwater system was on, the temperature of the injected water was not constant, but a function of time which was derived from experimental data.

The transient sequence of events for S-NC-8 predicted by RELAP5 appears in Table 4.3. At the start of the transient, the break valve was opened, beginning subcooled blowdown. As shown in Figure 4.2.1, the agreement between calculated and measured primary system pressures is excellent during the early stage of blowdown. Both data and analysis show the primary system pressure dropping sharply when the break opens, and even more rapidly when core power decay begins at about 131 s. The depressurization rate decreases when the hot leg fluid flashes at 190 s. When the liquid level drops to the hot leg elevation and the two-phase flow rate is at its peak at 290 s, increased condensation in the steam generator apparently increased the depressurization, until 370 s, when the cold leg begins to flash. This eventually leads to single-phase vapor blowdown, with the pressure falling slowly and continuously in the experiment, but leveling off at 6.45 MPa in the analysis. This difference may be caused by errors in primary-secondary heat transfer and/or in break mass flow rate and total primary mass inventory, as discussed below. It may also be partly due to assuming the primary system to be adiabatic, which becomes less valid the longer the transient.

Figures 4.2.2 and 4.2.3 show the steam generator secondary pressures for the intact and broken loops, respectively. As occurred in the experiment, the calculation shows the steam generators acting as heat sinks all through the blowdown phase, with the secondary pressures remaining below the primary pressure. The secondary pressures in both loops agree well with data for the first several hundred seconds, after the steam generators are isolated at ~120 s. However RELAP5 did not predict as much pressure decrease as was seen in the experiment by 2000 s, leading us to suspect that there might be some leakage in the steam generator secondaries, similar to that seen in test S-NC-8A, or that the primary-secondary heat transfer is being miscalculated. (Secondary side environmental heat loss was modelled, so the constant pressure calculated is not caused by assuming an adiabatic system, as in the primary.) When we stopped this calculation at 2000 s, the predicted intact loop secondary pressure was steady at 6.31 MPa, while in the test it had decreased slowly to 5.70 MPa.

A large part of the discrepancy in calculated and measured primary side pressures at late times is caused by underprediction of the break flow, as shown in Figure 4.2.4; in our analysis, the total mass flow rate out of the break was generally lower than measured. Both subcooled and saturated discharge coefficients were set to 1.0, and the abrupt area change model was used at the break. Other assessment calculations [15,16] have indicated that there are problems with the abrupt area change model for "pinhole-leak" geometries, and it would probably have been better to use the smooth area change model and input a user-determined loss coefficient. However, this would have required numerous calculations to adjust the loss coefficient such that the resulting break mass flow rate agreed with the data, which would be costly and time consuming.

The break flow shows the broken loop cold leg voiding earlier in the calculation (~600 s) than in the test (~700 s), also shown by the calculated and measured fluid densities upstream of the break in Figure 4.2.5. The analysis predicts an earlier onset of single-phase vapor blowdown and thus a reduced break mass flow rate. Density and flow oscillations are calculated, as seen in the experiment, when slugs of liquid pass through the cold leg piping. (Due to high frequency numerical oscillations and excessive mass error, the maximum time step had to be held down (~0.05 s), and sometimes even reduced further (~0.005 s), thus increasing the ratio of CPU to problem time for these calculations to 12:1. Sensitivity studies showed that the remaining oscillations were not eliminated by reducing the time step.)

The earlier voiding in the broken loop cold leg near the break is due to the difference in the calculated and measured broken loop mass flow rates, shown in Figure 4.2.6. (Two experimental data curves are given, one from the data tape, and the other digitized from a figure in the Quick-Look Report [13]. However,

the early-time broken loop flow measurement is probably unreliable, with no flow shown until 400 s because the broken loop flow turbine was in the dead-band prior to then.) The calculated mass flow rate for the broken loop peaked earlier (480 s rather than 638 s) and at a larger value (0.277 kg/s instead of 0.174 kg/s) than measured. At later times (>600 s) and low primary inventories, the analysis predicted reflux natural circulation in the broken loop, with a correspondingly small flow. When the flow rate dropped, the broken loop cold leg fluid eventually flashed. However, in the experiment, the broken loop mass flow was still at peak two-phase natural circulation during the same time period and reflux cooling did not begin until later in the test (>700 s).

Figure 4.2.7 shows the calculated intact loop cold leg mass flow rate compared with data. During the early blowdown period, the agreement is excellent, for single-phase and two-phase natural circulation. Peak two-phase flow occurs a little late but at about the right magnitude, and the earlier secondary flow peak when the pressurizer empties is correctly calculated. For times later than 400 s, during the transition between the two-phase and reflux modes of natural circulation, the code overpredicts the mass flow rate. This is most likely caused by the lower break flow calculated resulting in a higher primary inventory in the calculation, especially after ~600 s. After 690 s, the analysis predicted the intact loop entering reflux natural circulation, with flow oscillations calculated as were seen in the experiment. However, the flow oscillations predicted were much larger in amplitude than those measured, partly because the time step used (0.05 to 0.005 s) was not always small enough.

Mass flow rates in the vessel downcomer are plotted in Figure 4.2.8. The prediction and the measurement agree reasonably well with each other. The mass flow rate slowly increases at early times and decreases to zero at later times, with the most discrepancies as the system approaches the reflux cooling mode. The predicted downcomer flow rate of course reflects the errors in calculating the individual loop flow rates just discussed. The too-early and too-high broken loop peak two-phase flow, when added to the almost-correct intact loop peak two-phase flow, results in the high downcomer peak flow. The higher calculated downcomer flow after it peaks at ~400 s until 600 s is due to both calculated loop flows being high from 400 to 600 s. The loop flow oscillations are also visible in the downcomer flow.

The collapsed liquid level drops to the top of the core at 280 s, and continues dropping until it finally settles at 2.62 m above the bottom of the core (shown in Figure 4.2.9). Temperatures for two of the heated rods in the core are plotted in Figures 4.2.10 and 4.2.11, compared with experimental results; the agreement is very good, with both data and analysis showing the rods

remaining cool throughout blowdown. However, at the transition between blowdown and recovery (at 2000 s), the operator began feed and bleed, and one of the rods started to heat up in the experiment (just before 2000 s in Figure 4.2.10). No such heatup was calculated, probably because the analysis has much more mass left in the primary system late in the transient, due to the lower calculated break flow.

The fluid temperature distribution is shown in Figures 4.2.12 through 4.2.15, and shows the same general behavior as the rod clad temperatures. The cold leg temperatures for the intact and broken loops are shown in Figures 4.2.12 and 4.2.13 respectively. The agreement between calculation and measured data is reasonably good; the unphysical discontinuities and spikes in the liquid temperature shown in Figure 4.13 are a numeric artifact of the code requirement that the more massive phase be at saturation, as the cell voids with time. The broken loop fluid temperature is lower in the experiment because of a higher mass flow rate at the break. The hot leg fluid is saturated during much of blowdown and agrees well with experimental data (Figures 4.2.14 and 4.2.15).

As previously mentioned, when recovery began, the operator opened the steam outlet valve and turned on the auxiliary feed-water; this secondary side feed and bleed substantially lowered the primary system pressure, eventually allowing the accumulator to inject subcooled liquid into the cold legs. However, problems with the accumulator model in RELAP5 surfaced as the accumulators turned on at 2563 s, when the cold leg pressure fell below the set point pressure of the accumulators. As soon as the accumulator valves opened, a flow surge dropped the pressure in the accumulator drastically, producing a positive pressure gradient across the valve and causing the valve to shut off again. This prevented any more delivery of subcooled liquid to the primary system. Since the same problem with accumulator injection has been encountered in our other assessment problems [17], we decided to conclude our analysis at the end of the blowdown period and not to continue the analysis through the recovery period. Most of the interesting phenomena in S-NC-8, the different natural circulation modes and the transitions between each mode during a transient event, had been observed prior to that time.

#### 4.3 Comparison with S-NC-7

In section 4.2, we compared the results of our S-NC-8 calculation with experimental data as a function of time. However, discrepancies in the measured and calculated break mass flow rates (shown in Figure 4.2.4) cause large discrepancies in the measured and calculated primary system mass inventories (shown by the normalized inventories in Figure 4.3.1). To allow comparison with the results of the earlier Semiscale basecase two-loop steady state natural circulation test S-NC-7, we also analyzed various

interesting parameters as a function of primary mass inventory. (The primary inventory in the analysis was calculated using control functions that summed the masses in each component. The experimental inventory was obtained by subtracting the integrated break flow given on the data tape from the quoted initial system mass.)

The mass flow rates in the intact and broken loop cold legs are plotted in Figure 4.3.2 as a function of primary mass inventory. For the intact loop, the calculated mass flow rate compares very well with the measured mass flow rate, except at low inventories between 75% and 65%. There, the data shows a relatively smooth decrease to reflux cooling with a few large oscillations while the calculation shows high two-phase flow persisting until a much more rapid and oscillatory drop to reflux flow. However, for the broken loop, the agreement is only fair. The calculated mass flow rate rises much faster than the experimental data, peaks at a higher primary mass inventory (78% rather than 62%) and at a higher flow rate (0.277 kg/s rather than 0.174 kg/s), and drops to zero flow much earlier than the data.

Figure 4.3.3 shows the calculated and measured mass flow rates in the downcomer plotted against primary mass inventory. The agreement between these two results is generally good; both peak at the same inventory, and both decrease to zero value (reflux mode) at the same inventory. However, quantitatively, RELAP5 overpredicts the mass flow rate at the peak value and at the inventory between 60% to 75%, due to the problems calculating the mass flow rates in the individual loops.

Including both the calculated and measured S-NC-7 results for comparison (in Figures 4.3.4 and 4.3.5) results in some very crowded and confusing plots. However, close and careful study shows that many of the same trends are seen in both calculations and thus the conclusions which can be drawn for test S-NC-8 are quite similar to those previously drawn from our S-NC-7 results, especially for the broken loop behavior.

For the mass flow rate in the broken loop, RELAP5 predicts the peak value located at a much higher primary mass inventory than the data in both S-NC-7 and S-NC-8, while much better agreement on the inventory at which the flow peaks is seen in the intact loop. The magnitude of the calculated peak broken loop flow in S-NC-8 agrees well with both the calculated and measured peak broken loop flows in S-NC-7, but the measured peak broken loop flow in S-NC-8 is substantially lower (although that measurement may not be very reliable); the magnitude of the calculated peak intact loop flow in S-NC-8 agrees well with the measured peak intact loop flows in both S-NC-7 and S-NC-8, but the calculated peak intact loop flow in S-NC-7 is somewhat higher. The differences in intact loop flow due to the pressurizer being valved out in S-NC-7, but present in S-NC-8, are accurately calculated.

Table 4.1 Measured and Calculated Initial Conditions  
for Test S-NC-8

Steady State Results Parameters	Experiment	RELAP5
Core Power (kW)	95.0	95.0
Primary Pressure (MPa)	15.4	15.4
Hot Leg Temperature (K)	581.4	580.3
Cold Leg Temperature (K)	545.0	548.4
Mass Flow Rate (kg/s)		
Intact Loop	0.396	0.411
Broken Loop	0.121	0.128
Total Loop	0.517	0.539
Vessel Downcomer	0.532	0.584
Bypass Line	?	-0.044
Pressurizer Liquid Volume (c.m.)	0.0215	0.0215
SG Secondary Pressure (MPa)		
Intact Loop	5.85	5.85
Broken Loop	5.89	5.89
SG Secondary Water Level (m.)		
Intact Loop	10.74	11.3
Broken Loop	10.94	11.37

Table 4.2 Test S-NC-8 Core Power

Time After Trip (s)	Core Power (kW)
0	95.0
28.0	95.0
30.0	81.32
60.0	68.305
100.0	60.610
1000.0	36.955
10000.0	17.575



Table 4.3 Sequences of Observed and Predicted Events  
for Test S-NC-8

Event	Time (s)	
	Observed	Data RELAP5
Blowdown Initiation	0	0
High Pressure Trip (12.5 MPa)	103	103
SG Steam Valves Closed	117	117
Core Power Starts to Decay	131	131
Break First Uncovered	824	611
Break Final Uncovery	1500	1108
Core Heatup First Observed	1920	---
SG Steam Valves Open	2100	2100
Auxiliary Feed Begins		
Accumulator Setpoint Reached	2460	2563
Calculation Ended	---	2636
Accumulator Tank Depleted		
Broken Loop	3975	---
Intact Loop	4800	---
PORV Opened	7550	---
Second Heatup Observed	8025	---
PORV Closed	8098	---
Start Fill and Dump of SGs	8160	---

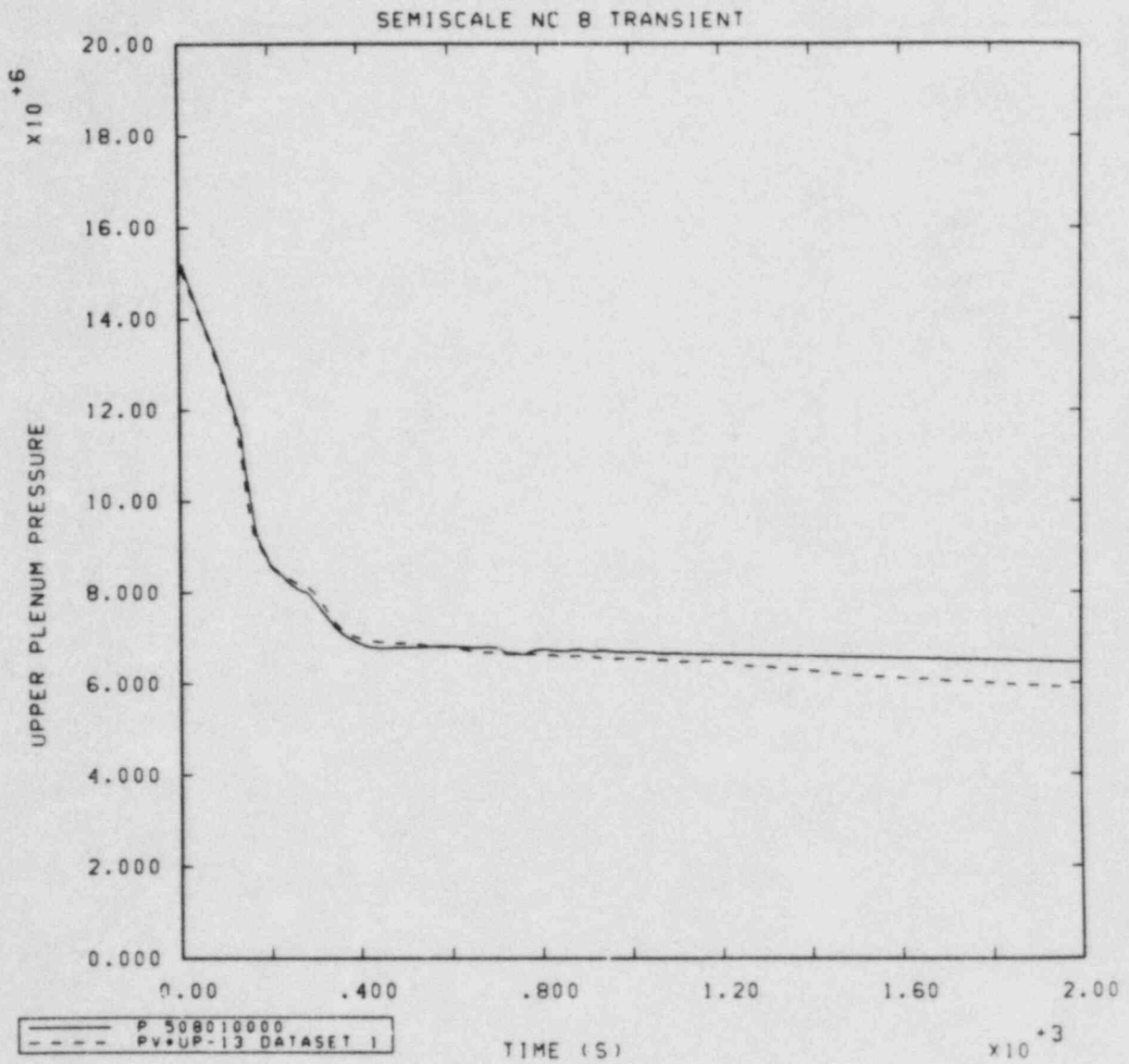


Figure 4.2.1 Measured and Calculated Primary System Pressures vs Time for Test S-NC-8

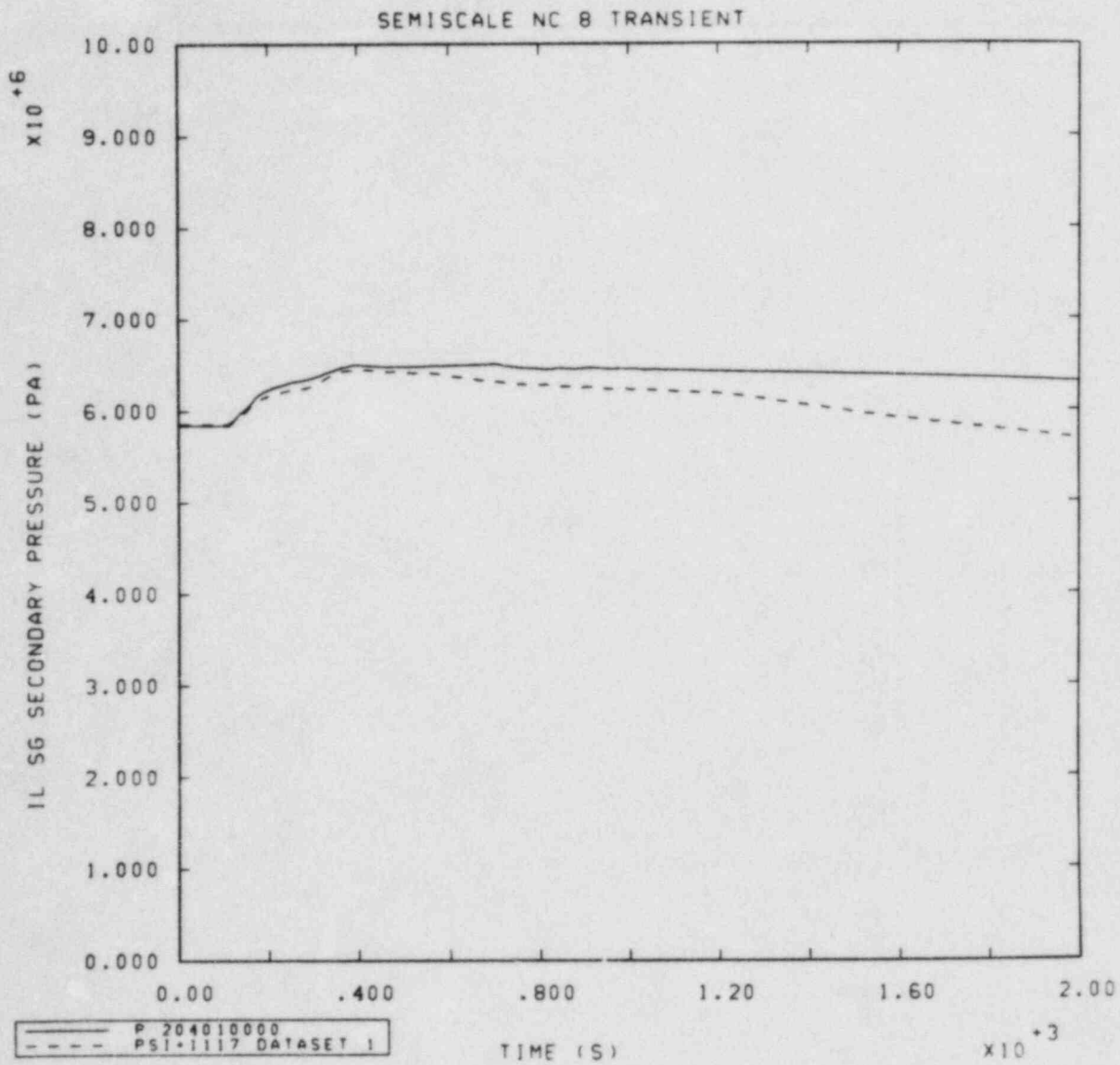


Figure 4.2.2 Measured and Calculated Intact Loop Secondary Pressures vs Time for Test S-NC-8

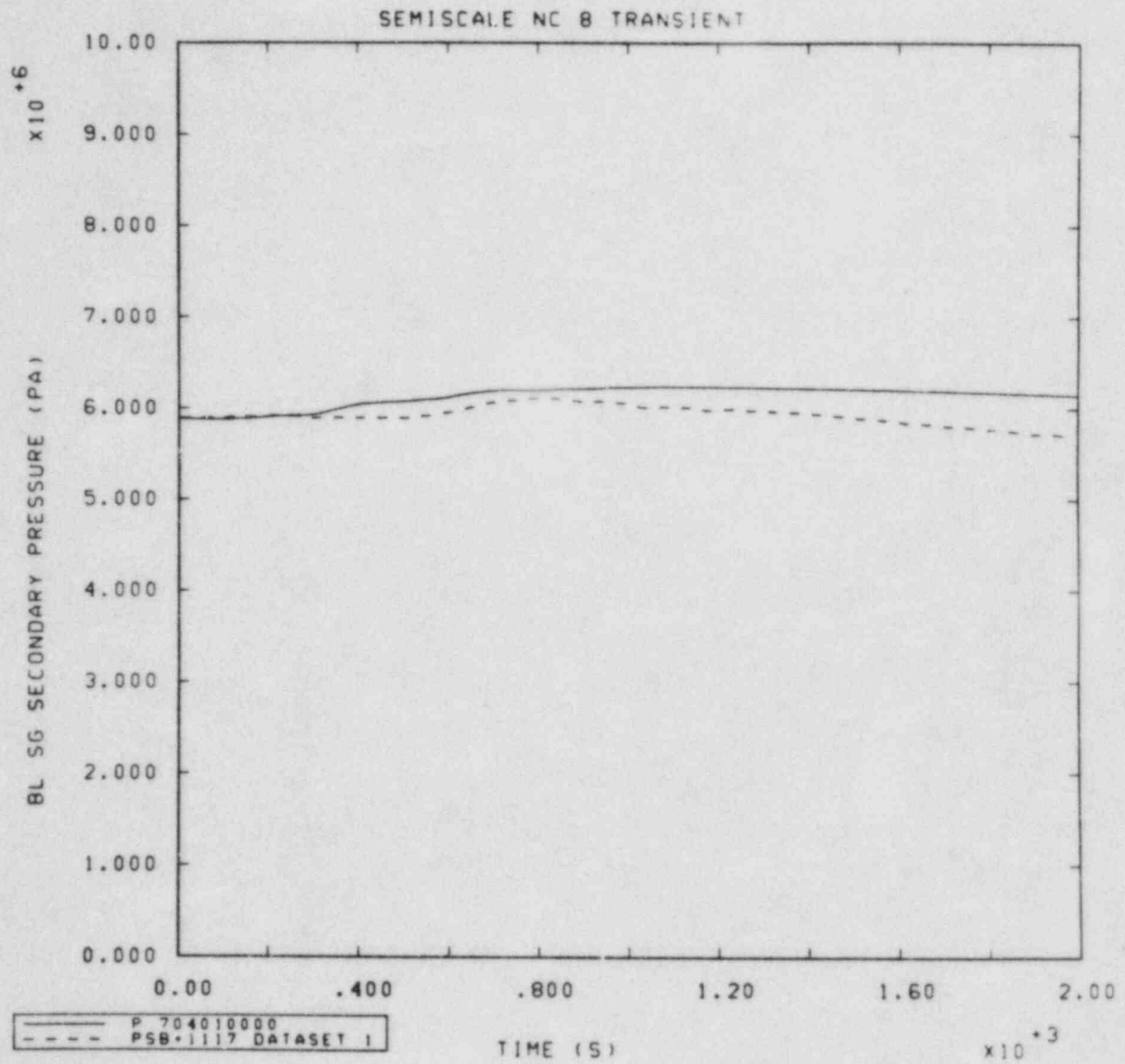


Figure 4.2.3 Measured and Calculated Broken Loop Secondary Pressures vs Time for Test S-NC-8

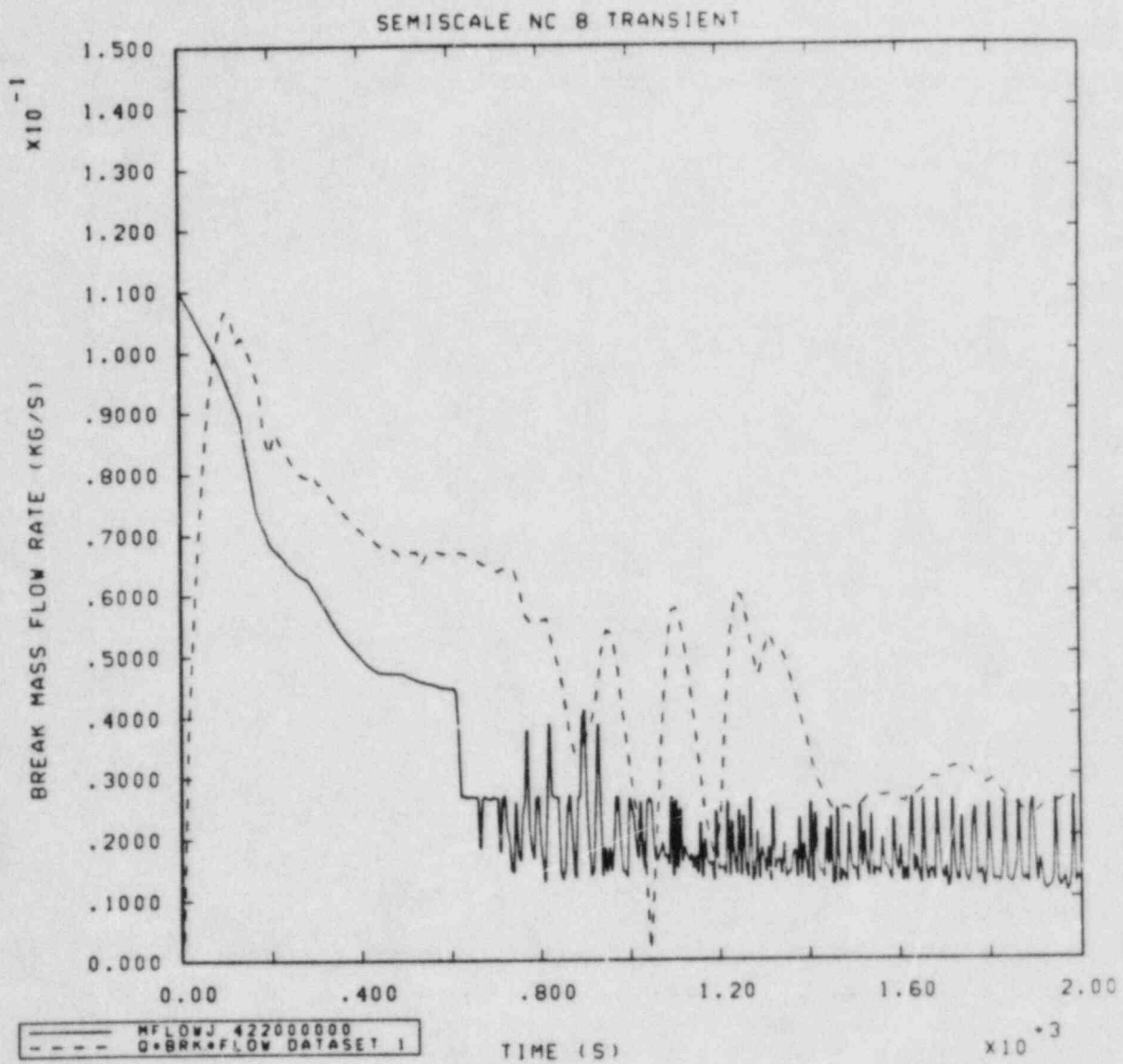


Figure 4.2.4 Measured and Calculated Break Mass Flow Rates vs Time for Test S-NC-8

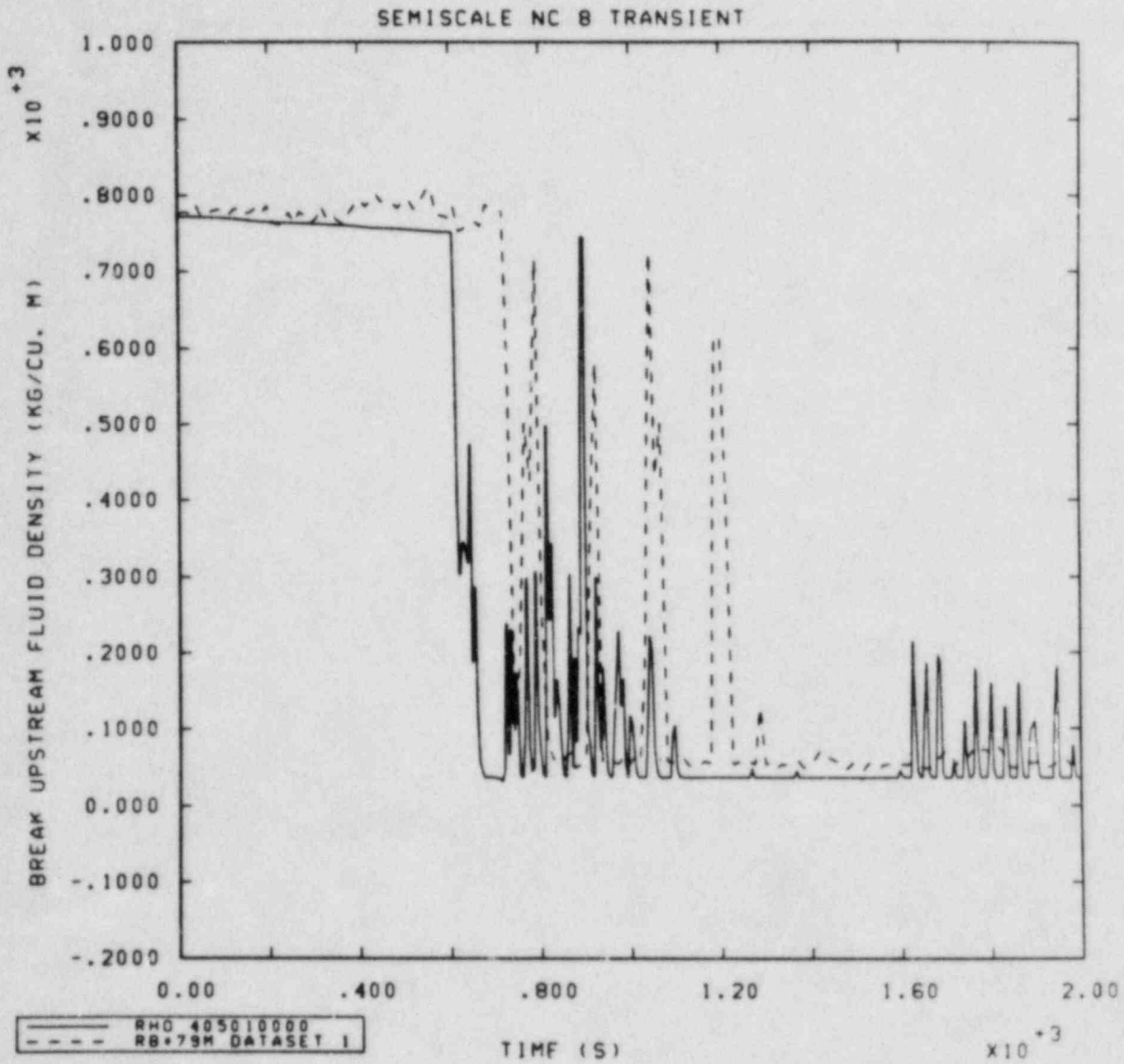


Figure 4.2.5 Measured and Calculated Fluid Densities Upstream from the Break vs Time for Test S-NC-8

SEMISCALE NC 8 TRANSIENT

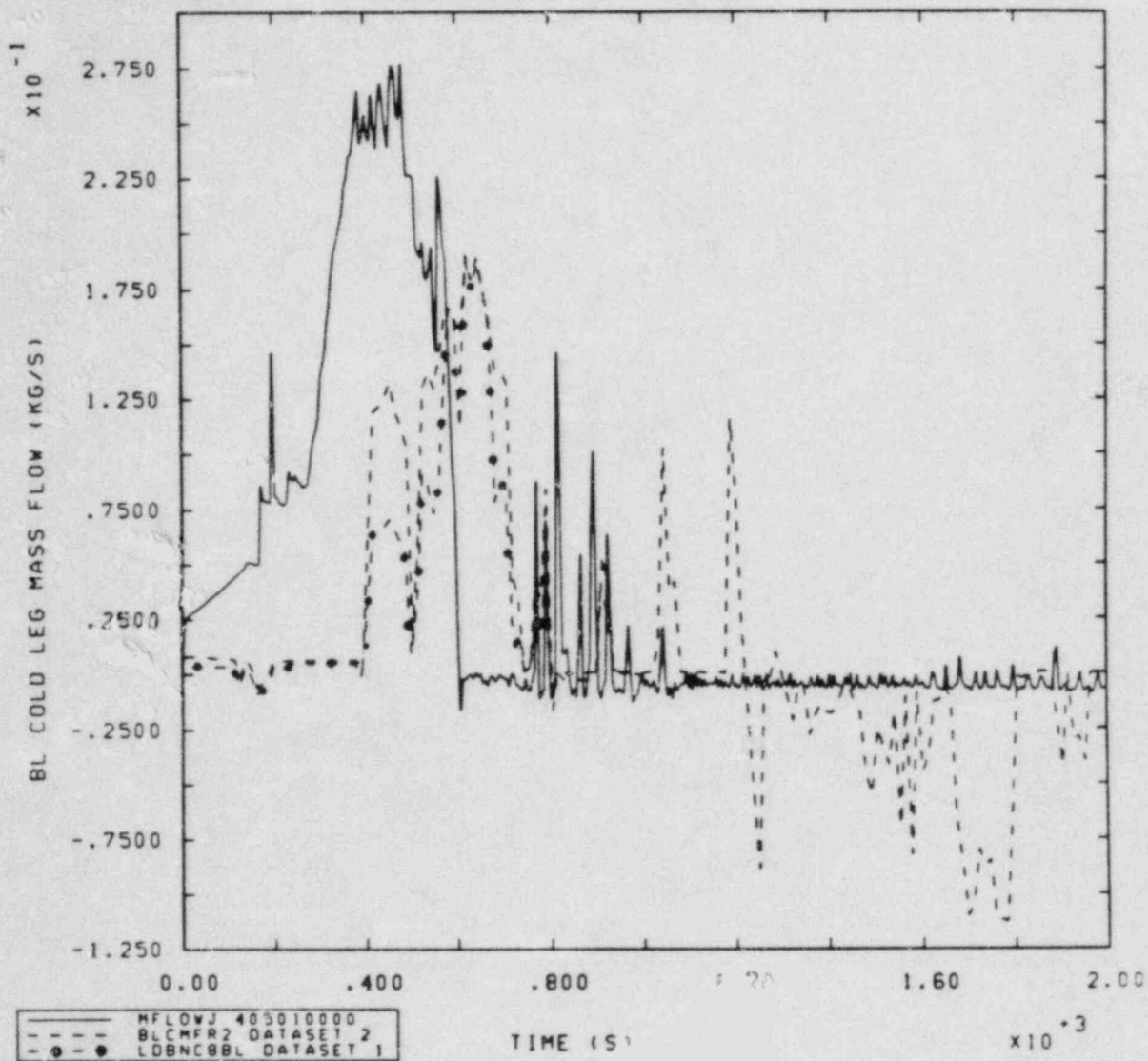


Figure 4.2.6 Measured and Calculated Broken Loop Cold Leg Mass Flow Rates vs Time for Test-NC-8

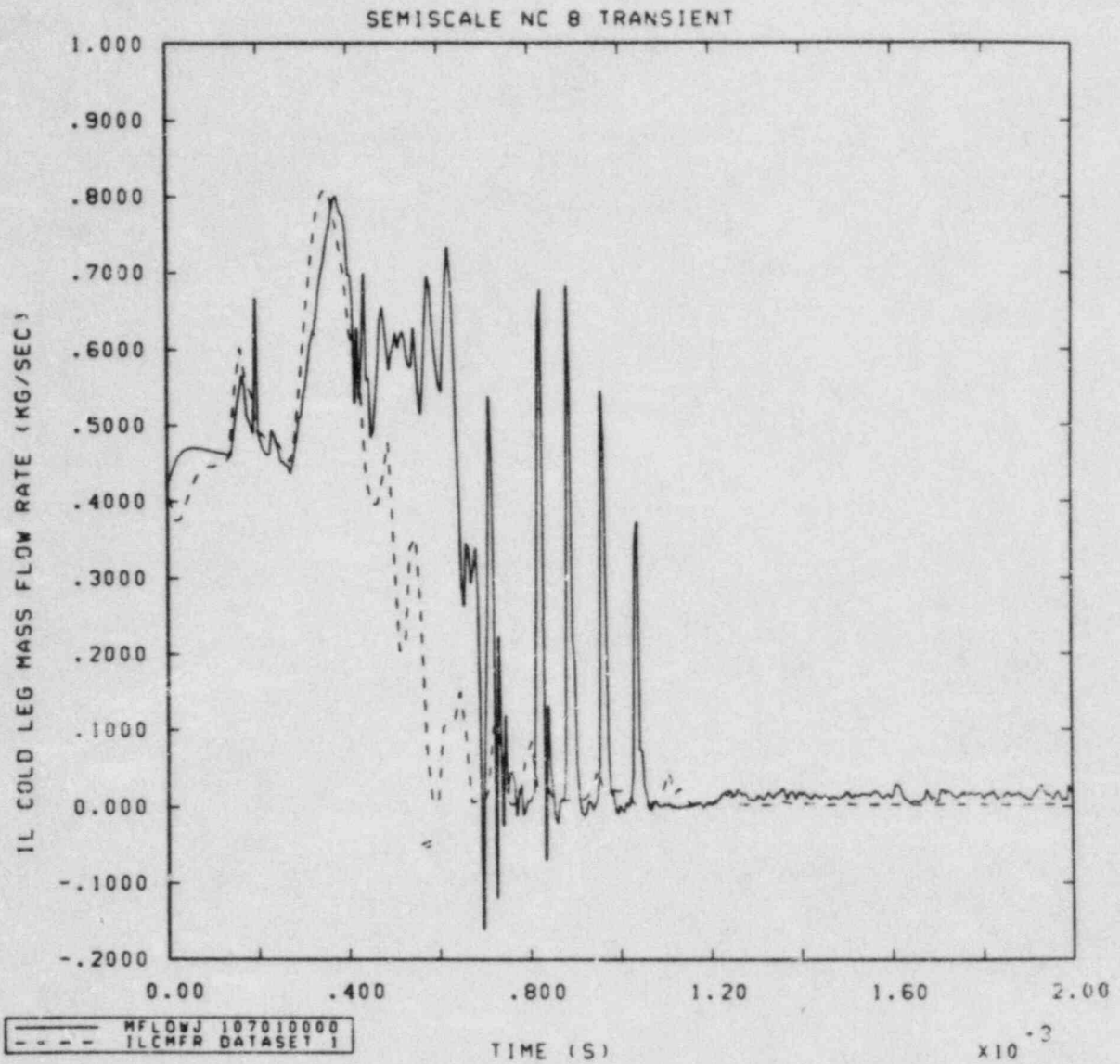


Figure 4.2.7 Measured and Calculated Intact Loop Cold Leg Mass Flow Rates vs Time for Test S-NC-8



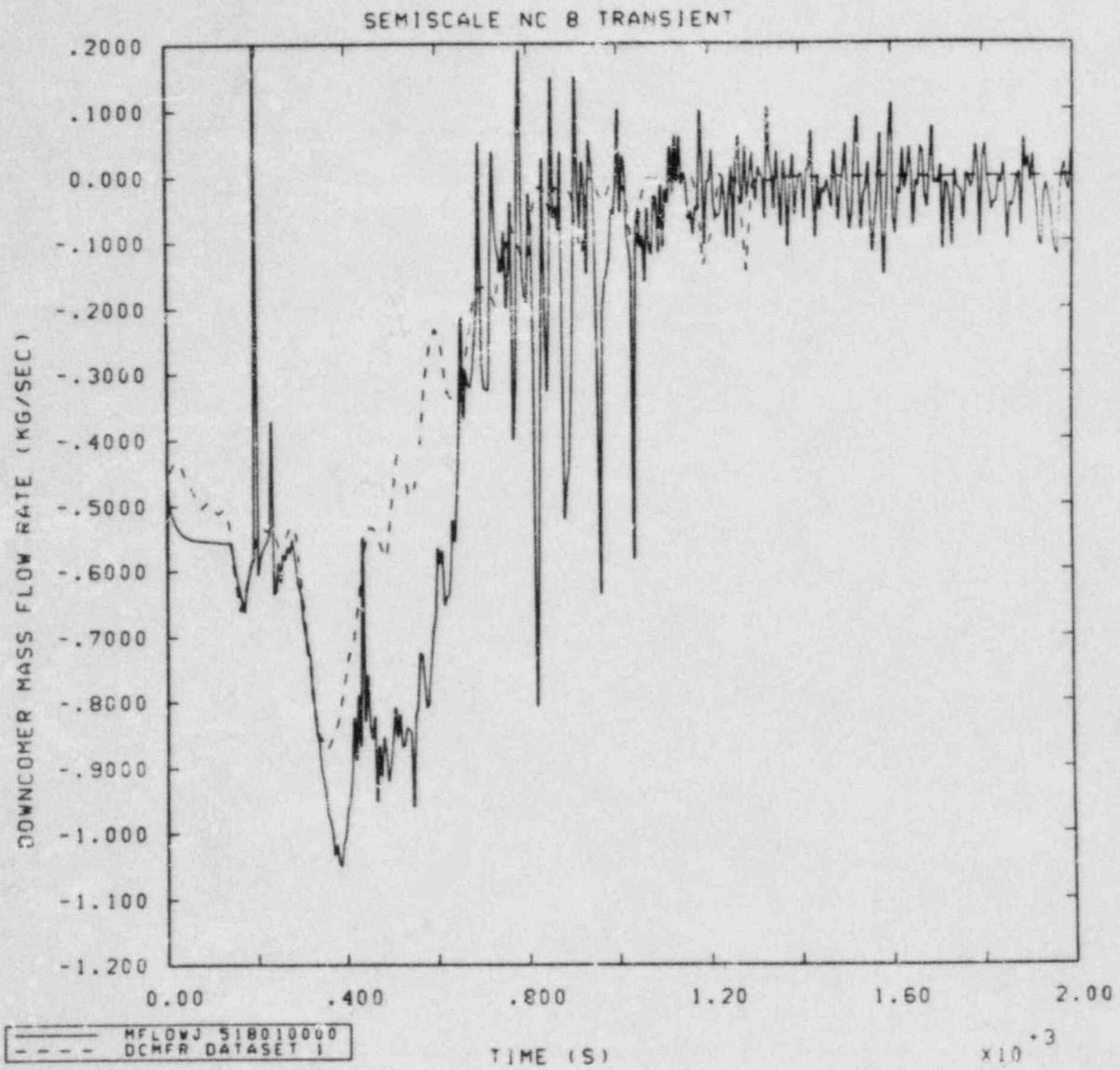


Figure 4.2.8 Measured and Calculated Downcomer Mass Flow Rates vs Time for Test S-NC-8

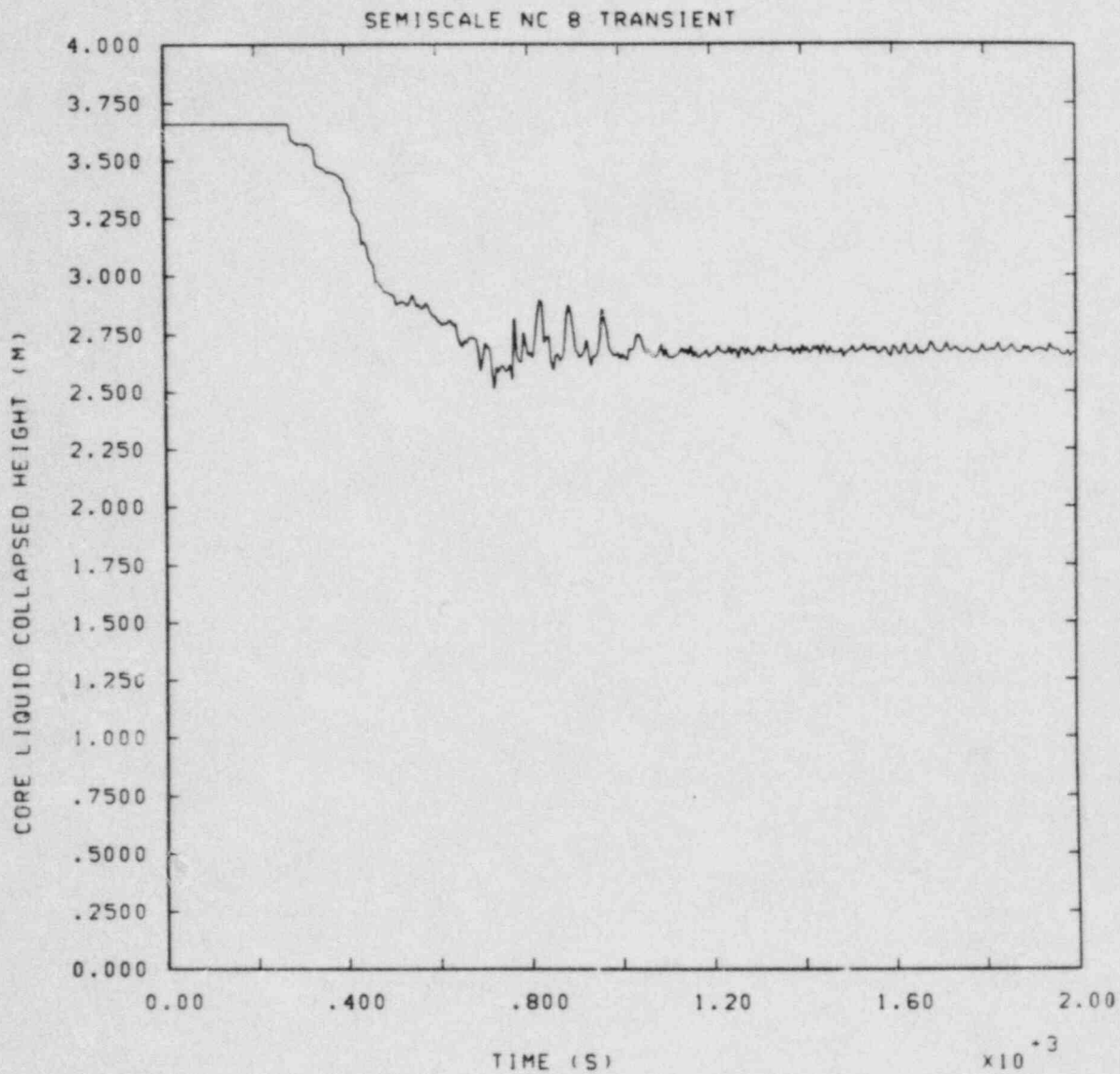


Figure 4.2.9 Calculated Collapsed Liquid Level in the Reactor Core vs Time for Test S-NC-8

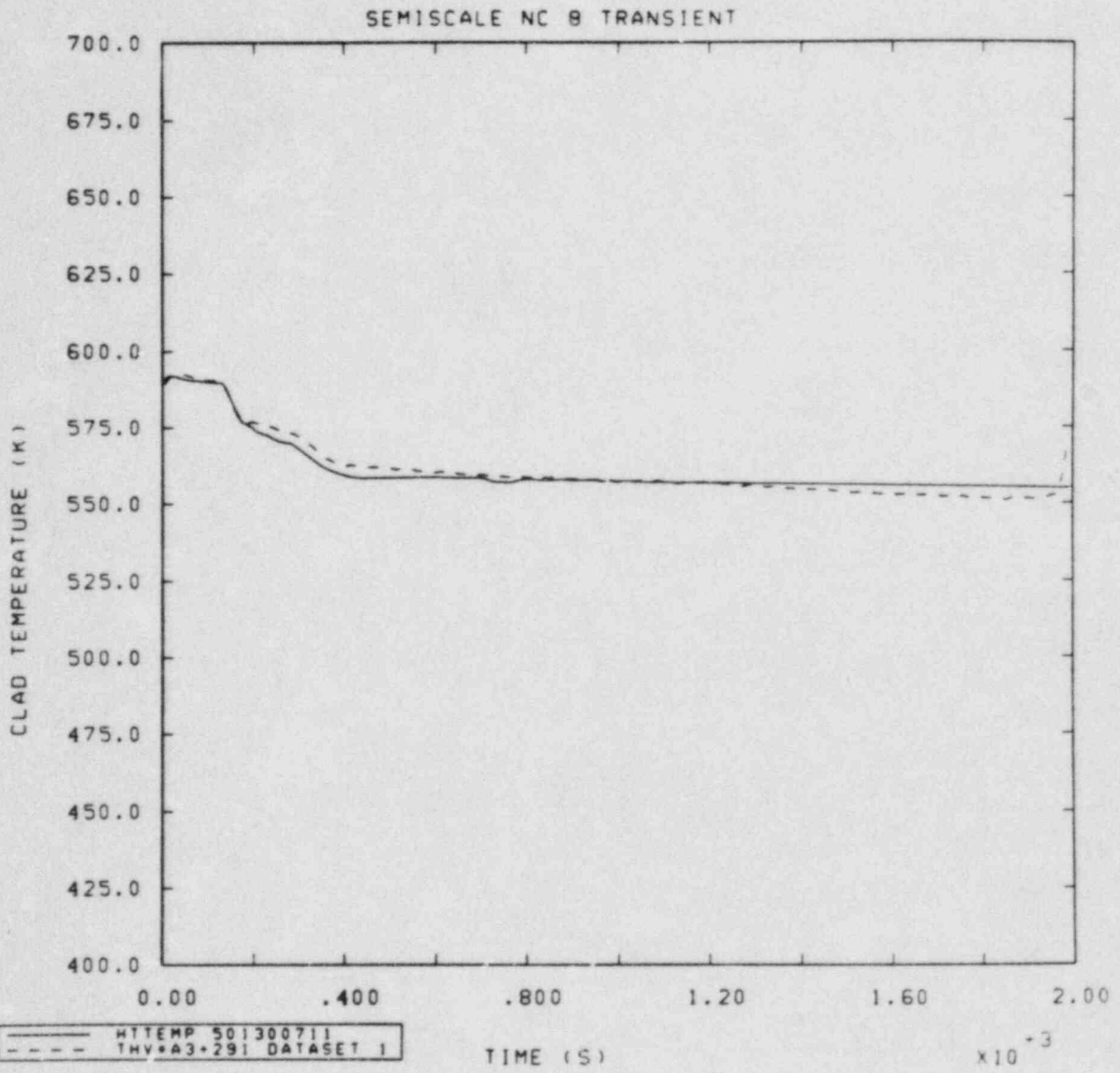


Figure 4.2.10 Measured and Calculated Clad Temperatures at 291 cm above the Bottom of Heated Length vs Time for Test S-NC-8

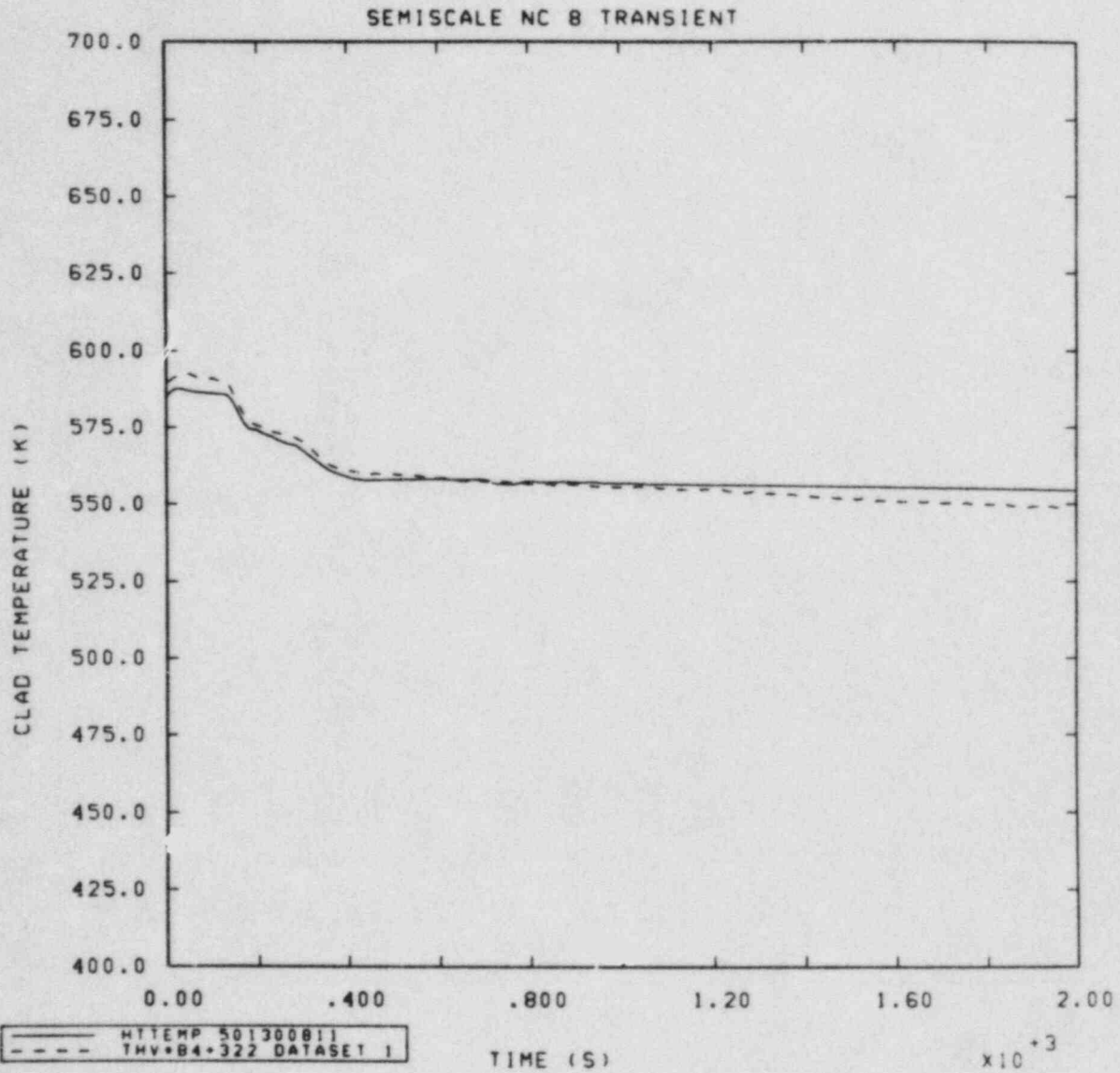


Figure 4.2.11 Measured and Calculated Clad Temperatures at 322 cm above the Bottom of Heated Length vs Time for Test S-NC-8

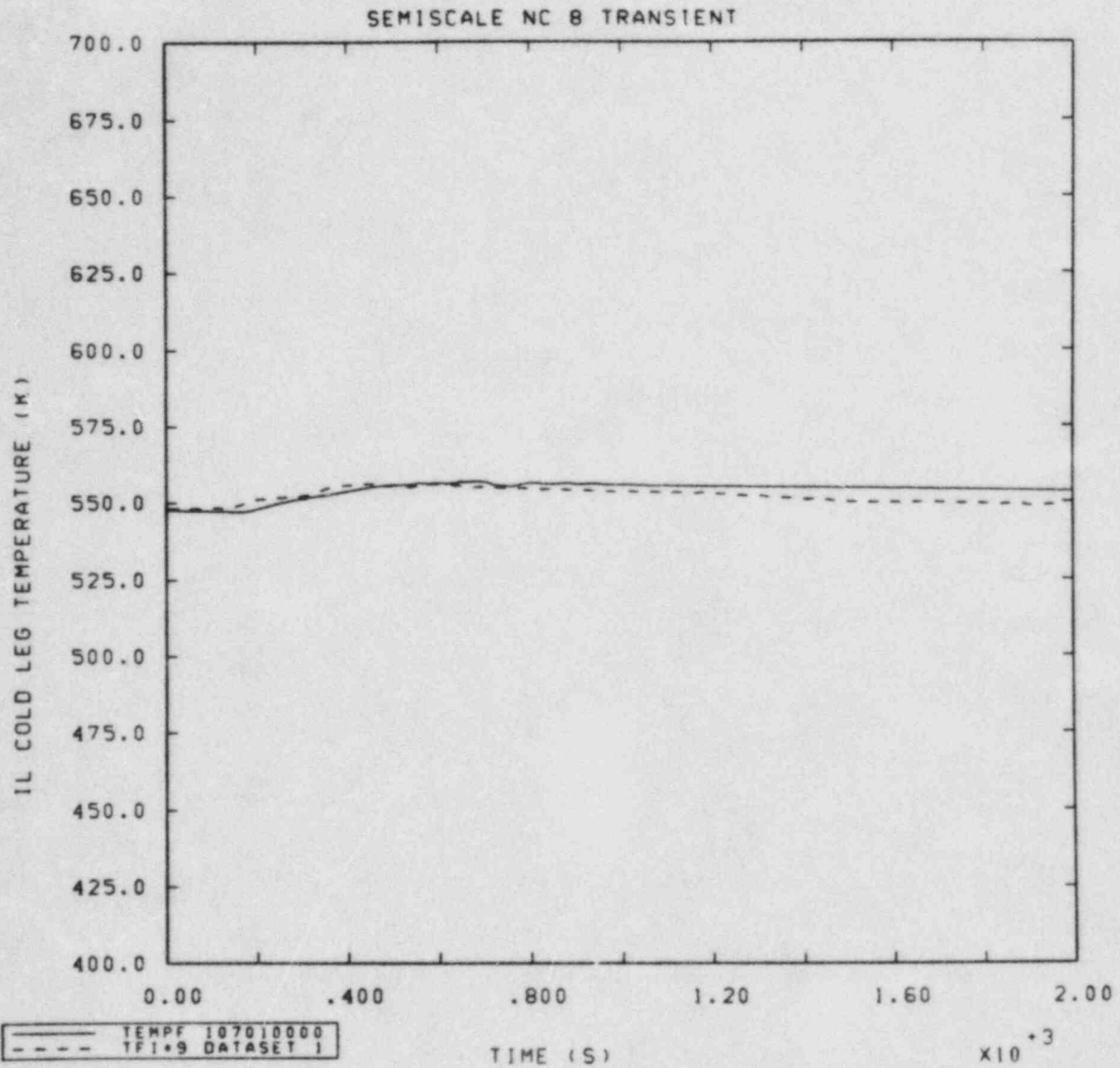


Figure 4.2.12 Measured and Calculated Intact Loop Cold Leg Fluid Temperatures vs Time for Test S-NC-8

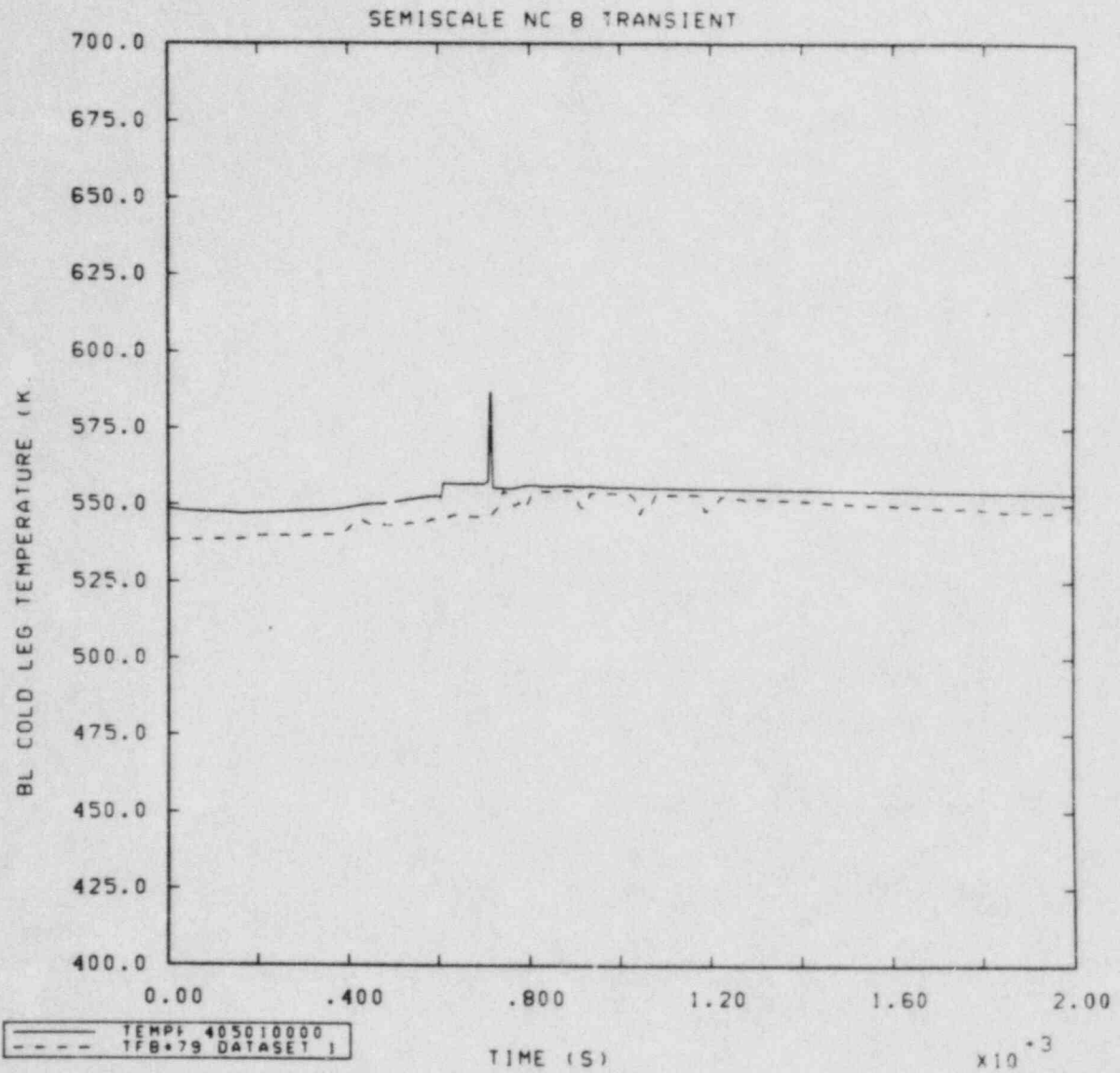


Figure 4.2.13 Measured and Calculated Broken Loop Cold Leg Fluid Temperatures vs Time for Test S-NC-8

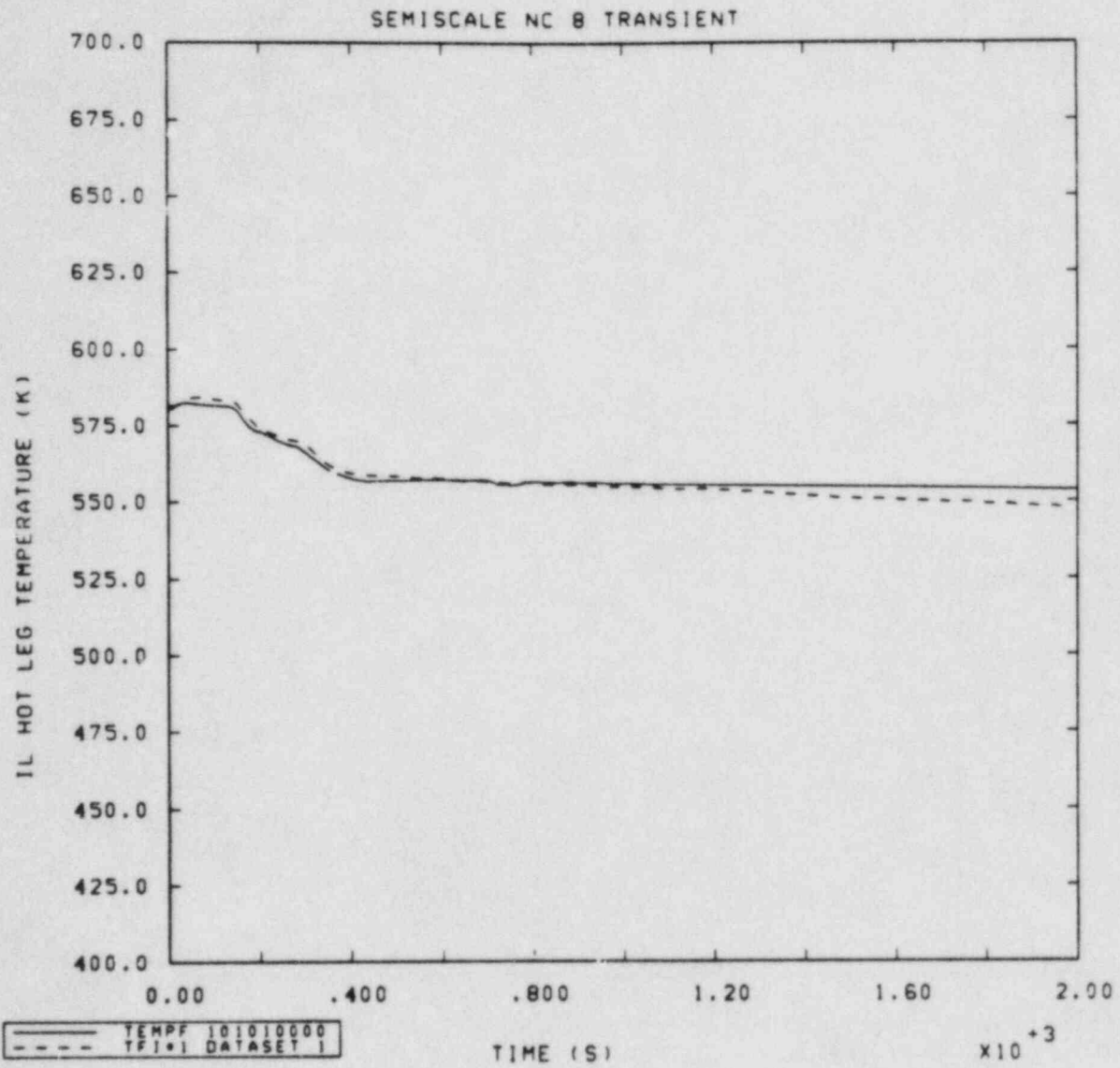


Figure 4.2.14 Measured and Calculated Intact Loop Hot Leg Fluid Temperatures vs Time for Test S-NC-8

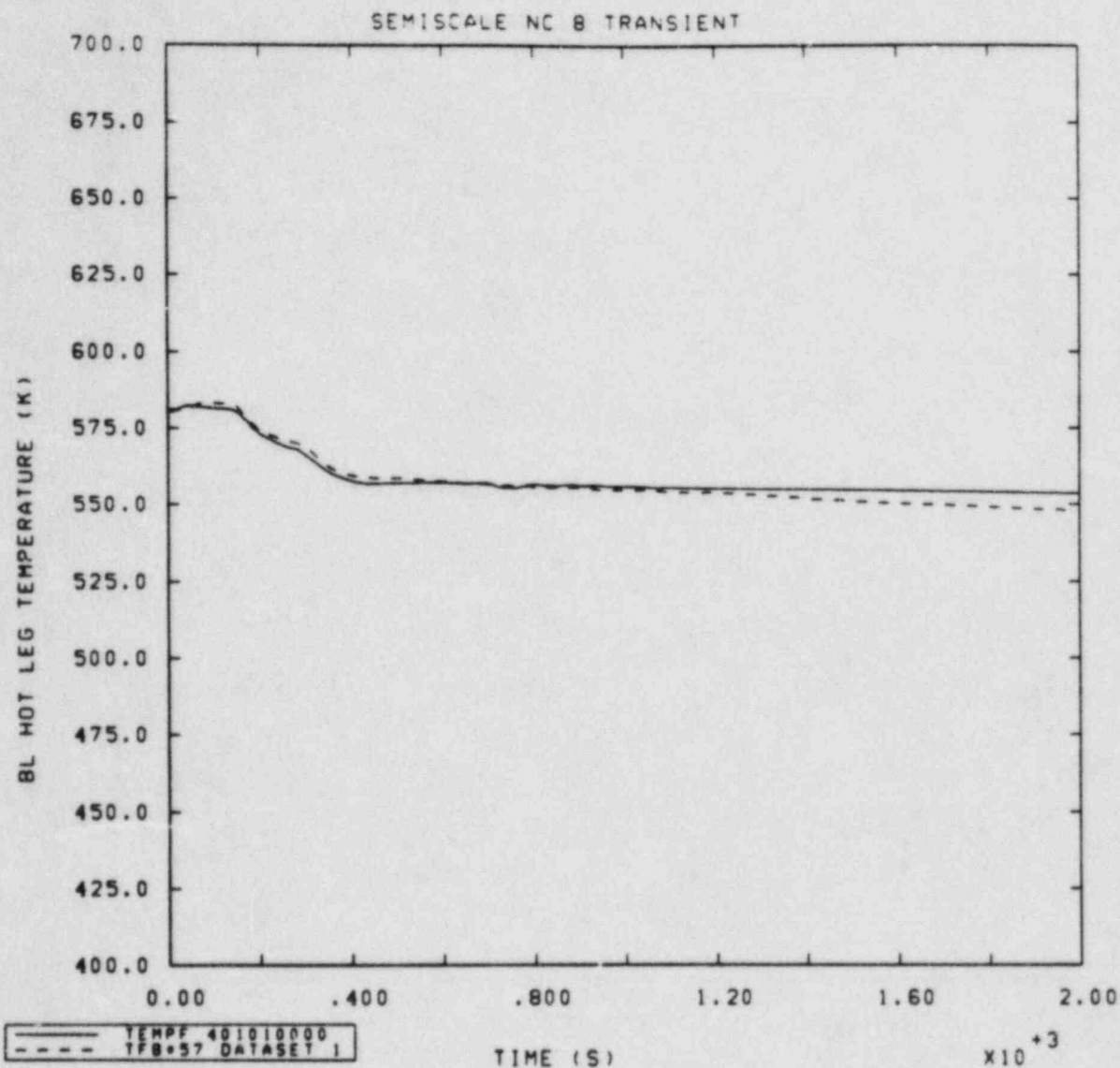


Figure 4.2.15 Measured and Calculated Broken Loop Hot Leg Fluid Temperatures vs Time for Test S-NC-8



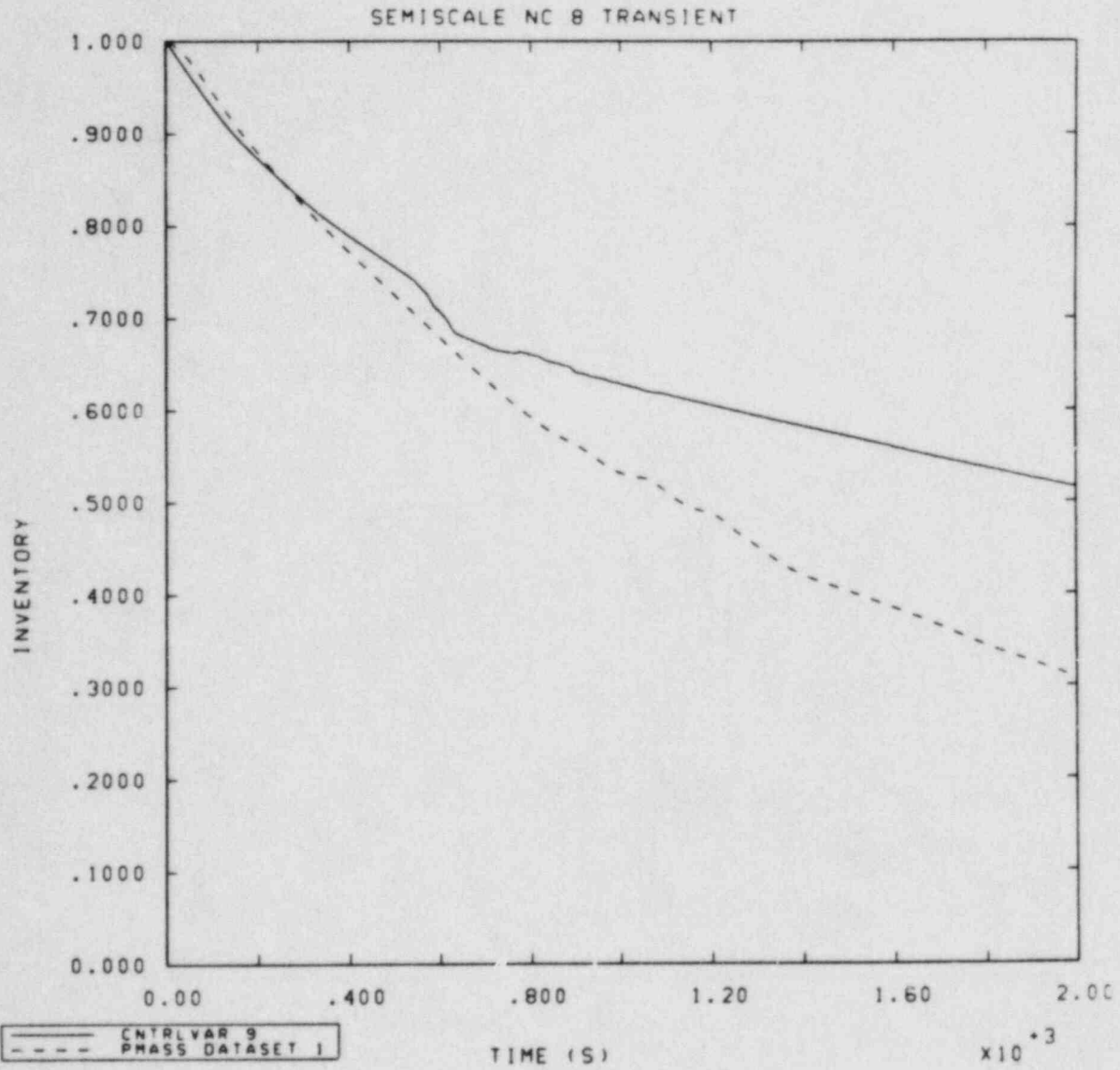


Figure 4.3.1 Measured and Calculated Primary Mass Inventories vs Time for Test S-NC-8

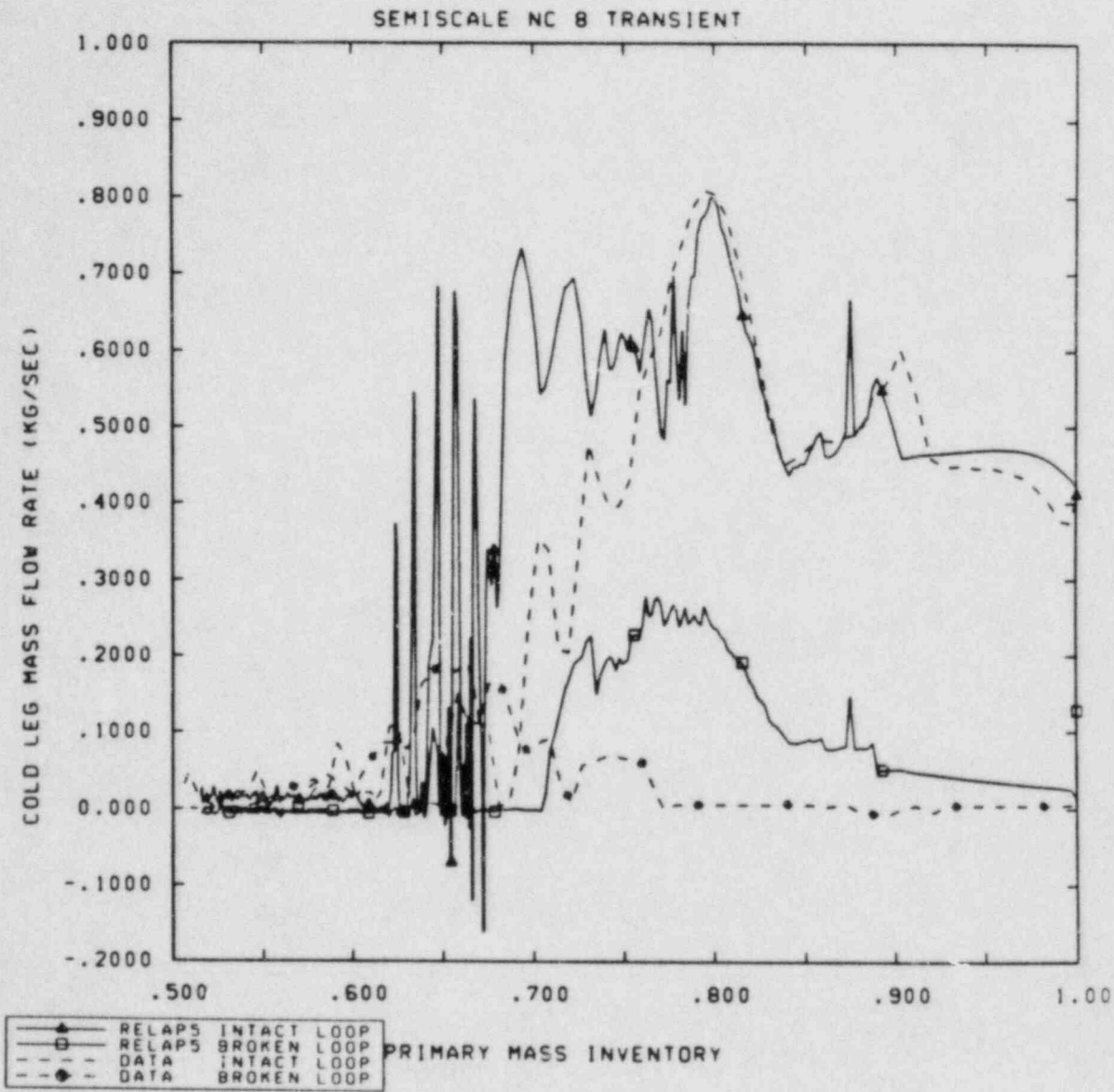


Figure 4.3.2 Measured and Calculated Cold Leg Mass Flow Rates vs Primary Mass Inventory for Test S-NC-8

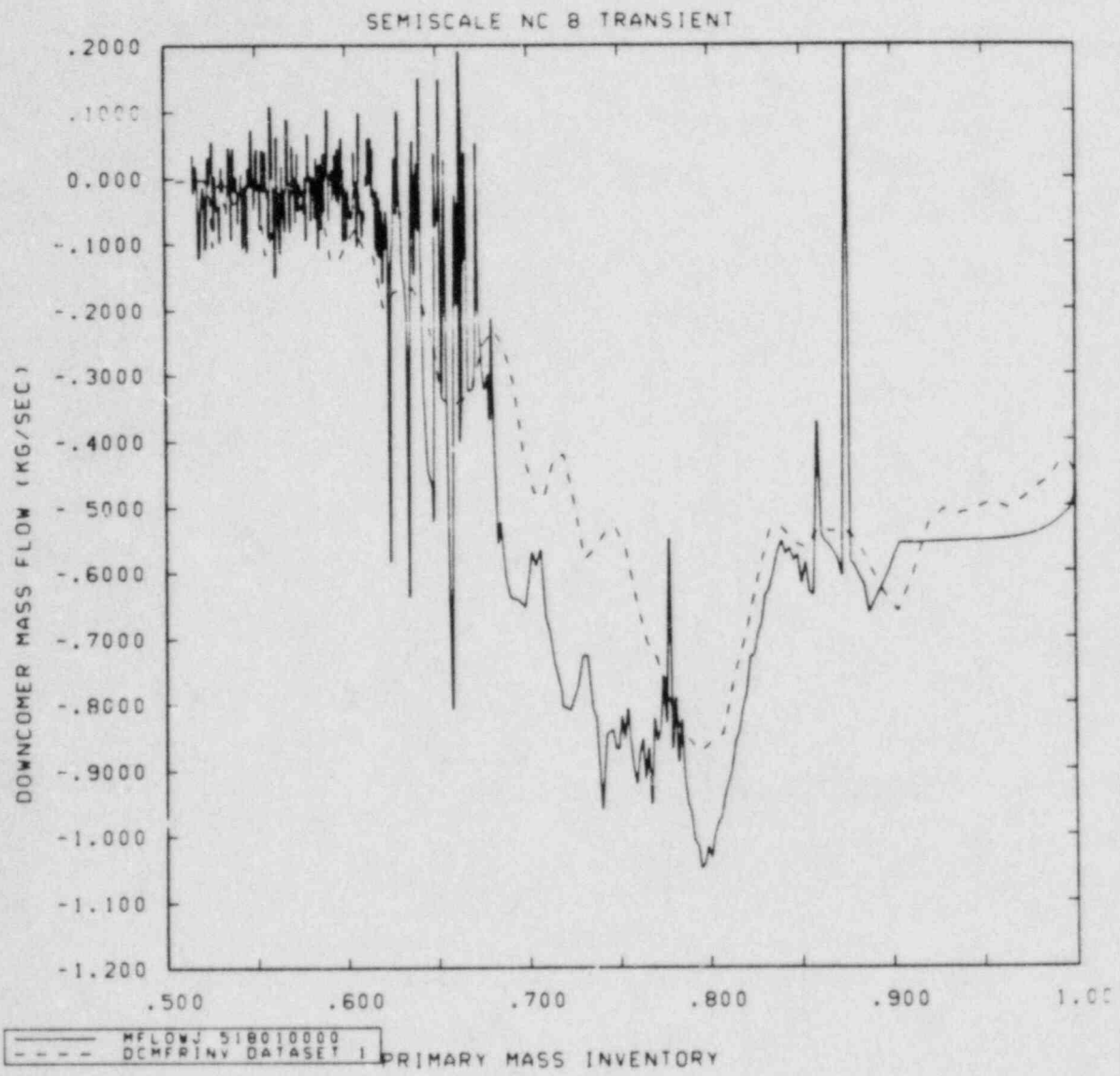


Figure 4.3.3 Measured and Calculated Hot Leg Mass Flow Rates vs Primary Mass Inventory for Test S-NC-8

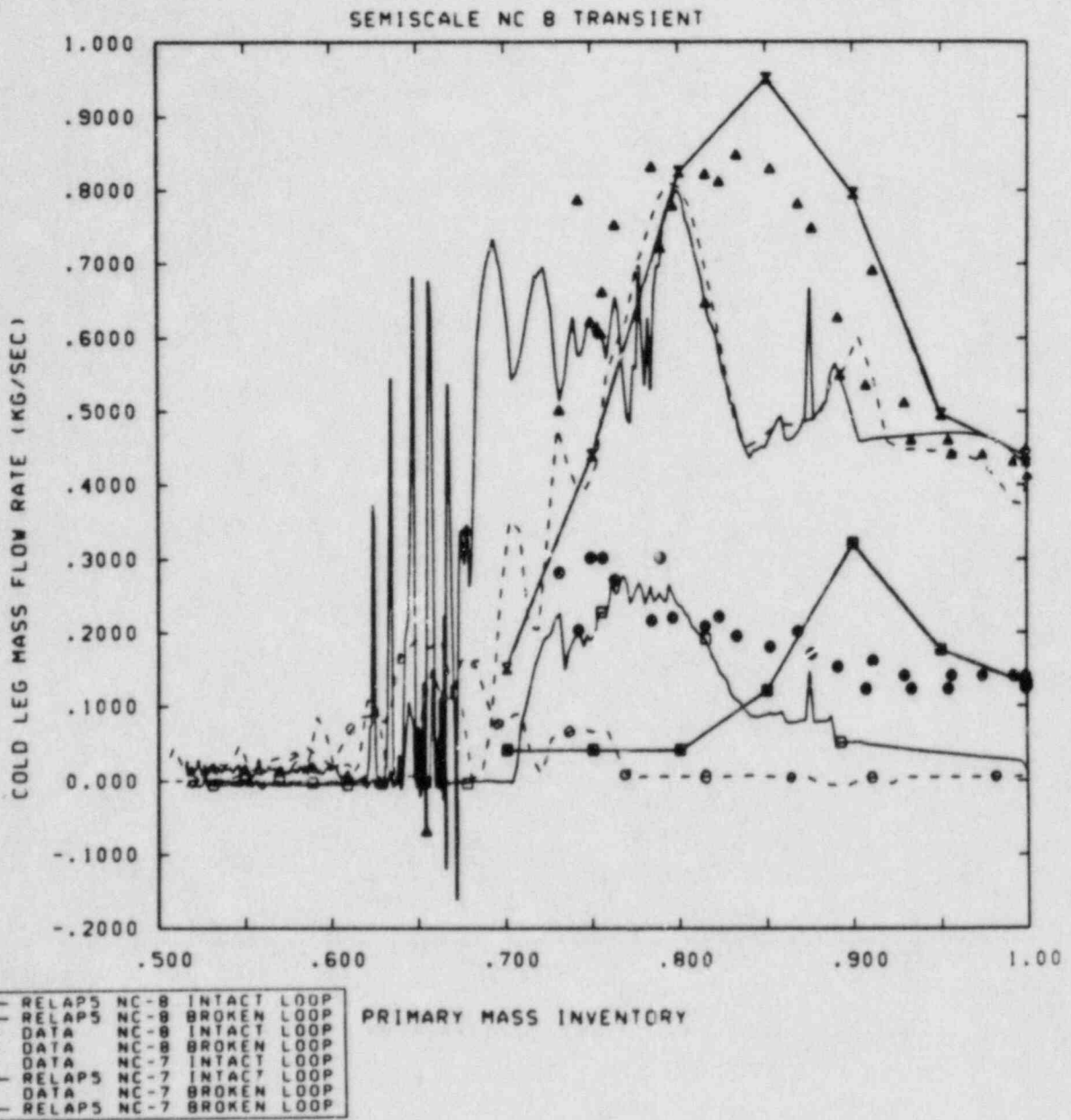


Figure 4.3.4 Measured and Calculated Cold Leg Mass Flow Rates vs Primary Mass Inventory for Tests S-NC-7 and S-NC-8

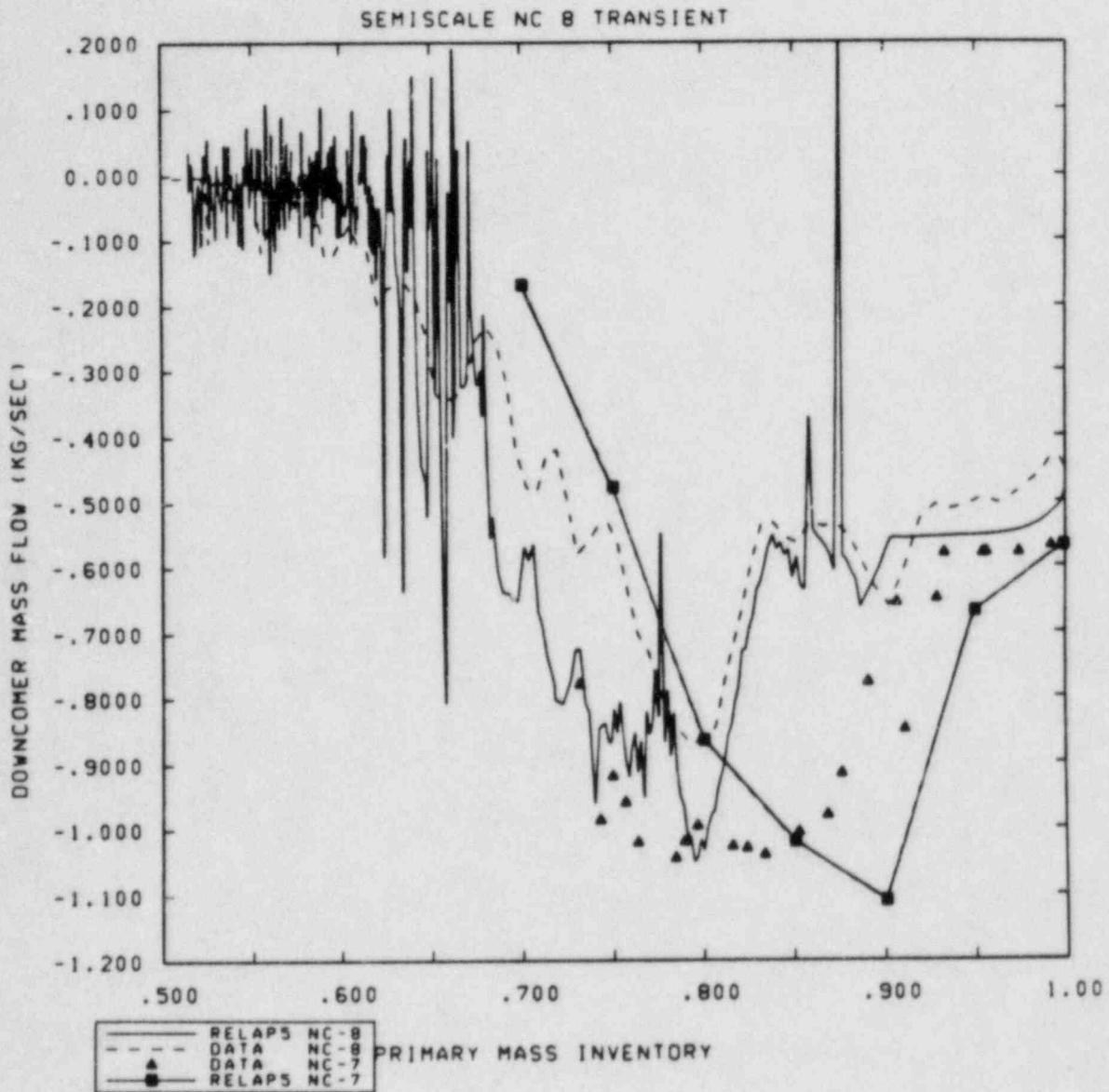


Figure 4.3.5 Measured and Calculated Downcomer Mass Flow Rates vs Primary Mass Inventory for Tests S-NC-7 and S-NC-8

## 5.0 DISCUSSION AND CONCLUSIONS

The results of our earlier analyses of Semiscale one- and two-loop and PKL three-loop steady state natural circulation tests [7,12] show that RELAP5/MOD1 qualitatively describes all modes of natural circulation (including reflux cooling), although with some quantitative discrepancies. The two-phase flows calculated are significantly higher (~10-40%) than those measured in these steady state natural circulation experiments, and the measured and calculated inventories at which the maximum mass flow occurs differ. In this study, RELAP5/MOD1 has now been used to analyze three additional experiments in the natural circulation series performed in the Semiscale facility: the single-loop degraded heat transfer natural circulation tests S-NC-3 and S-NC-4, and the two-loop ultra-small break transient natural circulation test S-NC-8.

Our results for test S-NC-3 show that RELAP5/MOD1 predicts the correct qualitative behavior, with some quantitative discrepancies at low secondary side inventories, for 92% primary mass inventory. For liquid levels as low as 55% of the total tube heat transfer area, primary side natural circulation does not change much at all, while dropping the heat transfer area below 55% causes a corresponding reduction in loop mass flow. Quantitative agreement between calculated and measured flow rate is better if the primary mass inventory in the calculations is set at 85% rather than 92%; agreement for other important parameters such as primary pressure, cold leg temperature and hot leg temperature also improves substantially when the primary inventory is decreased from 92% to 85%.

Our S-NC-2 results for 60 kW core power [7] show peak natural circulation flow at a lower primary inventory (85%) than in the experiment (92%). Thus, at 92% inventory, the peaking two-phase flow in the test indicates bubbles just reaching the top of the U-tubes and being pulled over into the downside, while the still-increasing two-phase flow in the calculation shows all the bubbles condensing out lower in the upside of the U-tubes; in the S-NC-2 calculation, the primary inventory must be dropped to 85% before the calculated two-phase flow peaks and the predicted inventory distribution has bubbles at the U-tube bend. Matching the height and distribution of the two-phase mixture within the U-tubes relative to the height and distribution of secondary side liquid is essential to correctly calculate the degraded heat transfer behavior seen in S-NC-3.

In the reflux cooling test S-NC-4, calculated and measured results for mass flow are somewhat different, with reflux flow oscillations predicted by RELAP5 but not reported in the experiments. Neglecting the presence of these flow oscillations and considering only the time-averaged flow, the comparison between

calculated and measured results is reasonably good. Similar flow oscillations were both seen and calculated in tests S-NC-2 and S-NC-3 at the lower primary and secondary inventories, suggesting that they probably occurred in S-NC-4 also, although the measurements were not fine enough to verify their existence. (The large perturbations in system conditions introduced by the reflux flowmeter and the relatively large uncertainties on measured flow rates preclude more quantitative comparison for S-NC-4.)

Our analysis for the ultra-small cold leg break transient test S-NC-8 shows that RELAP5 simulates this transient event well during the blowdown period. Both hydraulic and thermal system response are predicted accurately. There is good agreement with data for the intact loop and downcomer mass flow rates, although some discrepancies in the broken loop mass flow rate are seen. Pressure response during blowdown agrees reasonably well with measurement. The break mass flow rate is underpredicted, causing some disagreement between calculated and measured primary mass inventory. The overall results verify that, during a small break LOCA, correct calculation of the primary system mass inventory and distribution is important because this controls when and how the core heats up; both the amount of mass left in the system and the long-term system depressurization are primarily determined by the mass flowing out the break, and correct prediction of the break flow appears to be the major requirement for correctly calculating the transient phenomena.

When the mass flow rates are plotted against primary mass inventory rather than problem time, and compared with results from the previous S-NC-7 calculation, similar behavior is seen. Qualitatively, single-phase and two-phase mass flows are correctly simulated for both the steady state two-loop test S-NC-7 and the transient two-loop test S-NC-8, with the maximum mass flow in each loop when the fluid in the upside of its steam generator U-tubes is two-phase and the fluid in the downside is single-phase liquid, as expected. The mass flows in the intact loop are in good agreement everywhere except near the maximum, where the calculation is high, and the shape of the calculated intact loop mass flow curve is very close to the shape of the measured curve, except that the calculated curve is shifted to a slightly higher inventory. The broken loop mass flow at first looks nothing like the experimental data, because of a relatively massive shift in the inventory dependence, but qualitative agreement is still visible on closer examination.

All these natural circulation experiments are stringent tests for the liquid entrainment models in RELAP5. At reduced inventories, essentially all the core power is used in generating steam because there is little subcooling. The mass flow associated with this steam is very small; most of the mass flow is due to the

liquid water entrained by the steam. Mass flows at 100% inventory are generally well matched by the code, implying no gross input errors. The mass flows at very low inventories are small because there is very little entrainment of liquid, and reflux flow is also usually well calculated. The mass flow between these two limiting cases is governed by the entrained liquid. All the natural circulation assessment calculations we have done to date indicate possible problems in the interface drag model (affecting the amount of liquid entrained at any given inventory), and in the two-phase wall friction and loss coefficients for abrupt area changes (affecting the peak values in two-phase natural circulation).

Nonphysical oscillations encountered in all these calculations for two-phase and reflux natural circulation indicate problems in the code's automatic time step control algorithm, since they could be eliminated by the user reducing the time step. Other assessment calculations [7,12,15,16] have also shown that the RELAP5 time step control is inadequate, especially in two-phase situations when there is considerable slip or countercurrent flow between liquid and vapor phases.



## 6.0 REFERENCES

1. V. H. Ransom, et al., RELAP5/MOD1 Code Manual Volume 1: System Model and Numerical Methods; Volume 2: Users Guide and Input Requirements, NUREG/CR-1826, EGG-2070, Idaho National Engineering Laboratory, March 1982.
2. V. H. Ransom, private communication, June 16, 1982.
3. G. G. Loomis and K. Soda, Experiment Operating Specification for the Natural Circulation Test Series (Series NC), Semiscale Mod-2A, EGG-SEMI-5427, Idaho National Engineering Laboratory, April 1981.
4. M. L. Patton, Semiscale Mod-3 Test Program and System Description, NUREG/CR-0239, TREE-NUREG-1212, Idaho National Engineering Laboratory, July 1978, Revision B, January 1981.
5. G. W. Johnsen, Semiscale System Description, Handout at Joint LOFT/Semiscale Modelling Workshop, August 18-19, 1981, at Idaho Falls, ID.
6. M. T. Leonard, RELAP5 Standard Model Description for the Semiscale Mod-2A System, EGG-SEMI-5692, Idaho National Engineering Laboratory, December 1981.
7. J. M. McGlaun and L. N. Kmetyk, RELAP5 Assessment: Semiscale Natural Circulation Tests S-NC-2 and S-NC-7, NUREG/CR-3258, SAND83-0833, Sandia National Laboratories, May 1983.
8. G. G. Loomis and K. Soda, Quick-Look Report for Semiscale Mod-2A Test S-NC-3, EGG-SEMI-5522, Idaho National Engineering Laboratory, August 1981.
9. T. M. O'Connel, Experimental Data Report for Semiscale Mod-2A Natural Circulation Tests S-NC-2B, S-NC-3, and S-NC-4B, NUREG/CR-2454, EGG-2141, Idaho National Engineering Laboratory, December 1981.
10. G. G. Loomis et al, Quick-Look Report for Semiscale Mod-2A Test S-NC-2, EGG-SEMI-5507, Idaho National Engineering Laboratory, July 1981.
11. K. Soda et al, Quick-Look Report for Semiscale Mod-2A Test S-NC-4, EGG-SEMI-5549, Idaho National Engineering Laboratory, August 1981.
12. S. L. Thompson and L. N. Kmetyk, RELAP5 Assessment: PKL Natural Circulation Tests, NUREG/CR-3100, SAND82-2902, Sandia National Laboratories, January 1983.

13. G. G. Loomis and C. M. Kullberg, Quick-Look Report for Semiscale Mod-2A Tests S-NC-8A and S-NC-8B, EGG-SEMI-5678, Idaho National Engineering Laboratory, December 1981.
14. K. E. Sackett and L. B. Clegg, Experiment Data Report for Semiscale Mod-2A Natural Circulation Test Series (Tests S-NC-8B and S-NC-9), NUREG/CR-2648, EGG-2184, Idaho National Engineering Laboratory, April 1982.
15. S. L. Thompson and L. N. Kmetyk, RELAP5 Assessment: LOFT Turbine Trip L6-7/L9-2, NUREG/CR-3257, SAND83-0832, Sandia National Laboratories, July 1983.
16. R. K. Byers and L. N. Kmetyk, RELAP5 Assessment: LOFT L9-1/L3-3 Anticipated Transient with Multiple Failures, NUREG/CR-3337, SAND83-1245, Sandia National Laboratories, August 1983.
17. J. L. Orman and L. N. Kmetyk, RELAP5 Assessment: LOFT Intermediate Breaks L5-1/L8-2, NUREG/CR-3406, SAND83-1575, Sandia National Laboratories, August 1983.

## APPENDIX I FACILITY DESCRIPTION

The standard Semiscale Mod-2A system [4,5,6], shown in Figure AI.1, consists of a vessel with its associated internals and an external downcomer, an intact loop and a broken loop both with active steam generators and pumps, a break effluent measuring system and a steam generator secondary system. Other subsystems include the emergency core cooling system, external heat loss makeup system, leakage makeup system and a noncondensable gas injection system. The Semiscale system was scaled from a reference PWR system based on the core power ratio, 2/3411; component elevations, dynamic pressure heads and liquid distribution were maintained as similar as practical, most notably in the design of a full-length core, full-length upper plenum and upper head, and full-height steam generators. The major primary coolant system elevations are given in Table AI.1.

The intact loop consists of a steam generator, primary coolant pump, and pressurizer connected by piping; the intact loop piping itself is composed of individual pipe sections called spool pieces. These spool pieces and their relative locations in the intact loop are identified by spool numbers in Figure AI.2; the upper drawing unfolds the intact loop for easier viewing by preserving the orientation of the components in the vertical plane without regard to the actual horizontal orientation, which is shown in the lower drawing. The spool piece lengths and blueprint numbers are given in Table AI.2. The intact loop piping, other than the vertical spool pieces leading to the steam generator inlet and outlet (spools 4 through 12) and spool 3, are constructed of 3-in. Sch 160 Type 316 stainless steel pipe; spool pieces 3 through 12 are constructed of 2-1/2-in. Sch 160 pipe. A special pump replacement spool piece connecting the pump suction to the cold leg was used instead of the intact loop pump in these natural circulation tests to minimize leaks in the Semiscale system. It was constructed of 1-1/2-in. Sch 160 piping, and included an orifice to simulate the locked rotor resistance of the pump.

The broken loop is designed to simulate a single loop of a four-loop PWR; in addition to a break assembly, it also contains an active steam generator and pump. The spool pieces in the broken loop are constructed of 1-1/2-in. Sch 160 Type 316 stainless steel piping; these spool pieces and their relative locations in the broken loop are identified by spool numbers in Figure AI.3, and the corresponding spool piece lengths and blueprint numbers are given in Table AI.3. The broken loop pump is a high-speed vertical centrifugal pump with a bottom suction and side discharge, similar to PWR pumps. A flow restriction is incorporated into the pump discharge to give the properly scaled locked rotor hydraulic resistance. (This pump was used in the two-loop natural circulation tests for warmup purposes and was therefore physically present during the S-NC-8 test, but the pump rotor was kept locked during the actual test.)

The break assembly for S-NC-8 was designed to simulate a 0.4% centerline break; it includes an orifice plate, shown in Figure AI.4, which provides a break area of 0.009 cm<sup>2</sup>. The blowdown transient is initiated by opening a valve downstream of the orifice plate. The blowdown effluent is first condensed, and then collected in vented catch tanks; differential pressure cell measurements in the tanks are used to calculate the break flow rate.

The intact and broken loop steam generators, shown in Figure AI.5 and summarized in Table AI.4, consist of a two-pass tube and shell design with primary fluid flowing through vertical inverted U-shaped tubes and secondary coolant passing through the shell side. With the secondary side operating at saturation conditions, a centrifugal separator at the top of the riser or boiler section increases the exit quality of the steam rising through the steam dome and out a discharge line, while liquid separated from the steam falls down a downcomer outside the boiler shroud creating a recirculation flow path. The intact loop steam generator has two short, two medium and two long tubes representative of the range of bend elevations in a PWR steam generator, while the broken loop steam generator contains just one short tube and one long tube. The same tube stock (2.22 cm, 0.124 cm wall) and tube spacing (3.175 cm triangular pitch) used for PWR U-tubes are used in this "Type II" steam generator. Since the heat transfer area is specified based on the ratio of PWR to Semiscale primary system volume, the number of tubes is thereby fixed by the specified tube diameter and lengths.

Fillers are installed on the shell side in both the boiler and downcomer regions to provide a more properly scaled secondary fluid volume. The addition of these filler pieces not only reduces the total secondary coolant volume, but also changes the flow geometry of the boiler and downcomer, as shown in the cross-sectional view in Figure AI.5. The boiler section filler pieces create a parallelogram-shaped flow channel along the length of the U-tubes, while the downcomer filler pieces reduce the downcomer annulus to a set of slotted flow channels. Baffle plates are located at several axial positions in the boiler section of the steam generator, creating a substantial flow restriction to the rising coolant. Feedwater enters the downcomer above the filler pieces at approximately the elevation of the top of the U-tubes; auxiliary feedwater is also added at this point. The elevations of the steam generator nozzles, plena and tubes are similar to those in a PWR; however, the steam dome is shorter than a PWR steam dome and the steam drying equipment is of a simpler and less efficient design. (As a result of these dissimilarities, the secondary fluid operating level at full power conditions is about 75% of the operating level in a PWR, with the lower level required to ensure stable steam generator operation.)

The pressurizer, which is connected to the intact loop hot leg, is shown in Figure AI.6. The pressurizer vessel is made of 10-in. Sch 160 Type 347 stainless steel pipe, is approximately 1.14 m high and has a total volume of 0.034 m<sup>3</sup>. Heat is supplied by 24 0.05-kW vertically oriented electric heater rods, which are inserted in 2.2 cm stainless steel tubes sealed at the bottom. A pressurizer spray system is not included in the Mod-2A system. The pressurizer operates in a manner similar to its counterpart in a large PWR in that the vessel is partially filled with water and maintained at a saturation temperature corresponding to the desired system pressure. The pressurizer surge line and tubing (1.27 cm OD, 0.165 cm wall, ~2.7 m length and ~1.53 m total elevation drop from bottom of pressurizer vessel to hot leg centerline) is sized for a flow restriction that provides representative flow rates.

The Mod-2A vessel, shown in Figure AI.7, consists of a multi-section pressure vessel containing a lower plenum, heated core, upper plenum and upper head, and an external inlet annulus and downcomer. The pressure vessel is constructed primarily of 6-in. Sch XXS stainless steel pipe, with stainless steel Grayloc clamps used to connect the various vessel sections; the complete pressure vessel is approximately 10 m long. The upper head was removed and the vessel capped at the upper support plate for these natural circulation tests, and a bypass line was installed between the upper plenum and downcomer.

The upper plenum region, shown in more detail in Figure AI.8, extends from the upper core support plate to the top of the heated core region, and is approximately 2.5 m long. The upper and lower sections of the upper plenum contain fillers and insulators similar to those in the upper head. Two hot leg nozzles extend from the vessel upper plenum approximately 21.6 cm above the cold leg centerline to provide connections for the intact and broken loop hot leg piping. The flow path above the core to the hot leg nozzles is quite tortuous; in addition to a core flow measurement assembly, a simulated control rod guide tube and two simulated core support columns obstruct the flow path, and a short set of vertical tubes creates a horizontal flow restriction across the vessel at the hot leg elevation. This flow restrictor assembly simulates the flow restriction in a PWR caused by control rod guide tubes and core support columns. Above the hot legs, the upper plenum contains a significant amount of fluid which is not involved in the main flow path. The simulated control rod guide tube and core support columns extend from the upper head through the upper plenum and terminate open-ended in the upper core plate located in the heater ground hub which forms the boundary between the upper plenum and the top of the active heated core region. The guide tube is slotted in the upper plenum region.

The 3.66 m heated length of the core, shown in Figure AI.9, extends downward from the heater rod ground hub to the top of the mixer box (approximately 4.96 m below the cold leg centerline), which separates the core and the lower plenum regions. This figure includes a cross-sectional view of the Mod-2A vessel over the core region. The 25-rod electrically heated core is enclosed in a square housing with no coolant bypass. The heater rods, 1.07 cm in diameter, are positioned and held in the core with 10 grid spacers (at elevations shown in Figure AI.10) which maintain the heater rods on a typical PWR pitch of 1.43 cm. The 16 peripheral rods are powered separately from the 9 central rods, permitting a radial profile (although normally no radial peaking is simulated); two of the 16 peripheral rods, however, are not powered. The Semiscale Mod-2A heater rod design consists of a helically-wound constantan filament, electrically insulated from the dual-sheath stainless steel clad by compacted boron nitride powder. Chromel-alumel thermocouples are swaged between cladding sheaths in six symmetrical polar locations and ten axial elevations distributed along the rod. The heater rods have a symmetric chopped-cosine axial power distribution (shown in Figure AI.10); the peak-to-average power ratio is 1.55.

The lower plenum, shown in Figure AI.11, consists of an annular region between the flow mixer box and the pressure vessel, which serves to distribute flow from the downcomer pipe around the vessel periphery, and a lower head chamber region below the mixer box which approximates the scaled volume of a PWR lower plenum. (The lower plenum is the only part of the vessel which is not height-scaled.) Coolant flow from the downcomer distribution annulus changes direction within the lower head, turning up into the core housing. A simulated lower core plate at the entrance of the core housing provides a significant reduction in coolant flow area. The outer walls of the downcomer distribution annulus and the lower head are lined with honeycomb insulation to reduce heat transfer between the outer vessel wall and the fluid in the lower plenum. The heater rods pass through the length of the lower plenum and penetrate the vessel through the bottom head. There is a drain line in the lower plenum (not shown in the figure) that allows controlled draining of the vessel so that the system mass inventory can be varied.

Coolant enters the vessel through an external downcomer inlet annulus (shown in Figure AI.8). This annular entrance section reduces to an instrumented pipe over the major length of the lower vessel, until the bottom of the downcomer rejoins the vessel at the lower plenum through an annular distribution annulus, as shown in Figure AI.9. The downcomer pipe is fabricated from 3-in. Sch 160 pipe, and the inner wall of the downcomer pipe is lined with a honeycomb insulator to limit heat transfer between the pipe wall and the fluid. An instrumented spool piece provides the connection

between the lower end of the downcomer pipe and the downcomer nozzle connecting to the downcomer distribution annulus. The inlet annulus assembly contains the cold leg nozzles and is designed to provide an annular inlet geometry similar to that in a PWR. Both surfaces of the inlet annulus are covered with insulators that maintain a steam gap to isolate the fluid from the hot walls of the assembly. The lower end of the inlet annulus contains a transition section that funnels the flow into the downcomer pipe. The downcomer inlet annulus is connected to the vessel upper head with 1/2-in. tubing which simulates the bypass flow paths in a PWR; as already mentioned, about 4% of the total combined loop flows is routed through the bypass line into the upper head.

Table AI.1

---

 SEMISCALE PRIMARY COOLANT SYSTEM ELEVATIONS<sup>a</sup>


---

<u>LOCATION</u>	<u>ELEVATION (IN.)</u>
<b>VESSEL</b>	
TOP OF UPPER HEAD	+166.6
TOP OF GUIDE TUBE	+132.1
BOTTOM OF UHI INJECTION TUBE	+127.1
TOP OF CORE SUPPORT TUBES	+67.1
TOP OF UPPER SUPPORT PLATE	+61.4
BOTTOM OF UPPER SUPPORT PLATE	+53.4
HOT LEG NOZZLE CENTERLINE	+8.5
COLD LEG NOZZLE CENTERLINE	0.0
TOP OF HEATED CORE	-51.1
BOTTOM OF HEATED CORE	-191.1
TOP OF LOWER PLENUM	-215.0
BOTTOM OF LOWER PLENUM	-227.6
<b>INTACT LOOP</b>	
BOTTOM OF STEAM GENERATOR TUBE SHEET	+81.6
SHORT TUBE TOP, SPILLOVER	+436.9
MIDDLE TUBE TOP, SPILLOVER	+465.4
LONG TUBE TOP, SPILLOVER	+491.9
PUMP SUCTION CENTERLINE	-111.0
BOTTOM OF PRESSURIZER INTERNAL VOLUME	+68.8
TOP OF PRESSURIZER INTERNAL VOLUME	+117.3
<b>BROKEN LOOP</b>	
BOTTOM OF STEAM GENERATOR TUBE SHEET	+81.6
SHORT TUBE TOP, SPILLOVER	+436.9
LONG TUBE TOP, SPILLOVER	+491.9
PUMP SUCTION CENTERLINE	-110.3

---

<sup>a</sup> ELEVATIONS ARE RELATIVE TO COLD LEG CENTERLINE



Table AI.2

## Intact Loop Spool Pieces

Spool Piece Number	Spool Piece Indent	Total Length (in)	Blueprint Number
H. L. Nozzle		8.65	407968
1	3-PC-1B	23.06	414684
2	3-PC-18	15.61	407346
3	2½-PC-2	52.51	415155
4	2½-PC-6	26.31	414431
5	2½-PC-7	13.995	414425
6	2½-PC-8	14.00	414426
7	2½-PC-9	19.195	414427
SG Inlet		6.32	414271
SG Outlet		6.32	414271
8	2½-PC-10	27.195	414428
9	2½-PC-11	13.995	414425
10	2½-PC-12	14.00	414426
11	2½-PC-13	14.00	414429
12	2½-PC-14A	19.41	414430
13	3-PC-20	85.25	409027
14	3-PC-20	20.638	409027
15	3-PC-20	62.00	409027
16	3-PC-20	23.06	414684
17*	3-PC-9A	19.319	404749
18*	3-PC-10A	20.53	408613
IL Pump*			
19*	3-PC-11A	17.00	412858
20*	3-PC-12	17.25	404759
21	3-PC-13	23.06	404794
22	3-PC-19A	37.90	414684
C. L. Nozzle		7.15	407986

---

\* Replaced by pump replacement spool piece in all natural circulation tests (drawings 415276 through 415281).

Table AI.3

## Broken Loop Spool Pieces

Spool Piece Number	Spool Piece Indent	Total Length (in)	Blueprint Number
H. L. Nozzle	(3 in. Sch. 160)	16.07	407975
50	1½-ABL-1	24.01	407670
55	1½-ABL-14A	59.517	414670
56	1½-ABL-30	11.83	414671
57	1½-ABL-31	13.872	414672
58	1½-ABL-32	13.75	414673
59	1½-ABL-33	19.826	414674
SG Inlet		4.142	414272
SG Outlet		4.142	414272
60	1½-ABL-34	15.316	414675
61	1½-ABL-35	13.75	414676
62	1½-ABL-36	13.872	414672
63	1½-ABL-37	13.75	414673
64	1½-ABL-6A	109.17	414677
65	1½-ABL-7	33.834	407384
72	1½-ABL-9	61.82	407380
73	1½-ABL-11	27.56	407673
BL Pump			
74*	1½-ABL-12	23.64	407674
76*	1½-ABL-17	19.77	407875
79	1½-ABL-15	28.01	407675
CL Nozzle	(3 in. Sch 160)	15.314	407986

---

\* Replaced by cold leg piping used in hot leg breaks for NC-7 since cold leg break assembly not needed (1½-ABL-13 from 407386 and 1½-ABL-2 from 407381).

Table AI.4

TYPE II STEAM GENERATOR DATA (MOD-2A)

	<u>INTACT LOOP</u>	<u>BROKEN LOOP</u>
Number Tubes	6	2
Tube Dimensions	(0.875 in. OD x 0.049 in.	Wall x 1.25 in. Pitch)
Tube Height <sup>(1)</sup>	2 @ 391 in. 2 @ 364.5 in. 2 @ 336 in.	1 @ 391 in. 1 @ 336 in.
Primary Volume, Bundle	1.27 ft <sup>3</sup>	0.40 ft <sup>3</sup>
Primary Plenum Volume	0.058 ft <sup>3</sup> each	0.042 ft <sup>3</sup> each
Secondary Volume <sup>(2)</sup>	4.03 ft <sup>3</sup>	1.85 ft <sup>3</sup>
Downcomer Volume	0.91 ft <sup>3</sup>	0.58 ft <sup>3</sup>
Total Secondary Volume <sup>(3)</sup>	11.2 ft <sup>3</sup>	8.69 ft <sup>3</sup>
Secondary Heat Transfer Area	83.3 ft <sup>2</sup>	27.76 ft <sup>2</sup>

(1) Above top of tube sheet

(2) Tube sheet to top of tubes

(3) Tube sheet to top of steam dome

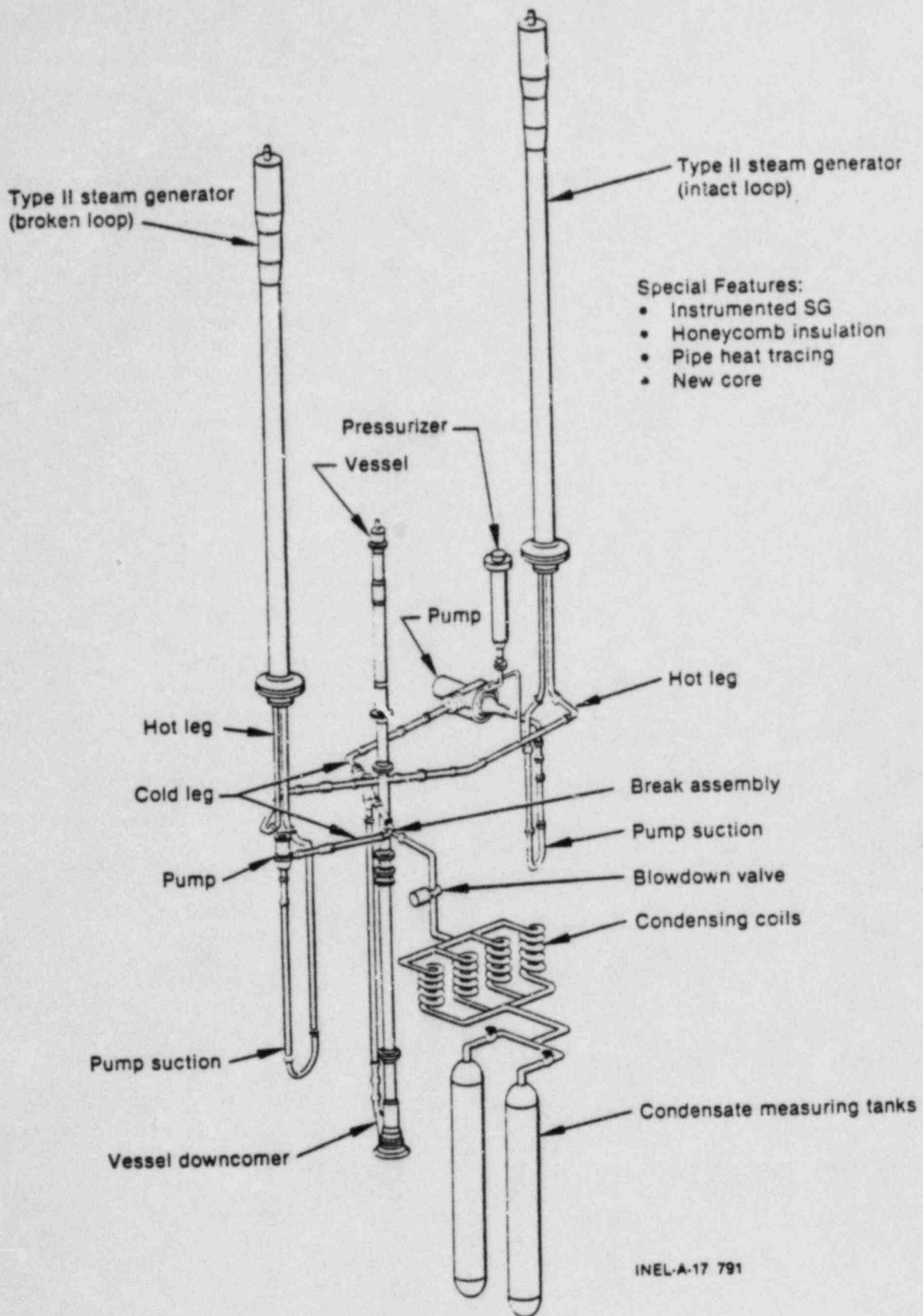
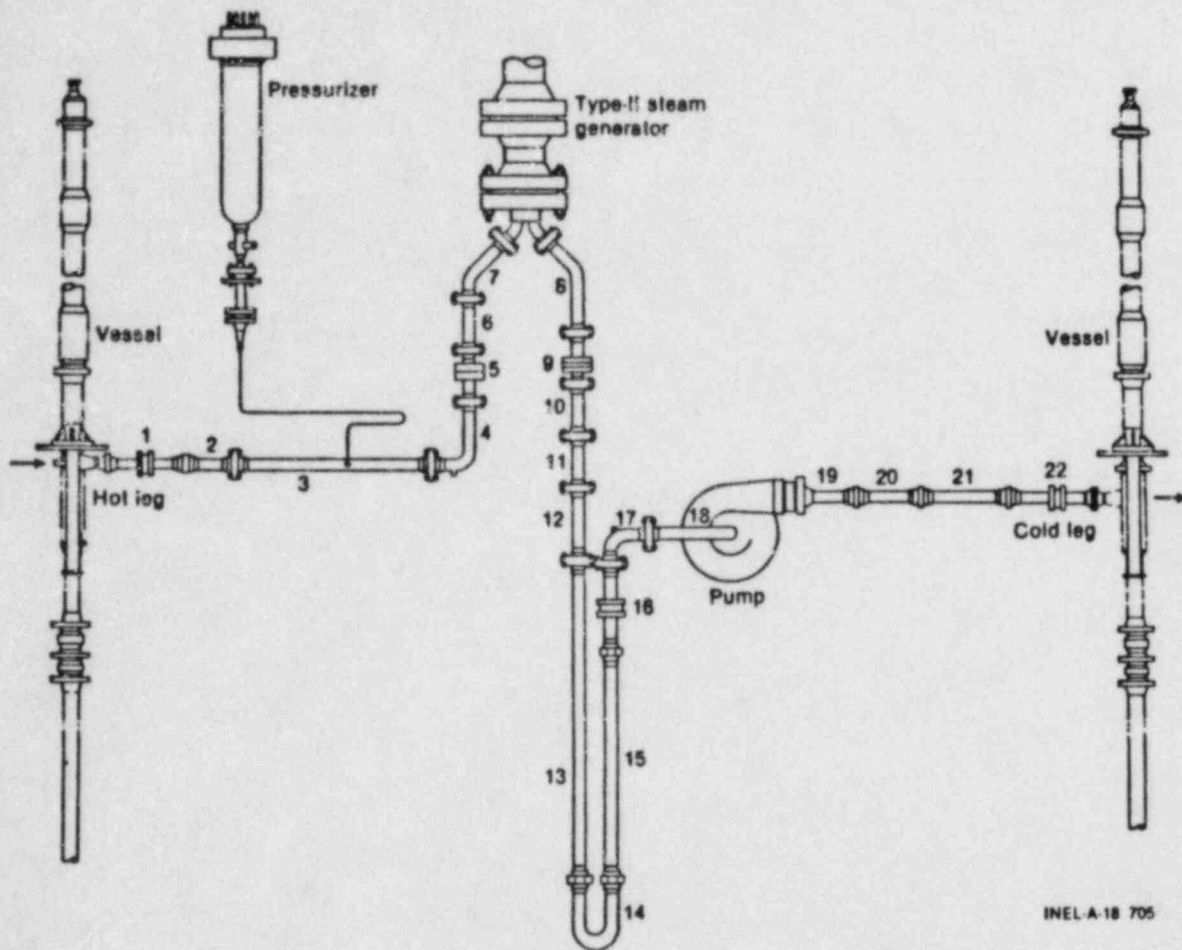
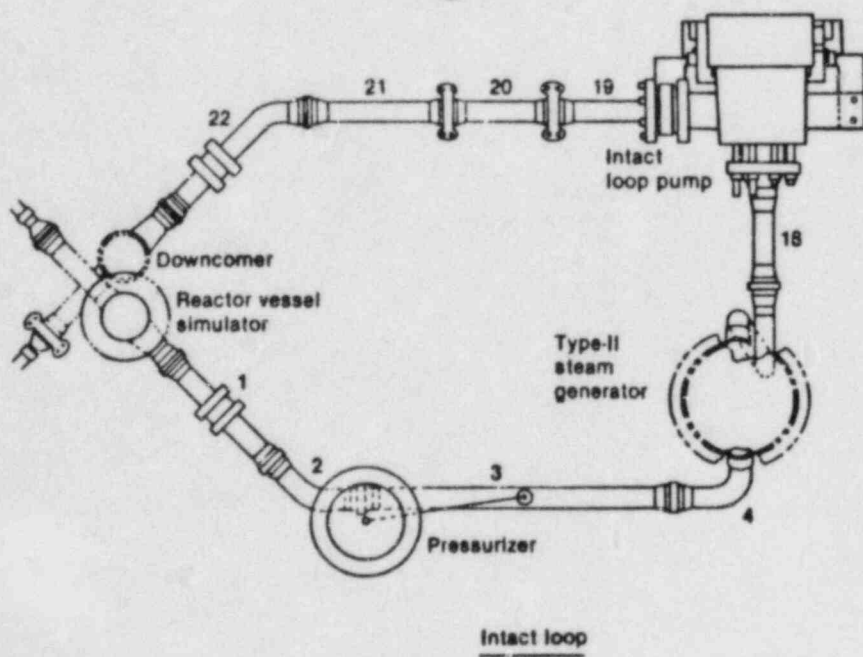


Figure AI.1 Isometric View of the Semiscale Mod-2A System



INEL-A-18 705



Intact loop

INEL-A-18 707

Figure AI.2 Intact Loop Spool Pieces

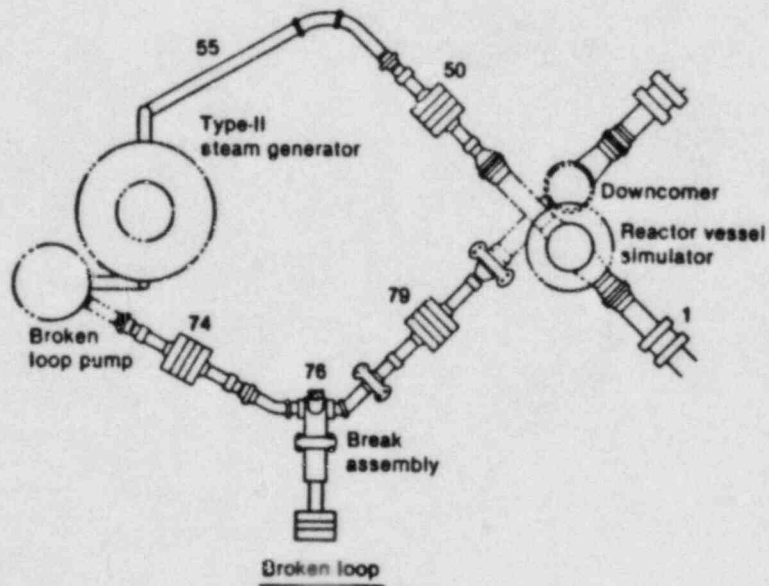
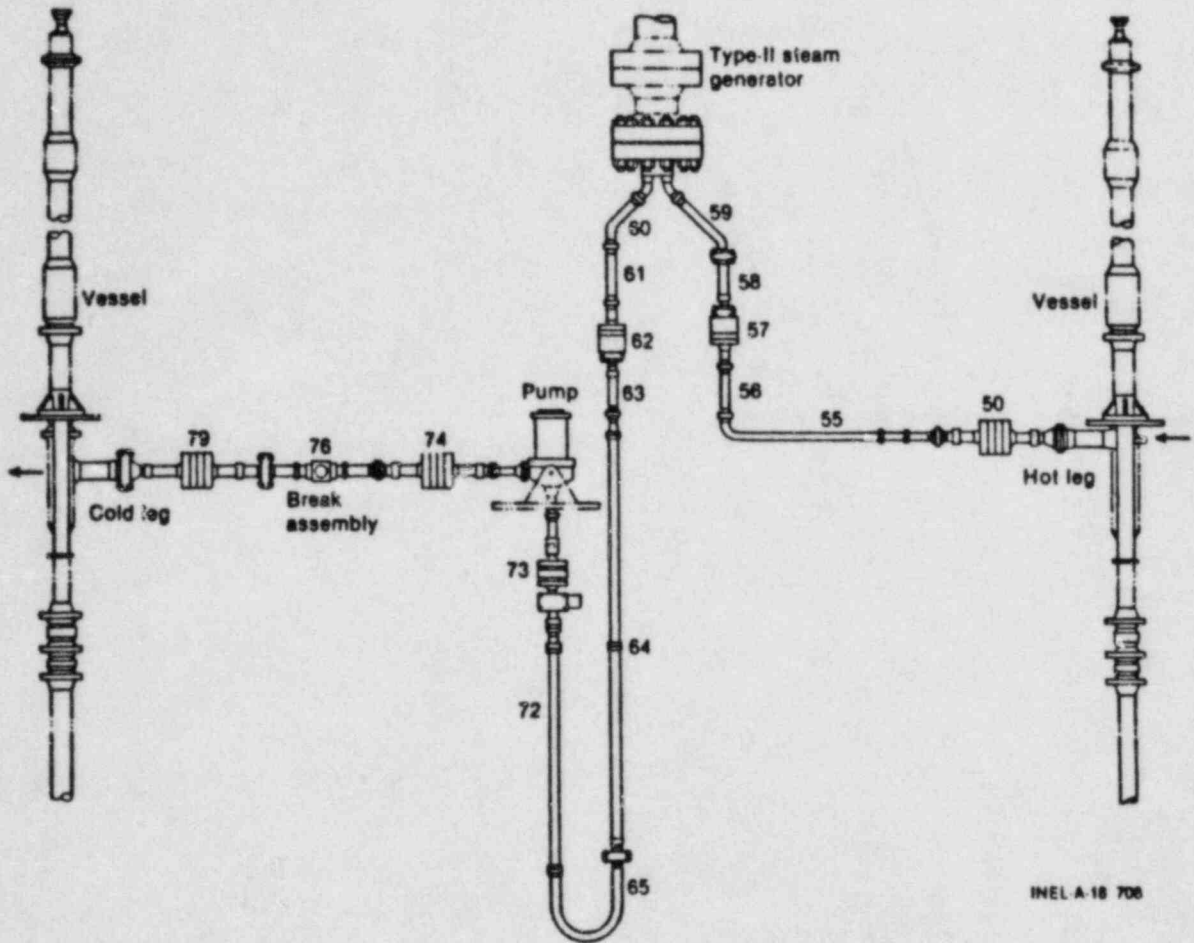


Figure AI.3 Broken Loop Spool Pieces

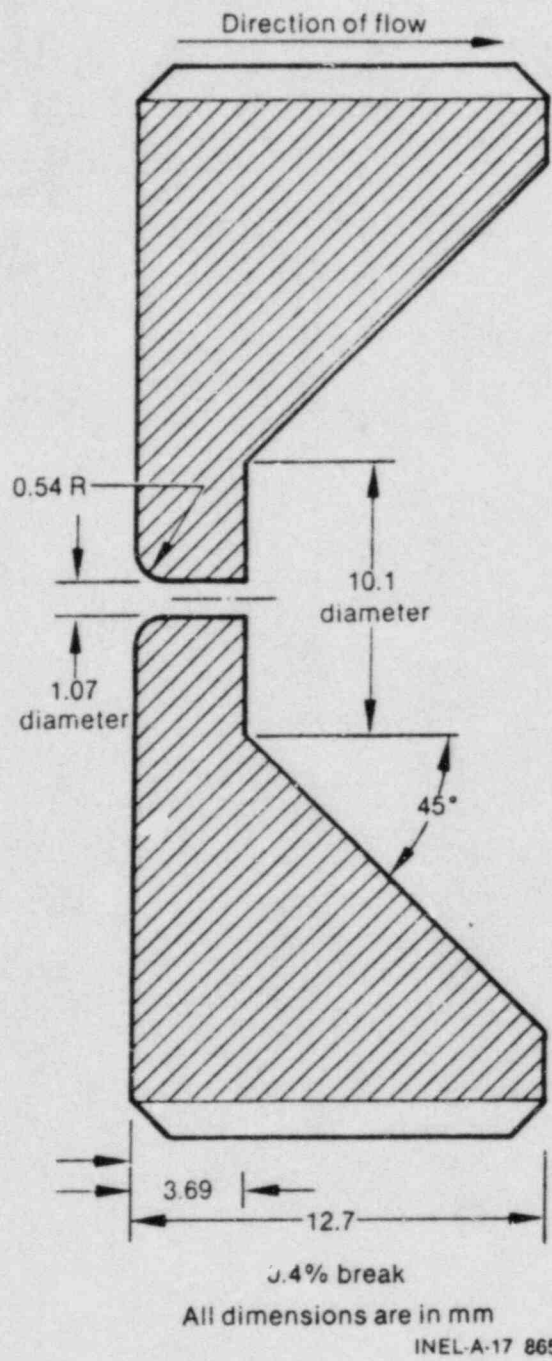


Figure AI.4 Break Orifice for S-NC-8

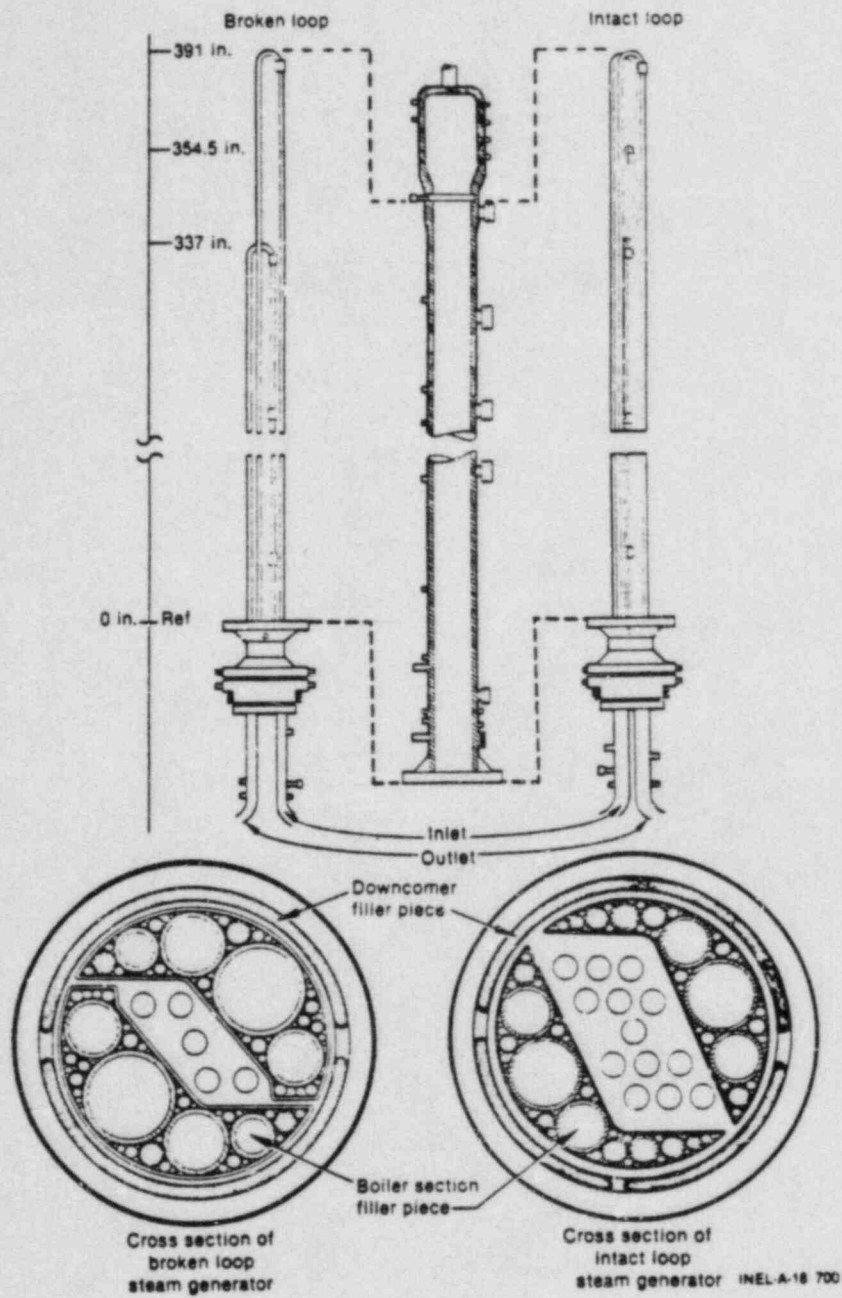


Figure AI.5 Steam Generator Assembly



# PRESSURIZER

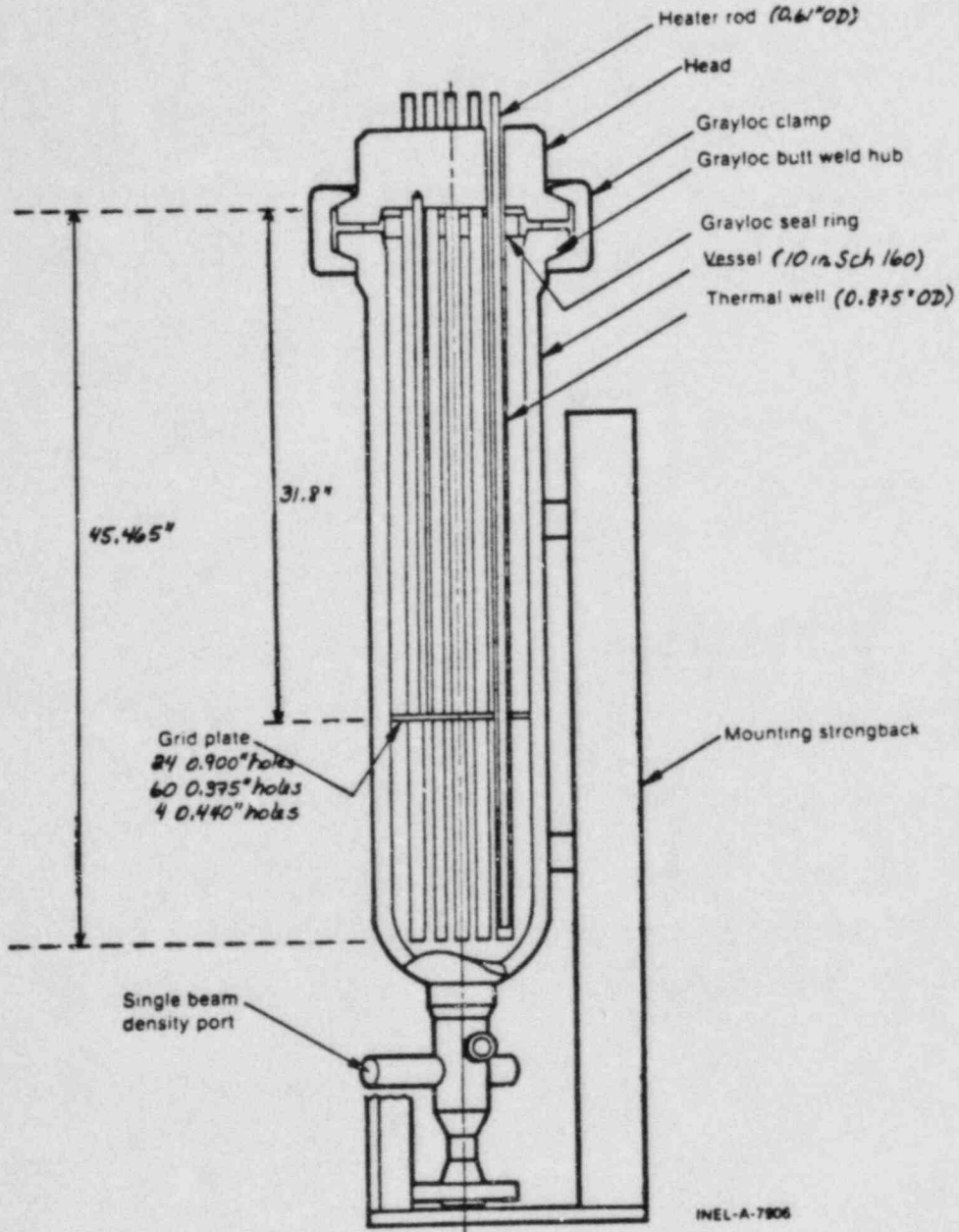


Figure AI.6 Pressurizer Vessel

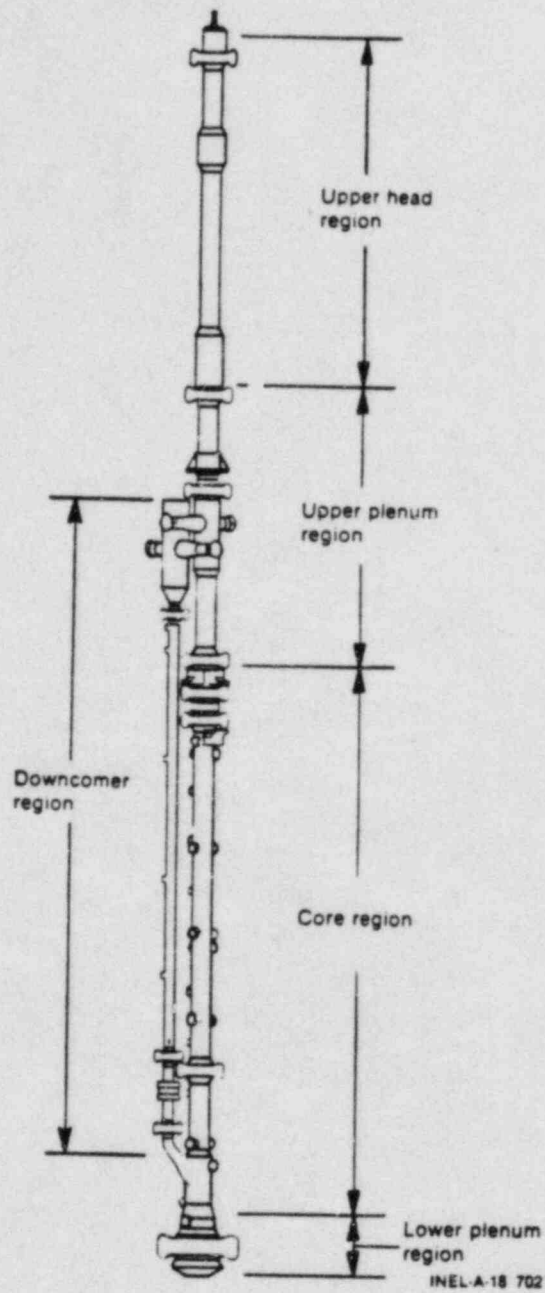


Figure AI.7 Semiscale Mod-2A Vessel Assembly

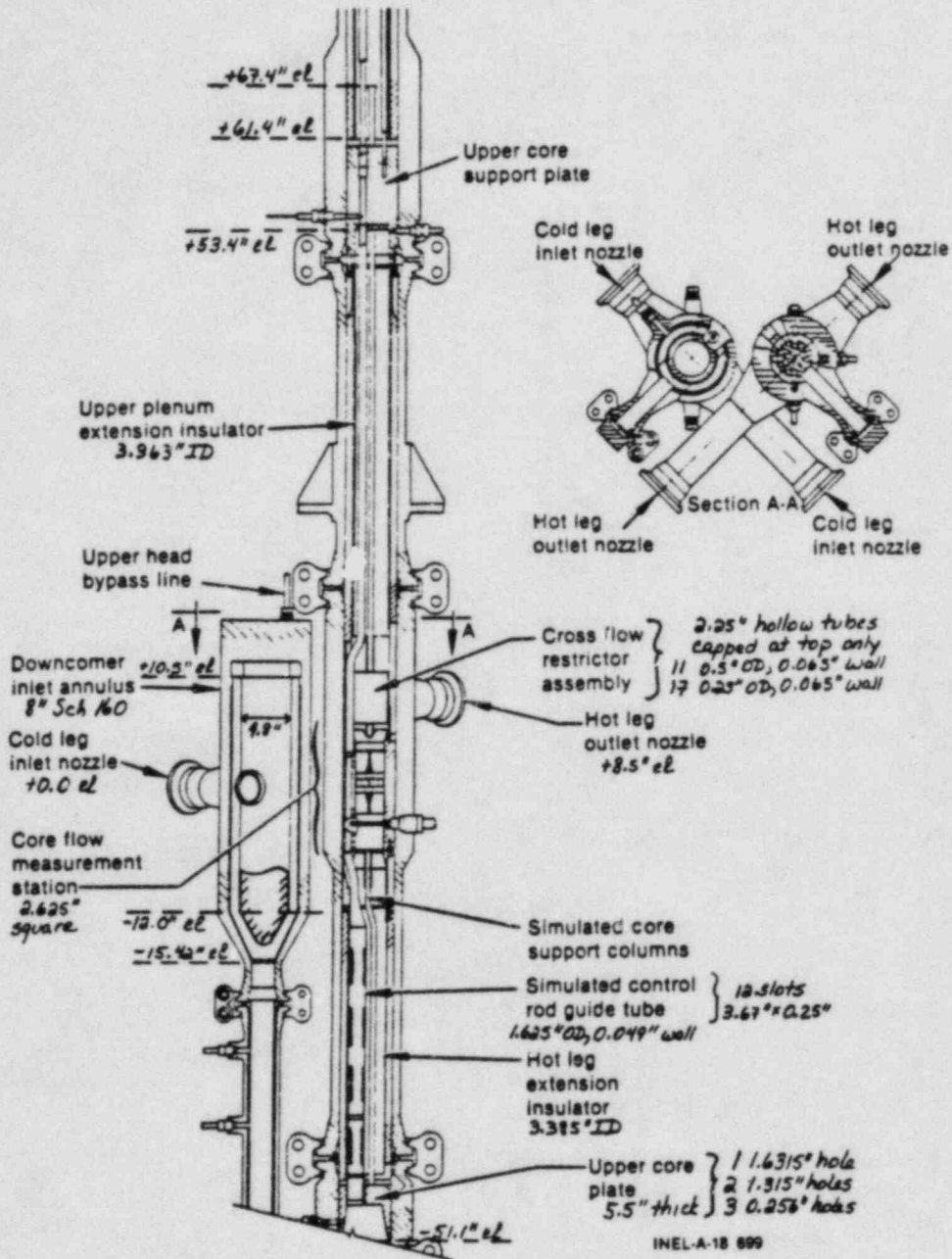


Figure AI.8 Semiscale Mod-2A Vessel Downcomer Inlet and Upper Plenum Region

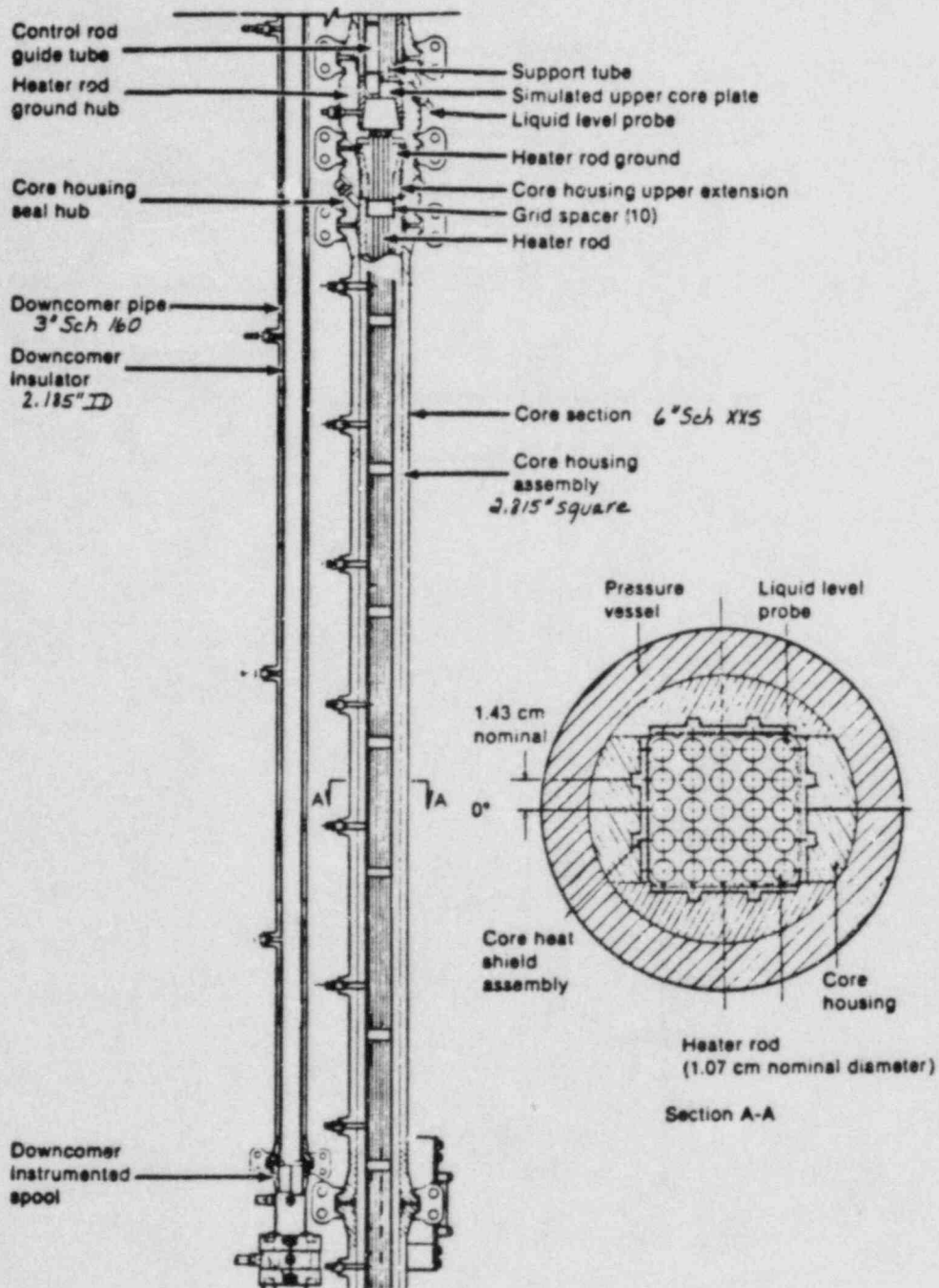


Figure AI.9 Semiscale Mod-2A Vessel Core Region

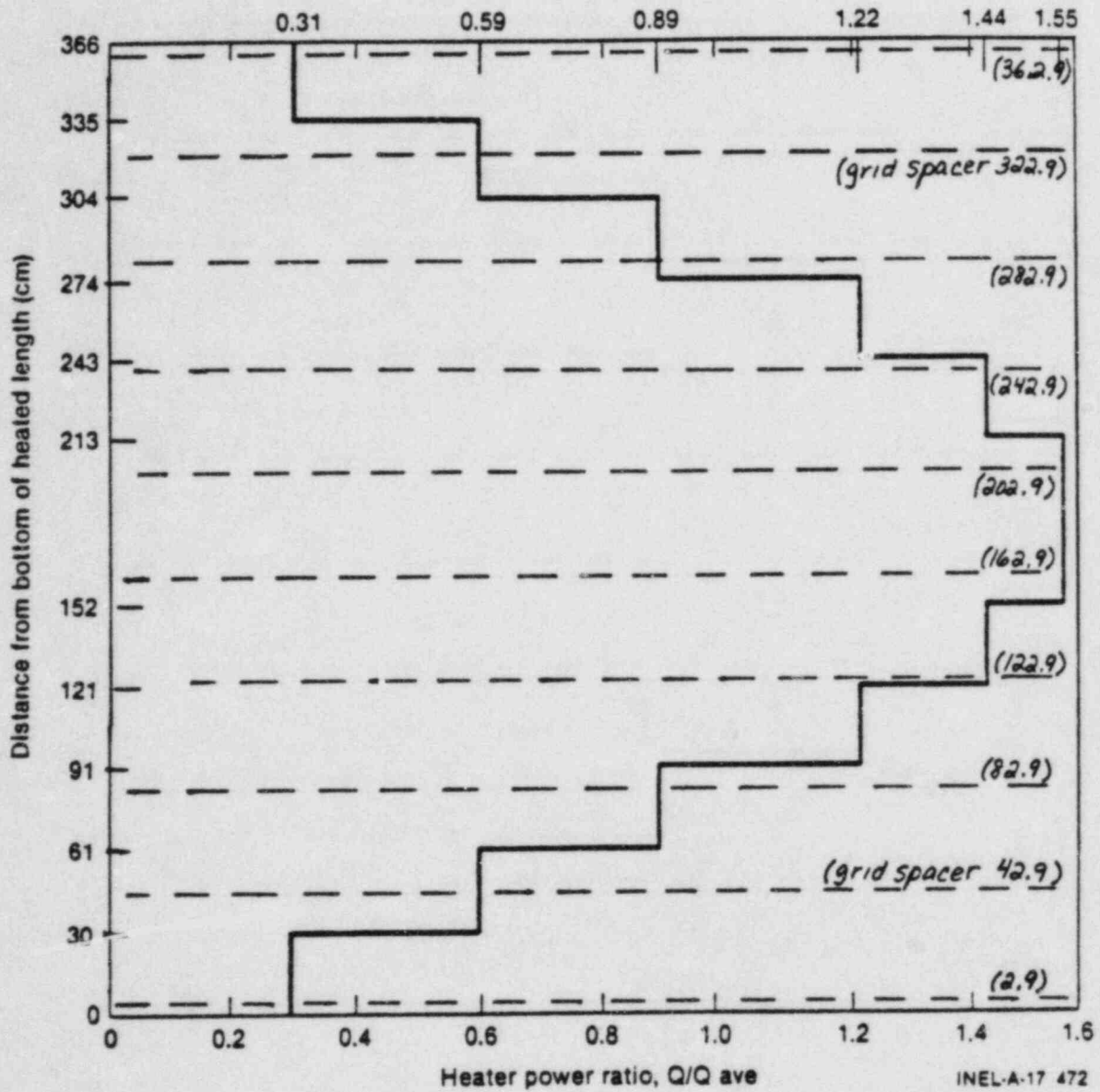


Figure AI.10 Core Axial Power Profile

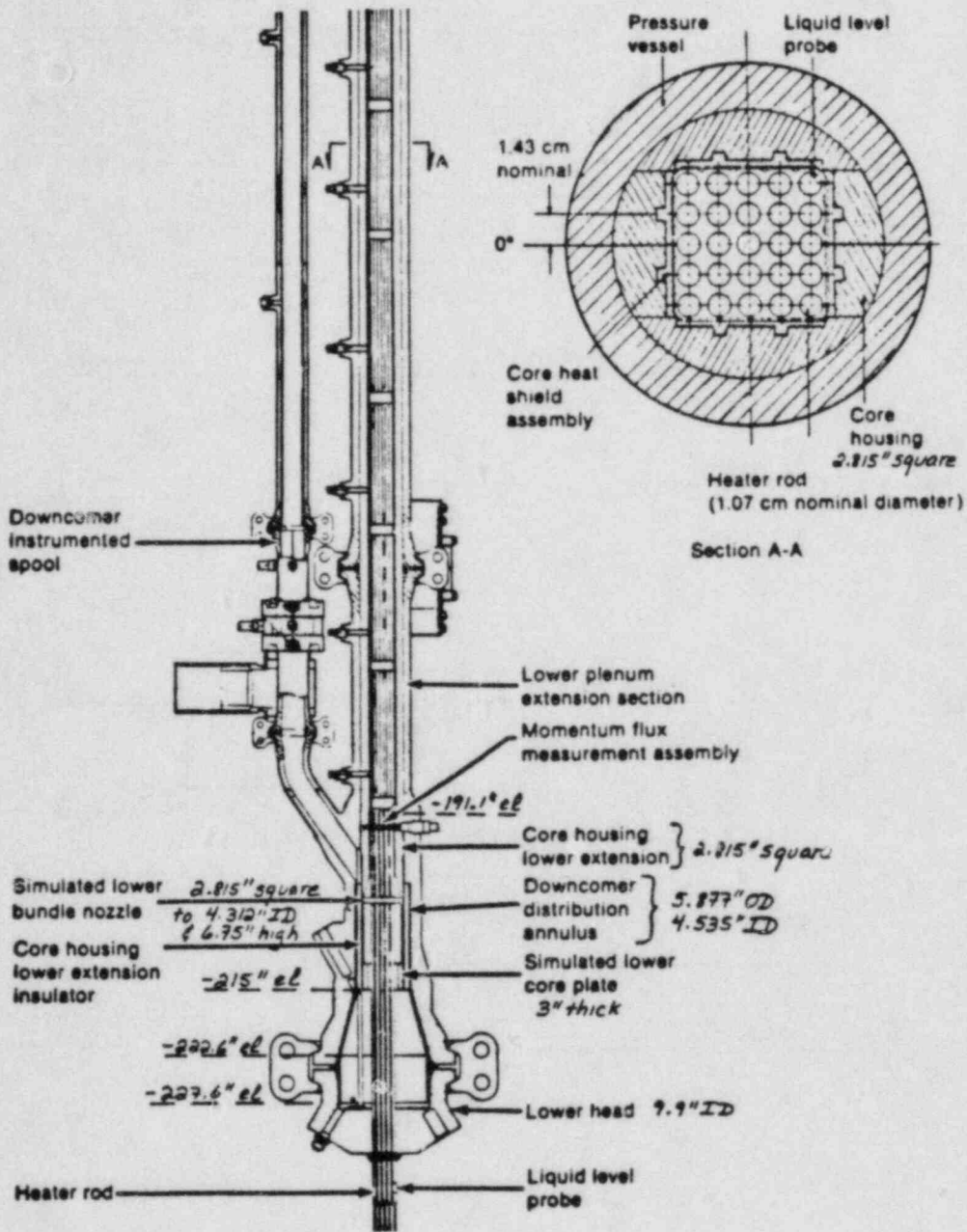


Figure AI.11 Semiscale Mod-2A Vessel Lower Plenum And Lower Downcomer Region

## APPENDIX II INPUT LISTINGS

Input listings for the S-NC-3 and S-NC-4 100% secondary inventory calculations, and for the S-NC-8 steady state and transient calculations, are given on attached microfiche.

### APPENDIX III

#### ADDITIONAL UPDATES USED FOR CYCLE 18+

In June 1982, updates to bring RELAP5/MOD1 to the cycle 18 level were received from INEL. Also added to our version of cycle 18 were some other recommended updates from INEL. The recommended updates which were added are listed below by their identifier names for reference.

- KERRO15: This update adds a subroutine to check elevation changes around piping loops. The check is done during input processing.
- DEBUGJ: Adds diagnostic printout during computation of junction properties.
- DMKTIM: Adds mass error debug printout during computation of equation of state variables.
- BRFIX: Attempts to fix a branching problem by multiplying viscous terms in momentum equation by the square of the ratio of the junction area to the volume flow area.

Also included in INEL's recommended updates was a new inter-phase drag model (identifier HXCRXXX). This update was not implemented in our version of RELAP5/MOD1/CYCLE18.



DISTRIBUTION:

U. S. NRC Distribution Contractor (CDSI) (300)  
7300 Pearl Street  
Bethesda, MD 20014  
300 copies for R4

U. S. Nuclear Regulatory Commission (4)  
Reactor Systems Research Branch  
Division of Accident Evaluation  
Office of Nuclear Regulatory Research  
7915 Eastern Avenue  
Silver Spring, MD 20910  
Attn: Louis M. Shotkin  
Fuat Odar  
R. Landry  
H. S. Tovmassian

EG&G Idaho (6)  
Idaho National Engineering Laboratory  
P. O. Box 1625  
Idaho Falls, ID 83415  
Attn: T. R. Charlton  
G. W. Johnsen  
Edna Johnson  
J. C. Lin  
V. H. Ransom  
R. J. Wagner

Thad D. Knight  
Dennis R. Liles  
Los Alamos National Laboratory (2)  
K553 Q-9  
Los Alamos, NM 87545

P. Saha, 130  
Department of Nuclear Energy  
Brookhaven National Laboratory  
Associated Universities, Inc.  
Upton, New York 11973

N. H. Shah  
Babcock & Wilcox Co. (NPGD)  
P. O. Box 1260  
Lynchburg, VA 24505

Jesse Fell (5)  
Deputy Director, Water Reactor Programs  
Atomic Energy Establishment  
Winfrith  
Dorchester, Dorset DT28DH  
ENGLAND

6400 A. W. Snyder  
6410 J. W. Hickman  
6417 D. C. Carlson  
6420 J. V. Walker  
6421 T. R. Schmidt  
6422 D. A. Powers  
6423 P. S. Pickard  
6425 W. J. Camp  
6427 M. Berman  
6427 C. C. Wong  
6440 D. A. Dahlgren  
6442 W. A. von Rieseemann  
6444 S. L. Thompson (16)  
6444 L. D. Buxton  
6444 R. K. Byers  
6444 R. K. Cole, Jr.  
6444 P. N. Demmie  
6444 D. Dobranich  
6444 M. G. Elrick  
6444 L. N. Kmetyk  
6444 R. Knight  
6444 J. M. McGlaun  
6444 J. Orman  
6444 A. C. Peterson  
6444 W. H. Schmidt  
6444 R. M. Summers  
6444 S. W. Webb  
6449 K. D. Bergeron  
3141 C. M. Ostrander (5)  
3151 W. L. Garner  
8424 M. A. Pound

**BIBLIOGRAPHIC DATA SHEET**

NUREG/CR-3690  
SAND84-0402

2 Leave blank

4 RECIPIENT'S ACCESSION NUMBER

5 DATE REPORT COMPLETED

MONTH April YEAR 1984

7 DATE REPORT ISSUED

MONTH YEAR 1984

9 PROJECT/TASK/WORK UNIT NUMBER

10 PIN NUMBER

A-1205

12a TYPE OF REPORT

Technical

12b PERIOD COVERED (Inclusive dates)

3 TITLE AND SUBTITLE

RELAP5 Assessment: Semiscale Natural Circulation Tests S-NC-3, S-NC-4, and S-NC-8

6 AUTHOR(S)

C. C. Wong and L. N. Kmetyk

8 PERFORMING ORGANIZATION NAME AND MAILING ADDRESS (Include Zip Code)

Thermal/Hydraulic Division 6444  
Sandia National Laboratories  
P. O. Box 5800  
Albuquerque, NM 87185

11 SPONSORING ORGANIZATION NAME AND MAILING ADDRESS (Include Zip Code)

Reactor Systems Research Branch  
Division of Accident Evaluation  
Office of Nuclear Regulatory Research  
U. S. Nuclear Regulatory Commission  
Washington, DC 20555

13 SUPPLEMENTARY NOTES

14 ABSTRACT (200 words or less)

The RELAP5/MOD1 independent assessment project at Sandia National Laboratories (SNLA) is part of an overall effort funded by the NRC to determine the ability of various systems codes to predict the detailed thermal/hydraulic response of LWRs during accident and off-normal conditions. The RELAP5 code is being assessed at SNLA against test data from various integral and separate effects test facilities. As part of this assessment matrix, we have analyzed a number of natural circulation tests performed at the Semiscale facility. Our results for the single-loop and two-loop steady state basecase tests S-NC-2 and S-NC-7 have already been documented separately; this report gives the results of calculations for two single loop degraded heat transfer tests, S-NC-3 and S-NC-4, and for the two-loop ultra-small break transient test S-NC-8.

For tests S-NC-3 and S-NC-4, our analyses show that RELAP5/MOD1 describes correctly the qualitative influence of steam generator secondary side heat transfer degradation on both two-phase and reflux natural circulation. The agreement between calculated and measured two-phase mass flow rates in test S-NC-3 is better with a primary mass inventory of 85% (where the peak two-phase mass flow rate is calculated to occur) instead of 92% (where the measured peak mass flow rate occurred in S-NC-2). Flow oscillations are calculated for both tests, and were seen during S-NC-3, but were not reported in the S-NC-4 experiment. Some of these predicted oscillations are real, but others are nonphysical and can be inhibited by reducing the time step being used (indicating problems in the time step control algorithm).

The results for test S-NC-8, an ultra-small (0.4%) cold leg break, also compare reasonably well with the outcome of that experiment. Mass flow rates calculated in the intact loop and in the downcomer match data, although there are some discrepancies in the broken loop mass flow rates. The calculated pressure response throughout the blowdown period is good. However, the mass flow rate at the break is underpredicted, resulting in discrepancies in the primary system mass inventory.

15a KEY WORDS AND DOCUMENT ANALYSIS

15b DESCRIPTORS

16 AVAILABILITY STATEMENT

17 SECURITY CLASSIFICATION  
(This report)

Uncl

18 NUMBER OF PAGES

112

-107-

19 SECURITY CLASSIFICATION  
(This page)

Uncl

20 PRICE

\$

ORG.	BLDG.	NAME	REC'D BY*	ORG.	BLDG.	NAME	REC'D BY*

120555078877 1 1AN1R4  
 US NRC  
 ADM-DIV OF TIOC  
 POLICY & PUB MGT BR-PDR NUREG  
 W-501  
 WASHINGTON DC 20555